LIQUEFACTION STUDIES ON SAND AND ITS MITIGATION USING STONE COLUMNS

A THESIS

submitted by

UNNI KARTHA G.

(Reg. No: 3756)

for the award of the degree

of

DOCTOR OF PHILOSOPHY

Division of Civil Engineering

School of Engineering

Cochin University of Science and Technology

November 2018

THESIS CERTIFICATE

This is to certify that the thesis entitled **LIQUEFACTION STUDIES ON SAND AND ITS MITIGATION USING STONE COLUMNS** submitted by **Unni Kartha G. (Reg. No: 3756)** to the Cochin University of Science and Technology, Kochi for the award of the degree of Doctor of Philosophy is a bonafide record of research work carried out by him under my supervision and guidance at the Division of Civil Engineering, School of Engineering, Cochin University of Science and Technology. The contents of this thesis, in full or in parts, have not been submitted to any other University or Institute for the award of any degree or diploma.

I further certify that the corrections and modifications suggested by the audience during the pre-synopsis seminar and recommended by the Doctoral committee of **Unni Kartha G.** are incorporated in the thesis.

Prof. (Dr) K. S. Beena
Research Guide
Professor
Division of Civil Engineering
School of Engineering
CUSAT, Kochi 682 022

Place: Kochi
Date : 26 - 11 - 2018

DECLARATION

I hereby declare that the work presented in the thesis entitled **LIQUEFACTION STUDIES ON SAND AND ITS MITIGATION USING STONE COLUMNS** is based on the original research work carried out by me under the supervision and guidance of **Dr. K. S. Beena**, Professor, Division of Civil Engineering, School of Engineering, Cochin University of Science and Technology for the award of the degree of Doctor of Philosophy with Cochin University of Science and Technology. I further declare that the contents of this thesis in full or in parts have not been submitted to any other University or Institute for the award of any degree or diploma.

Kochi - 682 022	**Unni Kartha G.**
26 - 11 - 2018	(Reg No: 3756)

DEDICATION

This thesis is dedicated to my father, Late **P. Gopalakrishna Pillai**, who would have loved to see me complete this work and awarded the degree.

ACKNOWLEDGEMENTS

First and foremost, my sincere gratitude goes to the research supervisor and guide, **Dr. K. S. Beena**, Professor, Division of Civil Engineering, CUSAT. She has been the constant motivation and support in carrying out this research work. I consider it a great honour to pursue my doctoral programme under her guidance and to learn from her long research experience. I gained a lot from her, through the personal and scholarly interactions during the research.

I am thankful to **Dr. George Mathew**, Professor, Division of Fire and Safety, CUSAT, Doctor Committee Member, for reviewing the work and giving crucial suggestion during the course of the work. My sincere thanks to the Principal, **Dr. M. R. Radhakrisha Panicker**, SOE, Head of the department, **Dr. Glory Joseph**, and other Faculty members and lab staff of Division of Civil Engineering, for their great support. The help and guidance provided by **Dr. Job Thomas**, Associate Professor, needs special mention.

I acknowledge and appreciate all my heads at FISAT; **Mr. Paul Mundadan**, Chairman, **Dr. George Issac**, Principal, **Dr. C. Sheela**, Vice Principal, **Dr. K. S. M. Panicker**, Director, who provided the best support for pursuing this research work. They have encouraged and supported me to complete the research without affecting my work. I wish to mention the support provided by Late **Mr. P. V. Mathew**, Ex-Chairman, FISAT, who gave the permission to get admission and also to develop the shake table for conducting the experimental work in the lab. I remember with gratitude, my colleagues at the Department of Civil Engineering, FISAT, for all the support and encouragement throughout the research work.

I am obliged to **Dr. S. K. Prasad**, Professor, SJCE, Mysuru, who has been one of the key contributors to this research work. His suggestions during the development of the experimental set-up have been very valuable.

I am thankful to **Mr. Jose**, **Mr. Eldho** and **Mr. Alby** for helping me fabricate the experimental set-up. My deepfelt gratitude to **Mr. Mahesh C.**, **Mr. Bejoy Varghese**, **Mr. Jestin Joy** and **Mr. Muhammed Noufal C.**, my faculty colleagues, who introduced me to the world of sensors and programming which was the key element in pursuing this research. They also enabled me to use the facilities like the centre for high-performance computing and robotics lab for conducting research. My sincere thanks to the M.Tech Students, **Ms. Chandana**, **Mr. Mohammed Thahir**, **Ms. Greeshma**, **Ms. Shafnas**, **Ms. Lakshmi** and **Ms. Chesma** who collaborated with me for their project.

I wish to acknowledge the support provided by the library at CUSAT and also at my home campus, FISAT which played a significant role in gathering the literature for conducting this research work. My sincere thanks to **TEQIP** for providing the seed money for setting-up the shake table in the Geotechnical Engineering laboratory of School of Engineering.

All the software used for this work are either free or open source. I feel that the free-software and *OpenSees* community played a crucial role in helping me to understand, learn and pursue this work. I am indebted to the contributions of the community.

I offer the highest credit to **Ms. Parvathy R.**, my wife who always wish me luck and will probably be the happiest person in the submission of this thesis. My family, Mother, **Ms. Savithri Devi Kunjamma**, my in-laws, **Mr. Gopalakrishna Pillai** and **Prof. Rani Rajini Devi** has been a constant encouragement.

Finally, I wish to mention all my teachers at school and college, who gave me the foundations in knowledge and enabled me to continue with my studies and reach this milestone in life.

ABSTRACT

KEYWORDS: Liquefaction; Shake table; Floating Stone Column; *OpenSees*; Parallel FEA

Liquefaction is one of the most dramatic behaviour observed in soil it and has captured the imagination of many researchers even before the formal evolution of the field of geotechnical engineering. This phenomenon is mostly observed when saturated sand or silt deposits are subjected to dynamic loading, the most common being the loading caused during earthquakes. During ground shaking, pore water pressure builds up in soil, and it loses strength and behaves like a viscous fluid. Liquefaction most often results in very disastrous consequences, since the loss of strength during the event is total and rapid, and any structure resting on it may collapse totally with little warning. Predicting and mitigating liquefaction poses a big challenge for engineers due to the wide diversity of nature of the soil and its composition and the complexity of the phenomenon.

Liquefaction studies in the Indian context are meagre mainly because of the expensive experimental set-up required for such studies and also due to the assumption that the country is not vulnerable to earthquakes. This thesis deal with the development of a cost-effective shake table test set-up with acceleration and pore water pressure sensors for conducting liquefaction studies in the laboratory. Even with certain limitations, the low-cost uniaxial shake table with innovative sensor and data acquisition system is found to give good results, suggesting that it can be used for studying liquefaction and related phenomenon in the laboratory. Further, experimental investigations were carried out on three different samples

from sand deposits in the central region the state of *Kerala* to identify its liquefaction susceptibility. The sands tested were found to be highly liquefiable in loose state, i.e. 30% relative density, when it is subjected to an acceleration of $0.24g$.

The effectiveness of stone columns as a mitigation technique was studied using experiments, and it is found to be a suitable mitigation method. An FEA model was developed on *OpenSees* platform and the results of the laboratory experiments were used to validate the model. Further, an exhaustive and systematic parametric study was conducted to study the behaviour of the system for different soil matrix and geometry of stone column along with the intensity of shaking. These studies were conducted using a high-performance computer with a parallel system of computing in order to handle the massive quantum of data.

The results indicated that stone column is very effective in reducing the excess porewater pressure build up during shaking, in its periphery and the effectiveness increases with increase in its diameter. At the same time, excess pore water pressure buildup below the stone column is found to increase due to its presence. This behaviour can be critical, since, the soil below the stone column will become vulnerable to liquefaction in such a case. A fully penetrating column is thus a better solution in loose sand deposits for mitigating liquefaction.

The results obtained from FEA was used to develop an empirical model for predicting the excess pore water pressure in sand bed improved with stone columns and the developed prediction charts assist the design of the mitigation solution.

TABLE OF CONTENTS

LIST OF FIGURES

LIST OF TABLES

ABBREVIATIONS

CPT	Cone Penetration Test
CSR	Cyclic Stress Ratio
EPWP	Excess Pore Water Pressure
EPWPR	Excess Pore Water Pressure Ratio
FDM	Finite Difference Method
FEA	Finite Element Analysis
GSM	Grams per Square Meter
MEMS	Micro-Electro-Mechanical Systems
MPI	Message Passing Interface
NWL	Non Woven Lined
OpenSees	Open System for Earthquake Engineering Studies
PDMY	Pressure Dependent Multi Yield model
PVC	Polyvinyl chloride
SPT	Standard Penetration Test
SC	Stone Column
TCL	Tool Command Language
USB	Universal Serial Bus

NOTATIONS

a	Ground motion acceleration in g
a_{max}	Maximum ground motion acceleration in g
A_r	Aspect ratio of stone column
B	Strain displacement matrix
B_r	Bulk modulus
C_0, C_1, C_2, C_3	Coefficients of empirical equation
C_c	Coefficient of curvature
C_u	Coefficient of uniformity
d	Depth of soil stratum
d_{SC}	Depth of stone column
D_r	Relative density
D_{10}	Size at 10% finer by weight
D_{30}	Size at 30% finer by weight
D_{50}	Size at 50% finer by weight
D_{60}	Size at 50% finer by weight
D_{SC}	Diameter of stone column
e	Void ratio
e_{max}	Maximum void ratio
e_{min}	Minimum void ratio
$f^{(s)}$	Body force vector
$f^{(p)}$	Fluid force vetor
g	Acceleration due to gravity
G	Specific gravity
G_r	Shear modulus

h	Height
H	Permeability matrix
k	Permeability
k_H	Horizontal permeability
k_p	Equivalent plane strain permeability
k_V	Vertical permeability
k_r	Permeability ratio
L	Length
M	Mass matrix
m_v	Volumetric compressibility of the soil
N	Number of cycles of shear stress
N_l	Number of cycles of shear stress required to cause liquefaction
p_u	Pore fluid pressure
p_r	Mean effective confining pressure
p_a	Atmospheric pressure in kPa
P	Pore pressure vector
Q	Discrete gradient operator
r_d	Shear stress reduction factor
r_u	Excess pore water pressure ratio
S	Spacing of stone column
t	Time
t_r	Time ratio
T	Time of shaking
u	Pore water pressure
u_g	Pore water pressure generated due to shaking
u_{xy}	Displacements in x, y
U	Displacement vector
X, Y	Location of point in the model
ρ_{sat}	Saturated density

σ	Total stress
σ'	Effective stress
σ'_0	Initial effective stress
γ	Unit weight of soil
γ_w	Unit weight of water
γ_{xymax}	Maximum shear strain
τ	Shear stress
τ_{av}	Average shear stress

CHAPTER 1

INTRODUCTION

1.1 Introduction

Liquefaction is one of the most dramatic behaviour observed in soil and it has captured the imagination of many researchers even before the formal evolution of the field of geotechnical engineering. This phenomenon is mostly observed when saturated sand or silt deposits are subjected to dynamic loading, the most common being the loading caused during earthquakes. During ground shaking, pore water pressure builds up, and soil loses its strength and behaves like a viscous fluid. Liquefaction most often results in very disastrous consequences, since soil often loses its complete strength during the event and any structure resting on it may collapse totally. The collapse can be rapid with little warning.

The two major earthquakes in 1964, Niigata, Japan with magnitude 7.5 and Alaska of magnitude 9.2 brought to the attention of the engineers the devastation that can be caused due to liquefaction. Both earthquakes produced examples of liquefaction-induced damage, including slope failures, bridge and building foundation failures and flotation of buried structures (Kramer, 1996). Fig. 1.1 shows the famous photograph of Kawagishi-cho apartment buildings at Japan which witnessed liquefaction induced bearing capacity failures during the Niigata earthquake. Over the past 50 years, many spectacular examples of liquefaction have been reported in Loma-Prieta Earthquake, USA (1989), Kobe Earthquake, Japan (1995), Chi-Chi Earthquake, Taiwan (1999), Kocaeli Earthquake, Turkey (1999) and Canterbury earthquake, New Zealand (2010).

Figure 1.1: Liquefaction induced bearing capacity failure at Kawagishi-cho apartment buildings at Japan during Niigata earthquake, 1964, Source:(Kramer, 1996)

Though not common, liquefaction has been reported in some of the earthquakes that occurred in the Indian subcontinent. During the 2011 Bhuj Earthquake, there was widespread occurrences of liquefaction-induced damage (Hazarika and Boominathan, 2009; Makran, 2001). Bhuj earthquake was a trigger and reviewed interest in liquefaction studies among the researchers in India.

1.2 History of liquefaction studies

One of the first studies about the phenomenon of liquefaction was reported by Japanese researcher Mogami (1953) who observed that sand under vibration behaved like a viscous liquid and loses its shear strength. Russian Engineers Maslov (1957) and Florin (1961) have also reported similar behaviour of saturated sands subjected to liquefaction in the 1960's.

Since then, many researchers have studied the phenomenon using laboratory tests to understand the behaviour of sands subjected to vibration and earthquakes. Some of the prominent early researchers like Seed, Lee, Finn, Idriss & Ishihara have studied liquefaction potential assessment, hazard mitigation and development of suitable mitigation techniques in detail. Their research work has resulted in a greater understanding of the phenomenon and also brought to light the various aspects to be pursued (Seed, 1968; Seed and Lee, 1966; Liam Finn *et al.*, 1977; Seed and Idriss, 1971; Ishihara *et al.*, 1980).

In the year 1971, Seed and Idriss came out with a simplified procedure for evaluating soil liquefaction potential which is still very popular among engineers (Seed and Idriss, 1971). Interestingly, defining liquefaction itself and the related phenomenon like flow liquefaction and cyclic mobility was also a major point of debate among researchers. A commonly accepted definition of liquefaction was given by Marcuson (1978) as *"The transformation of a granular material from a solid to a liquefied state as a consequence of increased pore-water pressure and reduced effective stress"*. Sladen *et al.* (1985) in their paper tried to incorporate more detail and defined it as *"A phenomenon wherein a mass of soil loses a large percentage of its shear resistance, when subjected to monotonic, cyclic, or shock loading, and flows in a manner resembling a liquid until the shear stresses acting on the mass are as low as the reduced shear resistance"*.

There has also been a good number of studies about liquefaction in Japan during the 70's, and in fact, the famous work by Tsuchida to predict the zones of liquefiable soil is still being used for identifying liquefiable soils (Koester and Tsuchida, 1988). A few researchers were also keen on studying the criteria for liquefaction during the late 70's in mainland China which resulted in the idea of *"Chinese Criteria"* for liquefaction of fine sands (Wang, 1979). Probably, one of the first research in liquefaction in India can be attributed to the work by Gupta (1977) of University of Roorkee, now IIT Roorkee. In his research, he developed a medium sized uniaxial shake table and conducted a detailed investigation into the liquefaction behaviour of locally available sand. Many studies followed, and the 80's and 90's saw consolidation of knowledge and also the widespread development of laboratory infrastructure and sophisticated instrumentation for measurements. Most of the studies tried to relate SPT and CPT values to the liquefaction potential of soil. These studies were based on the data that was obtained from the field. Centrifuge testing also gained some popularity during this period. The state model of liquefaction also got a lot of attention (Wood and Belkheir, 1994; Yamamuro and Lade, 1998; Ishihara, 1993).

Both the US and Japan have been able to build huge testing facilities to conduct earthquake and liquefaction studies using Shake tables and Centrifuges. Research from these testing facilities has resulted in a greater understanding of the phenomenon and validated some of the hypothesis regarding liquefaction. Different mitigation techniques have been tried, tested and the effectiveness was reported.

The workshops conducted by National Center for Earthquake Engineering Research (NCEER), USA, during 1996 and 1998 was a landmark and consolidated the knowledge acquired over the years on the evaluation of liquefaction behaviour of sand. The workshops resulted in a detailed review of the status of knowledge and development of recommendations about many aspects of liquefaction like the criteria based on SPT, CPT, Shear Wave Velocity, Magnitude scaling factors, correction factors for overburden pressures and sloping ground.

The early 21st century saw the emergence of software for simulating liquefaction using both finite difference and finite element techniques. Different constitutive models dealing with material as well as solid-fluid coupled models were being used for simulation studies. Availability of high-performance computational facilities enabled the researchers to develop programs which can simulate earthquakes and predict the stresses and pore water pressure development to a good relative degree of accuracy. Some of the notable commercial software are FLAC (Itasca, 2000), QUAKE/W (Krahn, 2004), Abacus (Abaqus, 2010) and Plaxis (with special license) (Petalas and Galavi, 2013). One of the noteworthy contributions in this direction is the *free software* named *OpenSees*, (Open System for Earthquake Engineering Studies) developed by the University of Berkeley (Mazzoni *et al.*, 2006). Being free and open source makes the software available for researchers and works out to be a very good alternative for commercial software.

The Earthquake Engineering Research Institute (EERI), US, has been one of the forerunners in the research on earthquake and liquefaction and has come out with a series of monograms with updated knowledge in this field. The monogram which was published in 2008, *"Soil Liquefaction During Earthquakes"* serves as an advanced reference on the topic (Idriss and Boulanger, 2008).

1.3 Motivation for the study

Earthquakes are often very disastrous for the stability of infrastructure and liquefaction is one of the main issues encountered for foundations in saturated loose sand deposits. As dramatic it is, the dynamics of liquefaction is quite complex and not completely understood. The behaviour of soil inherently is quite intricate and dynamic loading makes the problem more baffling. Maybe this is one of the reasons why liquefaction is one of the most widely studied phenomena across the developed nations. Studies in India in this direction are not very common mainly due to the high cost of laboratory infrastructure required. This is accompanied by the presumption that the country is not so prone to earthquakes like Japan or USA. Though there have been few studies in the recent past, experimental studies pertaining to the context of the state of *Kerala* are not reported in the literature.

Such studies are relevant and require immediate attention since the state of *Kerala* is classified under Zone III in the Indian Standard Code, IS 1893 (Part 1)-2002. With rapid urbanisation, it is essential that studies have to be performed to identify the liquefaction hazard of structures resting on liquefiable soils and suggest suitable mitigation methods.

1.4 Objectives and scope of the study

The current research work is aimed at studying the behaviour of sand deposits, specifically to the locality, and develop a better understanding of the behaviour of stone column as a liquefaction mitigation method in liquefiable sand. The specific objectives of the study are:

1. To develop a simple, cost-effective shake table and data acquisition system for conducting liquefaction studies on sand models.
2. To study the behaviour of sand samples in *Kerala* and find whether it is potentially liquefiable using shake table experiments.
3. To investigate stone columns as a liquefaction mitigation method using shake table experiments.
4. To develop a suitable FEA model for the experiment and validate it.
5. To investigate the development of excess pore water pressure of partially penetrating stone columns in liquefiable deposits due to sinusoidal loading using FEA.
6. To develop a model for predicting excess pore water pressure in stone column reinforced sand deposits.

1.5 Methodology

- Initially, a detailed review of the history of liquefaction studies and the status of knowledge and gaps in studies in the area of liquefaction mitigation using stone columns was carried out.
- The various experimental methods used for liquefaction studies were explored to identify the feasibility of developing a suitable experimental set-up for pursuing the study. A simple experimental set-up was designed, developed and calibrated.
- With the experimental set-up, liquefaction studies were conducted to understand the behaviour of sand samples sourced from different locations in the region.
- The experimental was used to study the mitigation effect of stone columns in soil samples.
- The different methods employed to model liquefaction was explored to identify a suitable software and to model the laboratory investigations.
- The model was validated using the data from experiments.
- A systematic and exhaustive parametric study was conducted using the validated model to study the effects of the factors affecting liquefaction.
- Finally, an empirical model for predicting the excess pore water pressure in soils improved with stone columns was developed using the results obtained from the parametric study.

1.6 Structure of the thesis

The thesis is structured in the following manner. Chapter 2 discusses the studies conducted by earlier researchers in the area of study. The development of an experimental setup and its performance evaluation is presented in Chapter 3. The experimental study on the effect of relative density and non-plastic fines content in liquefaction behaviour is discussed in Chapter 4. Liquefaction remediation using stone columns is discussed in Chapter 5 and the numerical modelling and its validation in Chapter 6.

The results of the parametric study performed using *OpenSees* is presented in the Chapter 7 and Chapter 8 describes the development of a statistical model for the prediction of excess pore water pressure in soils with partially penetrating stone columns. Finally, Chapter 9 consolidates the findings of the research and the scope for further work. The references and appendices are presented at the end. Appendix A presents the programs developed for acquiring data from the experimental setup, Appendix B presents *OpenSees* input file used for simulating the experimental model and Appendix C presents the input files used for the parametric study using *OpenSees*.

CHAPTER 2

LITERATURE REVIEW

2.1 Introduction

Though the phenomenon of liquefaction was identified way back in the 50's, it took some time for the researchers around the world to collect data and consolidate the knowledge. The knowledge still has gaps, since, the phenomenon is very intricate due to the complex behaviour of soil under dynamic loading. A wide diversity in the nature of the soil and its composition has compounded the challenges in arriving at a conclusive method for predicting liquefaction in soil. This survey extends to the current status of understanding about the phenomenon and studies related to it.

2.2 Understanding liquefaction

Earthquakes present serious problems for structures resting on saturated soil. The effect of an earthquake on structures depends on many factors including the intensity, frequency and location, nature of foundation soil and type of the structure. In loose soil, due to dynamic loading, the particles in sand matrix tries to rearrange to a closer configuration which results in the development of pore water pressure. It is understood that this build-up of pore pressure due to dynamic loading is responsible for the loss of strength.

Following the principle of effective stress states, the initial effective stress can be defined as the difference between total stress and pore water pressure. i.e.,

$$\sigma_0' = \sigma - u \tag{2.1}$$

where σ'_0 is the initial effective stress, σ, the total stress and u the pore water pressure. Undrained conditions in saturated cohesionless soil coupled with dynamic loading leads to build up of excess pore water pressure (Δu). The effective stress (σ') can then be calculated as:

$$\begin{aligned} \sigma' &= \sigma - (u + \Delta u) \\ \Rightarrow \sigma' &= (\sigma - u) - \Delta u \\ \Rightarrow \sigma' &= \sigma'_0 - \Delta u \end{aligned} \quad (2.2)$$

Now, When the excess pore water pressure value equals the initial effective stress, effective stress becomes zero. This condition is normally identified by calculating excess pore water pressure ratio (r_u), the ratio of excess pore water pressure to the initial effective stress. i.e.,

$$r_u = \frac{\Delta u}{\sigma'_0} \quad (2.3)$$

When $r_u = 1$, the effective stress becomes zero, and soil loses its complete strength and liquefies.

2.2.1 Factors affecting liquefaction

One of the challenges researchers faced was to identify the various factors that affect liquefaction and how exactly are these parameters related. The problem becomes complex with more number of parameters and non-linear relationships. The various factors that affect liquefaction are:

1. Soil type and grain size distribution
2. Relative density
3. Degree of saturation
4. Permeability

5. Thickness of sand layer

6. Earthquake loading characteristics

7. Vertical effective stress and over consolidation

8. Age and origin of soil

9. Seismic strain history

None of these parameters can be ignored while evaluating the liquefaction susceptibility of soil deposits.

The excess pore water pressure developed also depends on many factors, including, the nature of the deposit, intensity and duration of dynamic loading, drainage conditions, degree of saturation, grain size and relative density. Another major challenge in liquefaction studies has been to evaluate the susceptibility of soil deposits to liquefaction. The pioneering work by Seed and Idriss (1971) developed a simplified procedure for evaluating liquefaction and proposed the likelihood of liquefaction at a particular relative density for a given maximum ground surface acceleration. The significant factors that affect the behaviour were identified as (1) soil type, (2) relative density or void ratio, (3) initial confining pressure, (4) intensity of ground shaking, and (5) duration of ground shaking. This method was widely accepted due to its simplicity. In this method, the average cyclic shear stress τ_{av} due to maximum ground motion acceleration a_{max} is calculated as

$$\tau_{av} \approx 0.65 \times \frac{\gamma h}{g} \times a_{max} \times r_d$$

where γ is the unit weight of soil, h, the depth of the specimen, g, the acceleration due to gravity and r_d, the stress reduction factor, which depends on depth. The stress reduction factors also depend on the soil properties and are normally chosen from the chart. This equation provided a simple procedure for evaluating the stresses induced at different depths by any given earthquake for which maximum ground acceleration is known. Even with some shortcomings, this procedure is still widely used by researchers for evaluating the stresses induced due to shaking.

Another perspective in liquefaction research was to link the gradation or particle size distribution and the liquefaction susceptibility. Gradation was used as one of the main criteria for identifying the potential for liquefaction by many researchers throughout the history of liquefaction studies. The pioneering work in this direction was reported by Tsuchida (1970). In his research, the gradation of soil samples from sites from Japanese earthquakes were extensively studied in the laboratory and correlated with the observations in the field. Based on this, he proposed the zone of gradation for most liquefiable and potentially liquefiable soil. But Ishihara *et al.* (1980) has reported that the graph is unconservative for soil with low plasticity clay size particles, since, moderate to extensive liquefaction was reported in soil with more than 10% clay-size (5 microns) particles. The cyclic strength in such cases does depend on the Atterberg limits, and soil with fines having plasticity index 15 to 20 have much higher cyclic strength.
In the 1970's the Chinese building codes proposed a table of a set of parameters to identify the threshold to liquefaction shown in Table 2.1 (Jennings *et al.*, 1980). The Chinese criteria was widely used during the 80's, and it is generally considered as a conservative method for identifying liquefaction. At the same time, the Chinese criteria have been a subject for many studies (Donahue, 2007; Boulanger and Idriss, 2006; Phule and Choudhury, 2013).

According to Polito and Martin II (2001), there are also some contradicting results reported by researchers about the effect of non-plastic fines. Their detailed study using cyclic triaxial tests have brought out the concept of limiting silt content which can explain the behaviour of non-plastic fines in sand. It is interesting to note that the following two different behavioural patterns are predicted based on the limiting silt content.

1. If the silt content of the soil is below the limiting silt content, there is sufficient

Table 2.1: Chinese criteria for liquefaction

Condition	Threshold
Mean grain size (mm)	0.02 $<D_{50}<$1.0
Clay particle content (%)	10<
Uniformity coefficient	10<
Relative density (%)	75<
Void Ratio	>0.80
Plasticity index (%)	<10
Depth of water table (m)	<5
Depth of sand layer(m)	<20

room in the voids created by the sand skeleton to contain the silt. Here, the soil can be described as consisting of silt contained in a sand matrix. The cyclic resistance of such soil controlled by the relative density of the specimen. Increasing the relative density increases the soil's cyclic resistance.

2. If the silt content of the soil is greater than the limiting silt content, the specimen's structure consists predominately of sand grains suspended within a silt matrix with little sand grain to sand grain contact. The cyclic resistance of these soils is also controlled by the relative density of the specimen but is markedly lower than it is for soils below the limiting silt content. Here, the increase in cyclic resistance with an increase in relative density occurs at a slower rate.

The paper by Guo and Prakash (1999), brings out the lack of clarity on the criteria for evaluating the liquefaction and discusses the confusions regarding the influence of clay content, plasticity index, and pore pressure ratio by quoting field results as well as results from cyclic triaxial tests.
All these studies point to the fact that there is no single parameter or method which can be completely relied on for predicting the liquefaction behaviour of soil. In this context, experimental investigations can provide crucial information about the behaviour, which needs to be correlated to the site conditions.

2.2.2 Liquefaction experiments

Since the understanding of soil behaviour during shaking is still incomplete, different approaches like element tests, model tests, analytical/numerical model tests and field tests are required to understand the phenomenon completely. Laboratory tests for liquefaction studies can be broadly classified into three.

1. Cyclic triaxial tests
2. Shake table tests (medium and full scale) and
3. Centrifuge tests

Each method has its own advantages and limitations. The use of cyclic triaxial tests studying liquefaction has been reported as early as 1960's (Rocker Jr., 1968). Cyclic tests were the basis for most of the studies reported by Seed and his contemporaries (Seed and Idriss, 1971). Cyclic tests offer a very controlled method by which the behaviour of soil can be investigated under various confining pressures. With the advent of modern control systems and electronic sensor based measurements, cyclic triaxial equipment has become one of the most preferred methods in liquefaction research. The major advantage of the cyclic triaxial equipment is the control over the loading pattern and the dynamic measurement of pore water pressure. The test can be used to calculate the number of loading cycles required to initiate liquefaction in a sample. The cyclic strength curves obtained from the tests are normalised with the initial effective overburden pressure to produce a cyclic stress ratio (CSR). The cost of cyclic triaxial testing equipment is a constraint and so have not been commonly used in our country.

Shake table tests offer the advantage of modelling and visualising large sized models under dynamic loading. This can overcome the size limitation of the cyclic triaxial test to a certain extent. Shake table tests also helps to simulate field conditions to a great extent. One of the disadvantages of small shake table tests are that the scaling laws cannot be applied directly as it involves inertial forces. This can be overcome by using large-sized models, but large capacity shake tables are very expensive. A review of the shake table facilities across the world as well as in the country is detailed in Chapter 3. Managing boundary effects are also a crucial part in shake table simulations. Various techniques like laminar boxes, soft boundaries etc., have been successfully tried by researchers.

The experimental work by Dou and Byrne (1997), have investigated the effect of rigid boundaries on container boxes of small sizes during shake table tests. In their tests, a new technique of hydraulic similitude gradient was used to create a higher level of stress within the soil. The results have pointed out that the response of the soil layer constrained within rigid boundaries is essentially identical to free field response. The reason for such a behaviour is identified as the large difference in the input frequency (10Hz) and the fundamental frequency of the soil layer (150 to 180Hz).

Centrifuge tests offer a method for overcoming the modelling errors due to the scaling of models in shake table tests. But the equipment can be very expensive to make and run. The instrumentation involved is also quite complex. Several such studies have been reported by researchers in the recent past (Adalier and Elgamal, 2002; Brennan and Madabhushi, 2002; Coelho *et al.*, 2003; Sharp *et al.*, 2003). Such studies are not common in India, maybe because of the lack of laboratory infrastructure. An exception is the centrifuge facility at IIT Bombay (National Geotechnical Centrifuge Facility) which has been used by researchers to study liquefaction (Chandrasekaran, 2003).

Table 2.2: Liquefaction mitigation methods (Adopted from the report of National Research Council Committee on Earthquake Engineering Research (1985))

Method	Suitability	Principle
Blasting	Saturated and partially saturated sand	Compaction Densification
Vibratory probe	Saturated or dry sand	
Vibrocompaction	Cohesionless soil <20% fines	
Compaction Piles	Loose sandy soil, clay	
Heavy tamping	Cohesionless, any type	
Displacement or Compaction grout	Any type of soil	
Surcharge/buttress	Any type of soil	Overburden pressure Compression
Drains (Gravel, Sand, Wick, Wells)	Sand, Silt & Clay	Porewater pressure relief
Grouting (Particulate, Chemical, Pressure injected, Electrokinetic, Jet)	Medium to coarse gravel	Fill soil pores
Mix in place piles and walls	Sand, silt, clays	Stabilisation
Insitu Vitrification	All soil and rock	Thermal stabilisation
Vibroreplacement Stone and sand columns	Sand, Silts, Clays	Soil reinforcement
Root Piles, Sand nailing	All soils	

2.3 Liquefaction mitigation

Engineers have tried many methods for mitigating liquefaction. There are basically two approaches to mitigating liquefaction, namely, densification and drainage. The 1985 report of the Committee on Earthquake Engineering supported by National Research Council has identified the various techniques, its suitability and the approximate cost in mitigating liquefaction (National Research Council Committee on Earthquake Engineering Research, 1985). Table 2.2 summarises the findings in the report.

Stone columns (SC) have been traditionally used as a ground improvement technique in soft soil. SC offers the advantage of both densification and drainage and can be considered as an efficient method for mitigating liquefaction. The mechanism of action of stone columns is detailed in the following section.

2.3.1 Liquefaction mitigation using stone columns

The inclusion of Stone Column (SC) or granular pile is a common technique used to improve the foundation soil for structures resting on weak soil. Stone columns generally use gravel or crushed stone as backfill. The three most common methods of stone column installation are top feed, bottom feed and auger-casing with internal gravel feeding system. The first two methods are commonly called as vibro-replacement. Vibro-replacement can help in achieving densification of surrounding soil during the installation of the stone column. The auger casing system does nor provide densification and in this case, the stone column relies on drainage capabilities for mitigation of liquefaction. Liquefaction mitigation design approaches in the U.S. used to consider an increase in soil density only and the ability of the stone column to act as a drain and the stiffness are not usually accounted and these effects are taken as additional benefits. However, in Japan, stone columns that are installed without densification are designed to act as pore pressure dissipation sinks in the event of an earthquake (Martin and Martin, 1992).In addition to the enhancement of the bearing capacity, stone columns also work as drainage paths due to its high hydraulic conductivity. Stone columns can drain out pore water pressure as soon as it is generated during dynamic loading if designed properly.

As per the report by Mitchell and Wentz (1991) stone columns / granular piles/ gravel drains are the most commonly adopted ground improvement methods for liquefaction mitigation and its effectiveness have been verified in many field cases. This technique is preferred due to three basic reasons - technical feasibility, low energy utilisation and cost. Stone columns function in many ways including drainage, storage, dilation, densification and reinforcement.

Krishna and Madhav (2009) and Madhav and Krishna (2008) have conducted a detailed survey into the recent developments in Engineering of Ground for Liquefaction Mitigation Using Granular Columnar Inclusions and have indicated that Granular columnar inclusions (Granular piles) help in mitigating earthquake induced liquefaction effects through one or more of the following functions or effects:

- Granular piles function as drains and permit rapid dissipation of earthquake induced pore pressures by virtue of their high permeability with the additional advantage that they tend to dilate as they get sheared during an earthquake event.
- Pore water pressures generated by cyclic loading get dissipated almost as fast as they are generated due to significant reduction in the drainage path.
- Granular piles densify and reinforce the in-situ soil there by improving the deformation properties of the ambient soil.
- Granular piles, installed in to a very dense state, are not prone to liquefaction and replace a significant quantity of in-situ liquefiable soil.
- Granular piles modify the nature of earthquake experienced by the in situ soil.

The idea of using stone columns for liquefaction mitigation is not new. Seed and Booker (1977) developed the equations pertinent to the development and dissipation of pore water pressure in the presence of gravel drains (Seed and Booker, 1976). Here, the drainage mechanism of SC is developed based on Darcy's law by applying it to the flow of pore water and the permeability of soil in both vertical and horizontal directions.

$$\frac{\partial u}{\partial t} - \frac{\partial u_g}{\partial N}\frac{\partial N}{\partial t} = \frac{k_H}{\gamma_w m_v}\left(\frac{\partial^2}{\partial^2 r} + \frac{1}{r}\frac{\partial u}{\partial r}\right) + \frac{k_V}{\gamma_w m_v}\frac{\partial^2 u}{\partial r^2} \tag{2.4}$$

where u is the hydrostatic pore water pressure, and k_H and k_V, coefficients of permeability in horizontal and vertical directions respectively. γ_w is the unit weight of water and m_v is the volumetric compressibility of the soil. During shaking, the pore water pressure in an element of soil will undergo a change ∂u, while the element will also be subjected to ∂N cycles of alternating shear stress. Due to this, there will be an additional increase in pore pressure $\frac{\partial u_g}{\partial N}$, where u_g is the pore pressure generated due to shaking. These equations can be modified for conditions of pure radial drainage, if required. The values of $\frac{\partial u_g}{\partial N}$ are calculated from undrained tests. If the number of cycles N_l required to cause liquefaction is known, u_g corresponding to N cycles can be calculated using the relationship

$$\frac{u_g}{\sigma'_0} = \frac{2}{\pi} arcsin\left(\frac{N}{N_l}\right)^{\frac{1}{2\alpha}} \tag{2.5}$$

Where σ'_0 is the initial effective stress for triaxial test conditions, and α is an empirical constant. Researchers who have investigated further have tried to include the variations of permeability around the stone column (Krishna *et al.*, 2006; Ben Salem *et al.*, 2015). Even though three different decay patterns of permeability (constant, linear and parabolic) are studied, the exact mechanism of variation in permeability is not identified. It is predicted that slower rate of dissipation happens when the column spacing increases.

Experimental programs using shake table tests have supported the theoretical understanding of the behaviour of soil with stone columns. Shake table tests conducted by Sasaki and Taniguchi (1982) on gravel drain systems revealed that the pore water pressure is less near the gravel drains and that its presence accelerates the dissipation of the excess pore water pressure. The presence of drain is found to help in faster dissipation due to high permeability of the drain. This flow creates a radial hydraulic gradient in the horizontal plane. The drainage aspect of gravel drains has been investigated and clarified using centrifuge testing by Brennan and Madabhushi (2002). The study gave several insights into the flow of pore water during shaking. The drainage path has been investigated in detail, and the flow front is used to indicate the direction of flow of excess pore water. The flow happens through the top surface, and a vertical hydraulic gradient exists between the top surface and bottom, resulting in the upward flow of the fluid. The vertical drains are found to influence the flow fronts and impact the drainage of excess pore water pressure.

2.4 Numerical modelling of liquefaction problems

The analysis methods for liquefaction problems can be classified broadly into two:

1. Total stress method
2. Effective stress method

In total stress method, originally proposed by Seed *et al.* (1976), the soil behaviour is represented by a nonlinear backbone curve fit to match G_r/G_{rmax} curves. Here, the analysis should be repeated several times to obtain a better evaluation of the induced stresses. The major deficiency in the total stress method is that it is unable to take into account the progressive stiffness degradation caused by the pore pressure build-up in the soil. These models have been modified by researchers by coupling with extended Masing criteria that define unloading and reloading behaviour and establish the level of hysteretic damping (Uma Maheswari *et al.*, 2010). The Modified Kondner and Zelasko (MKZ) constitutive model (Matasović and Vucetic, 1993) is one of the methods used for cyclic characterisation of liquefiable sands.

In the effective stress analysis, in addition to the soil nonlinearity, the effect of excess pore pressure generation is also considered. Here, the modulus degradation and the stress degradation models is used in the normalised form. Only the effective stress method can model adequately the gradual loss of soil strength due to build-up of pore water pressures (Liyanathirana and Poulos, 2002). The liquefaction models used in effective stress analysis can be divided into four main categories:

1. Models based on plasticity theory - multi-yield plasticity, plasticity with nested surfaces, generalised plasticity, and bounding surface plasticity
2. Stress path methods
3. Correlations between pore pressure response and volume change tendency of dry soils
4. Direct use of experimentally observed undrained pore pressure response

Laboratory tests must be performed to obtain the parameters for all the above models except when pore pressure response is formulated directly from observed data.

2.4.1 Numerical modelling software for liquefaction analysis

The research in liquefaction studies on soil took new dimensions with the advancement of computing hardware and software available for studies. The main challenge in modelling liquefaction is to incorporate the development of pore water pressure during the dynamic load and modelling the associated reduction in the shear strength. This is normally achieved by coupling the motion and flow equations. The solution can be obtained either using the Finite Difference Method (FDM) or Finite Element Method (FEM). FLAC, a commercial software uses FDM while most of the commonly available software uses FEM for solving such problems. Other software which have similar capabilities are QUAKE/W (Krahn, 2004), Abacus (Abaqus, 2010) and Plaxis (with special license) (Petalas and Galavi, 2013) which employ FEM. Apparently, most of these software are expensive even with academic license.

A significant contribution in this direction is the Open System for Earthquake Engineering Simulation (*OpenSees*) a free and open source software framework developed by the University of Berkely and is an excellent alternative to commercial software. *OpenSees* has advanced capabilities for modelling and analysing the nonlinear response of systems and also for performing parallel finite element method. It has a wide range of material models, elements, and solution algorithms for simulating the response of structural and geotechnical systems subjected to earthquakes. The software employs Tool Command Language (TCL) for creating input files using the extended commands developed in the software framework. The only drawback is the lack of pre and post processors. Though there have been attempts to develop very specific pre and post processors like *OpenSeesPL* (Elgamal *et al.*, 2009), researches commonly employ freely available tools for this. Numerical studies using *Opensees* have been successfully conducted by researchers to study the liquefaction-related phenomenon (Elgamal *et al.*, 2009; Tang *et al.*, 2015). The Finite-element modelling studies typically focus on evaluating the extent of remediation measures and deformation characteristics. Another advantage of *OpenSees* is the capability for parallel computation (McKenna and Fenves, 2007). With the advent of multi-core processors, parallel computing is the means of harnessing the full performance of the computer. The computation is distributed among the different cores of the processors for fast computation. There are two situations in which parallel computation might be required. (1) when the model is really large, and it may not fit into the memory of the computer and (2) when multiple analysis is intended, like, in the case of a parametric study. There are two different interpreters in *OpenSees* for this, *OpenSeesSP*, for large models and

OpenSeesMP for parametric studies.

2.4.2 Modelling liquefaction using u-p formulation

The methodology for coupling displacements and pore pressure for geomechanics problems employing Biot's theory was developed by Zienkiewicz and Shiomi (1984). This u-p formulation captures the movements of the soil skeleton and the change of the pore pressure and is the most simplistic method available for modelling liquefaction problems (Jeremić *et al.*, 2008). The software *OpenSees* employs this formulation (Elgamal *et al.*, 2002; Yang *et al.*, 2003) and has been proved to be very effective in modelling liquefaction problems.

2.4.3 UCSD soil constitutive model

The UCSD soil model which is used in *OpenSees* employs the multi-surface plasticity based constitutive model in which the salient cyclic-mobility response characteristics are reproduced by specifying an appropriate flow rule. The yield function forms a conical surface in stress space with its apex along the hydrostatic axis as shown in Fig.2.1.

To generate hysteretic response under cyclic loading, a purely kinematic hardening rule is employed in this model. In kinematic hardening rule, the yield surfaces translate in stress space within the failure envelope.

Fig.2.2 shows the adopted flow rule for the different phases of soil response. Phase 0-1 is the contractive phase within the Phase Transformation (PT) surface (boundary between the contraction and dilation). Phase 1-2 is the liquefaction induced perfectly plastic phase during shear loading before the initiation of dilation. Phase 2-3 is the dilative phase during shear loading with stress state outside the PT

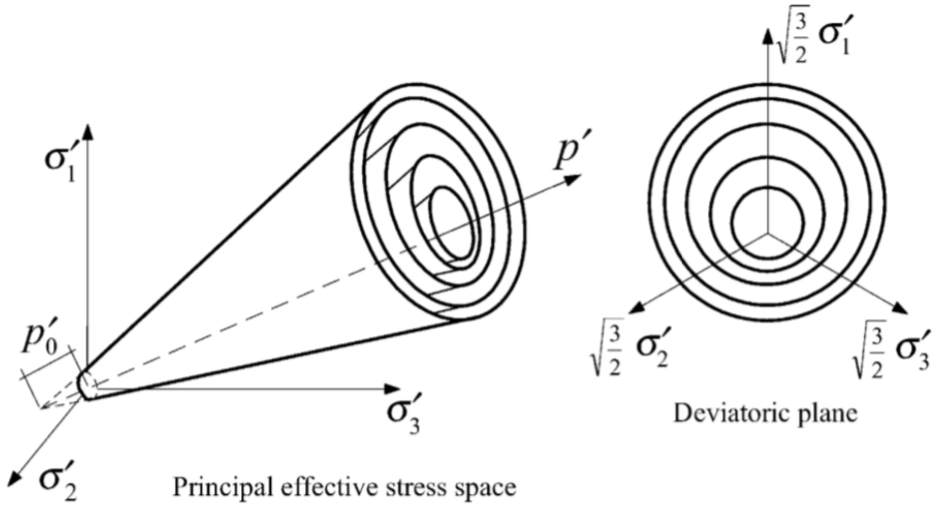

Figure 2.1: Yield surface (Elgamal *et al.*, 2002)

surface. The contractive phase during shear unloading is phase 3-4.

Researchers have used three dimensional as well as two-dimensional models for modelling liquefaction problems. Though 3D models are considered more accurate, including non-linearity makes it computationally very demanding. Procedures have been derived for converting axisymmetric problems to two-dimensional plane strain problems by researchers (Hird *et al.*, 1992; Indraratna and Redana, 2000). This is achieved by changing either the drain spacing or the horizontal permeability of the soil. Tan *et al.* (2008) has successfully used this technique for analysing stone column reinforced ground subjected to dynamic loading. In the permeability matching method, the equivalent plane strain permeability k_p can be computed using the simplified formula

$$\frac{k_p}{k} = \frac{0.67}{ln(n) - 0.75} \tag{2.6}$$

where k is permeability in the axisymmetric case and $n = R/r$, where R is the radius of the influence zone of the drain and r is the radius of the drain.

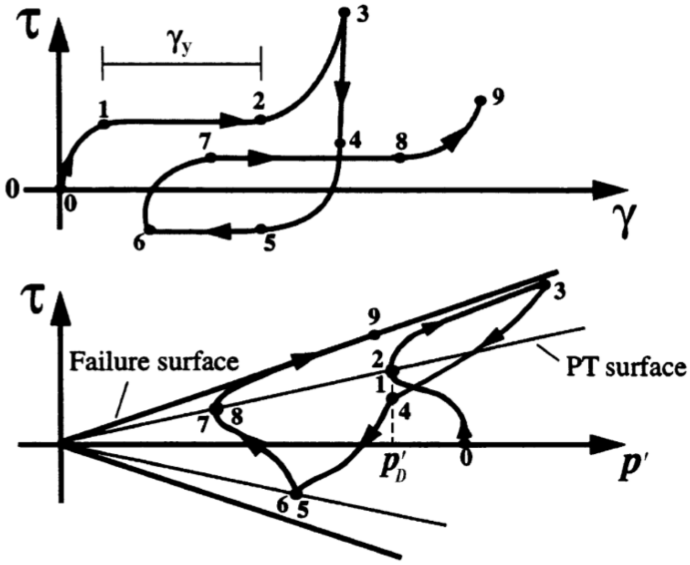

Figure 2.2: Constitutive Model (Elgamal *et al.*, 2002)

2.5 Liquefaction studies in the Indian context

Liquefaction studies in India are not common because of two underlying reasons. (1) lack of sophisticated infrastructure for conducting such studies and (2) many consider most of the regions in the country to be less vulnerable to earthquakes. However, studies have shown that the Indian plate is one of the fastest moving plates of the world (Kumar *et al.*, 2007). The recent earthquakes Nepal/India (2015), Sikkim (2011), Andaman (2009), Kashmir (2005), Gujarath (2001) have indicated the need for earthquake-related studies in the country.

The early studies by Gupta (1977) on Solani sand is probably the first attempts in the country to study liquefaction. A uniaxial shake table was developed, and extensive experiments were conducted to study the phenomenon. It was the 2001 Bhuj earthquake that gave Indian researchers an opportunity to conduct field study the phenomenon in detail. The failures reported during the earthquake have been documented, and many studies have been reported based on it (Singh *et al.*, 2005; Rajendran *et al.*, 2001; Dash *et al.*, 2009; Karanth *et al.*, 2001). Over a period of time, shake tables were available in universities and researchers have attempted not too many studies. It can be noted that most of the liquefaction studies in India have been conducted using medium sized shake tables (Varghese and Latha, 2014). There has also been attempts to develop low-cost manual shake tables without the use of actuators or motors (Prasad *et al.*, 2004).

Liquefaction hazard mapping using borehole data as well as probabilistic methods are also reported for various cities like Bangalore (Sitharam *et al.*, 2007), North-east (Nath *et al.*, 2008), Delhi (Rao and Satyam, 2007), Mumbai (Choudhury *et al.*, 2015), Gujrath (Vipin *et al.*, 2013). These studies make use of SPT data and soil profile to evaluate the liquefaction potential.

2.5.1 Liquefaction studies in *Kerala*

The Indian Standard Code IS 1893 (Part 1)-2002 has classified the state of *Kerala*, located at the south-western part of the peninsula, under zone III (Moderate Damage Risk Zone) with a maximum expected ground acceleration of $0.16g$. The state has not witnessed any major earthquakes in its history except a couple that occurred in the bordering regions of Idukki and Kottayam districts on 12 December 2000 with a magnitude 5.0 and an earthquake of magnitude 4.8 that occurred in the same region on 7 January 2001 (Bhattacharya and Dattatrayam, 2002). But, *Kerala* has a long coastline and many natural riverine sand deposits, and thus the infrastructure built on such deposits are vulnerable to liquefaction damages in the event of an earthquake. The liquefaction studies related to *Kerala* are very limited and rarely attempted.

2.6 Summary

The detailed review helps to gather the different aspects of liquefaction studies, including its understanding, different experimental and numerical techniques and mitigation methods.

1. It is clear that there are gaps in the complete understanding of the effect of different parameters that affect liquefaction. The criteria for liquefaction is still being reviewed by researchers.

2. The survey helps to understand the various experimental and numerical methods employed by researchers for studying the phenomenon. No single approach is complete, and the methods are constantly evolving.

3. The free software *OpenSees* has opened up huge possibilities for researchers to simulate and study liquefaction and related phenomenon using FEM.

4. The studies reported in literature about mitigation methods using stone columns deal with fully penetrating stone column and the effect of partially penetrating columns has not been explored.

5. Liquefaction studies in India is lagging behind, maybe because of the need for highly sophisticated and expensive equipment and the presumption that the country is not so earthquake prone.

6. Even though the state of *Kerala* has many saturated sand deposits, no previous shake table studies are reported in the literature so far.

CHAPTER 3

DEVELOPMENT OF EXPERIMENTAL SET-UP

3.1 Introduction

Experimental studies on liquefaction using shaking table tests are widely conducted in the countries like Japan and the United States, where a number of earthquakes occur every year. Earthquake geotechnical engineering in India had received a tremendous boost after the Gujarat earthquake of 2001. The present chapter describes the development of a simple uniaxial shake table and the data acquisition system using components which are commonly available in the market.

3.2 Shake table

Shake table is an equipment which can be used for studying the dynamic response of the ground as well as structures resting on them during earthquakes. A typical shake table will have a base plate on which the structure or model can be placed and a mechanism for creating a desired shaking. Shake tables are classified based on the degree of freedom. While a simple shake table has one degree of freedom (commonly called as uniaxial shake table or horizontal shake table), the most modern ones have up to six degrees of freedom. They are also characterised by the payload, the total weight of the model that can be tested and also the maximum acceleration and frequency that can generated. In advanced systems, linear actuators are used to achieve the desired shaking. Real earthquake input motions can be created with advanced control systems in such types of equipment. The cost of these equipments depend on the payload, degree of freedom and the sophistication

Table 3.1: Shake table across the world

Location	Key Specifications
University of California at San Diego, USA (Luco *et al.*, 2009)	12.2m x 7.6m, 2000 tonnes, 1 DOF
NIED 'E-Defence' Laboratory, Miki City, Japan (Ohtani *et al.*, 2003)	20m x 15m, 1200 tonnes, 6 DOF
Public Works Research Institute (PWRI), Japan (Matsuo *et al.*, 1998)	8m x 8m, 300 tonnes, 6 DOF
European Centre for Training & Research in Earthquake Engineering, Italy (Peloso *et al.*, 2012)	5.6m x 7m, 140 tonnes, 1 DOF
CGS Laboratory, Alger, Africa (Airouche *et al.*, 2014)	6.1m x 6.1m, 140 tonnes, 6 DOF
CEA, France (Fabbrocino and Cosenza, 2003)	6.0m x 6.0m, 100 tonnes, 3 DOF
Sanryo Heavy Industries Corp, Japan (Sollogoub, 2007)	6.0m x 6.0m, 91 tonnes, 3 DOF
University of California at Berkeley, USA (University of Berkeley, 2018)	6.1m x 6.1m, 85 tonnes, 6 DOF
Nuclear Power Institute, China (Sollogoub, 2007)	6.0m x 6.0m, 60 tonnes, 6 DOF
University of Nevada, Reno, USA, (2 tables) (Thoen and Laplace, 2004)	4.3m x 4.5m, 50 tonnes, 2 DOF

of the control system used. A few of the state-of-the-art facilities available across the world are show in Table 3.1. The list is not exhaustive, but mentions the shake table facilities with payload more than 50 tonnes and has highly sophisticated instrumentation systems. Some of the best facilities are available in USA and Japan. The test facilities in India have also improved over the years with many universities developing very good infrastructure. Some of the best earthquake testing facilities in India is listed in Table 3.2.

The choice of the shake table depends on the problem that is attempted. In an ideal case, earthquake testing has to be conducted on real size structures, but this is rarely practicable. This has lead researchers to develop scaled models which can perform similar to real size structures. Centrifuge testing is one way to overcome the use of

Table 3.2: Shake tables in India

Location	Key Specifications
Central Power Research Institute (CPRI), Bangalore (Sharma *et al.*, 2012)	3 m 3 m, 10 tonnes, 6DOF
SERC, Chennai (Prakashvel *et al.*, 2012)	4m x 4m, 30 tonnes, 3 DOF
IIT Roorkee (Jain and Nigam, 2000)	3.5m x 3.5m, 20 tonnes, 2 DOF
Indira Gandhi Centre for Atomic Research (IGCAR), Chennai (Kumar *et al.*, 2014)	3m x 3m, 10 tonnes, 6 DOF
IIT Guwahati (Das *et al.*, 2016)	2.5m x 2.5m, 5 tonnes, 1 DOF
IIT Kanpur (IIT, 2018)	1.2m x 1.8m, 4 tonnes, 1 DOF
IISc, Bangalore (Ammanagi *et al.*, 2006)	1m x 1m, 0.5 tonnes, 6 DOF
IISc, Bangalore (Varghese and Latha, 2014)	1.2m x 1.2m, 1 tonnes, 1 DOF
IIT, Chennai (Boominathan *et al.*, 2004)	3m x 3m, 1 tonnes, 1 DOF

large-sized models where scaling laws can be properly applied to get good results from experiments. However, creating and maintaining a centrifuge testing facility can be very expensive. Hence, the choices are to go for 1-g scaled models, which inherently have some limitations.

The similitude laws regarding stress and strain cannot be satisfied completely in small shake table tests since higher gravitational stresses cannot be produced. Even then, such research has provided valuable insight into liquefaction. One advantage of shake table test is simple instrumentation and easy visualisation of the behaviour of the system. The size of the table is decided based on the size of the container box. Table 3.3 summarises the size of the soil container, the range of acceleration and frequencies of uniaxial, medium scale shake table used by previous researchers. From these available studies, it should be noted that uniaxial shake table tests are sufficient to understand the response and failure mechanism of earth structures like embankment, retaining wall etc.(Prasad *et al.*, 2004). Hence, it is decided to design and fabricate a medium size shake table for the present study.

Table 3.3: Medium sized shake tables used for liquefaction studies

Researchers	Size & Type of soil container	Range of acceleration & frequencies used for study
Prasad *et al.* (2004)	1.65×0.5m×0.6m, Perspex, Rigid wall	0.5g, 2Hz
Maheshwari *et al.* (2012)	1.05 m×0.60m×0.60m, Steel	0.1-0.5 g, 5Hz
Varghese and Latha (2013)	1.2m×0.5m×0.8m, Perspex	0.1-0.15g, 1Hz
Orense *et al.* (2003)	0.9m×0.6m×0.8m, Steel	0.18g, 3hz
Joshi *et al.* (2000)	1.5 m×0.75m×0.9m	0.21-0.54g
Park *et al.* (2000)	1.94m×0.44m×0.6m	0.1-0.4g
Giri and Sengupta (2010)	1.0m×0.90m×0.48m	0.1g
Ramakrishnan *et al.* (1998)	2.05m×0.95m×0.81m	0.25-0.45g
Wang *et al.* (2013)	0.80m×0.30m×0.70m	0.1-0.5g, 3Hz

3.3 Shake table design and development

It is intended to fabricate a shake table system which can produce a sinusoidal input motion of 1Hz and a maximum acceleration of 0.5g. A provision to vary the acceleration was also considered during the design. For such a system, the most economical design will be to use a crank mechanism, driven by an electric motor. The basic system will have four components

1. Electric motor
2. Transmission system with pulleys, belts and crank mechanism
3. Base frame with rollers
4. Container box

Table 3.4: Calculation of power required for motor for shake table

Volume of the box	0.45 m^3
Total mass of soil (assuming ρ_{sat} as 2100 kg/m^3)	2100 $\times$ 0.45=945 kg
Mass of the container box and base frame (approx.)	55 kg
Total mass of the model and base frame (m)	1000 kg
Maximum design acceleration (a)	0.5g = 4.9 m/s^2
Inertial force ($F = m.a$)	4905 N
Maximum eccentricity of crank (e)	0.05 m
Angle of crank (θ)	30^o
Torque required ($T = F.e.cos\theta$)	283.2 Nm
Frequency of vibration,f	1 Hz
Angular velocity ($\omega = 2.\pi.f$)	2π
Power required, $P = T.\omega$ =1779 W	2.4 HP
Motor selected (allowing for losses)	5HP 3-Phase

3.3.1 Selection of motor

To choose the motor, the first step was to calculate the maximum pay load for the shake table. For this, the dimensions of the container box for soil had to be fixed. After reviewing the size of the container boxes used by researchers for similar studies (Table 3.3), the container box size was decided as 1.5 m $\times$ 0.5 m $\times$ 0.6 m. Table 3.4 gives the calculations in respect of the selection of motor for the shake table.

3.3.2 Transmission system

The transmission system has two purposes. One, to reduce the speed of the motor and two, to convert the rotational motion to linear motion. The designed system has a pulley-belt mechanism which can reduce the speed of the electric motor to 1Hz and a crank mechanism to create linear motion. Table3.5 shows the calculation of the pulley ratio required.

Table 3.5: Calculation of pulley ratio

Speed rating of AC motor	1500 rpm
Desired frequency of shaking	1Hz, 60 rpm
Pulley ratio required (=1500/60)	25

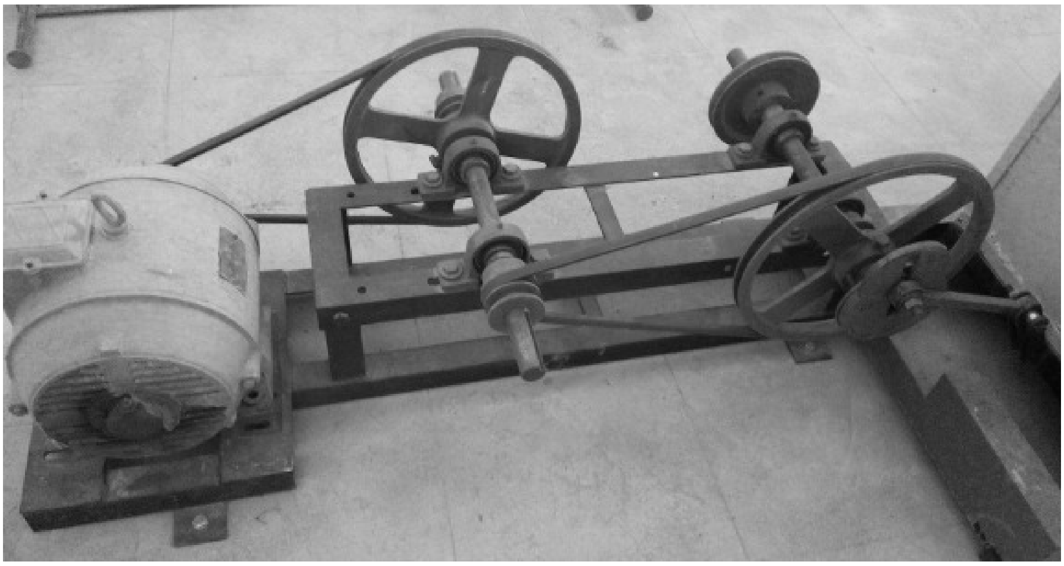

Figure 3.1: Motor and transmission system of shake table

Based on the availability of pulleys, it was decided to achieve this ratio in two steps. Fig.3.1 shows photograph of the fabricated system. In the crank mechanism, a slot is provided which enables the connecting rod to be positioned at different eccentricity (Fig.3.2). This helps to achieve different accelerations for shaking.

3.3.3 Base frame

The base frame consists of two steel cylindrical rods supported on four heavy duty ball bearings as shown in Fig.3.3. This base frame is bolted to the foundation for minimising unwanted vibrations. The shaking platform is placed on the steel rods. This design allows free movement of the system without any vibrations.

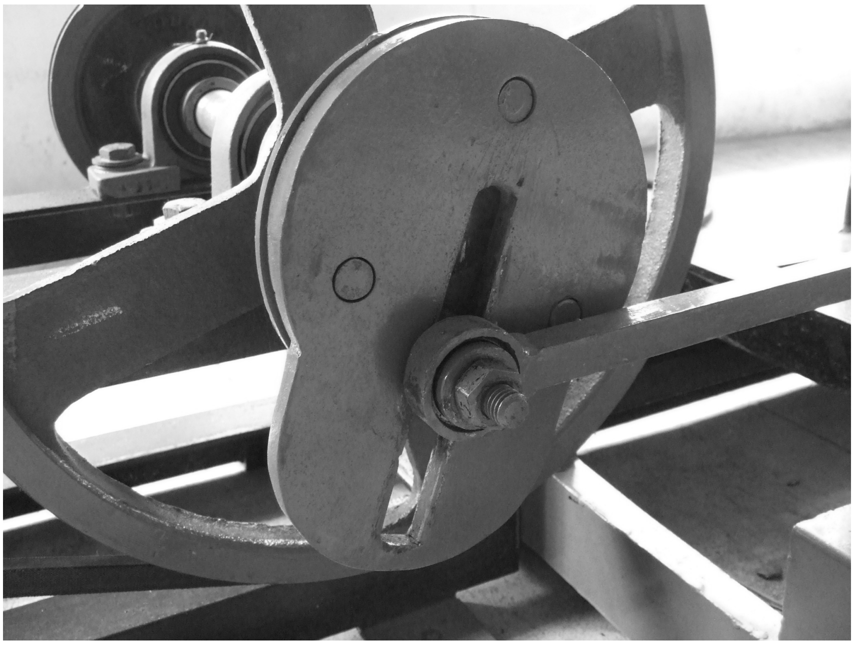

Figure 3.2: Crank design

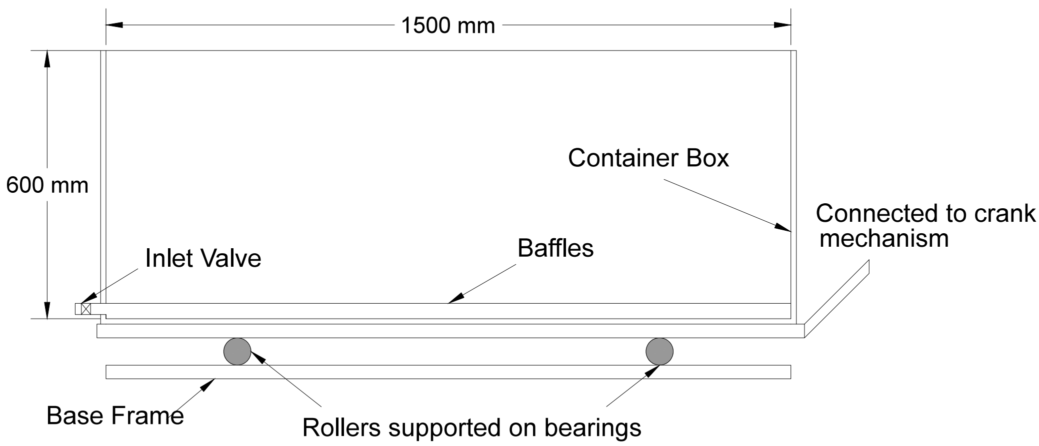

Figure 3.3: Shaking platform and soil container box

3.3.4 Container box for soil

A box with rigid boundaries is the simplest design of the container box. However, in the field of earthquake geotechnical engineering, the boundary conditions of the soil model is a major concern in all shake table tests, even for centrifuge testing. In the ideal case, to simulate free field conditions, the box should have large dimensions. One technique to overcome such situation is to use laminar boxes, which can simulate free field conditions to a certain extent if designed properly. Even though laminar boxes give good results, they are complex and expensive. Additional flexible membranes are required to support soil inside laminar boxes. Researchers have tried to solve this issue by using soft material for boundaries and also constraining the model to the center of the rigid box. It is reported that *"even without soft material at the side walls, the rigid tank may simulate the free-field conditions"* (Maheshwari *et al.*, 2012).

The attempts by Prasad *et al.* (2004) points that the rigid boundary effect is present upto 0.2 times the length of the container from the boundary for a rigid box of size 1800 mm. The acceleration recordings during their experimental investigations have supported this theory. Thus, it can be reasonably argued that rigid boundary effects may not affect the measurements of pore pressure and deformations in the center of the model.

Taking into considerations the above observations, a container box with rigid boundaries was selected for the present experimental study. The outer frame of the container box was fabricated using angle sections and flats. One of the longer sides of the box is made using transparent perspex sheet of 10 mm thickness so that the behaviour of the soil can be observed during shaking. The other sides as well as bottom are made of 3 mm galvanised steel sheet. Fig. 3.4 shows the fabricated container box.

For conducting liquefaction experiments, ensuring full saturation of the sample is

Figure 3.4: Container box

very essential. There are basically two different methods by which the sample can be prepared, (1) prepare the sample and then saturate and (2) prepare the sample in a saturated state using water pluviation.

Saturating the sample after preparation offers a few advantages like, better control over dry density of packing in different layers, easiness in handling materials and closeness to free field conditions in nature. The most suitable way of saturation is to introduce water from the bottom of the sample and allow it to get saturated on its own. The only concern is the uplift created during the introduction water, which can be easily managed by reducing the speed of saturation. Hence this method is adopted here.

The bottom of the container box was designed in such a way that water can be introduced uniformly underneath the sample. A series of channels were formed as shown in Fig. 3.5 to ensure this. The top of the channels was covered with a mesh and fabric cloth to prevent soil from entering the channels. This layer acts as the permeable boundary between the sample and the saturating water. The valve used to introduce water is also used to drain water after the experiment.

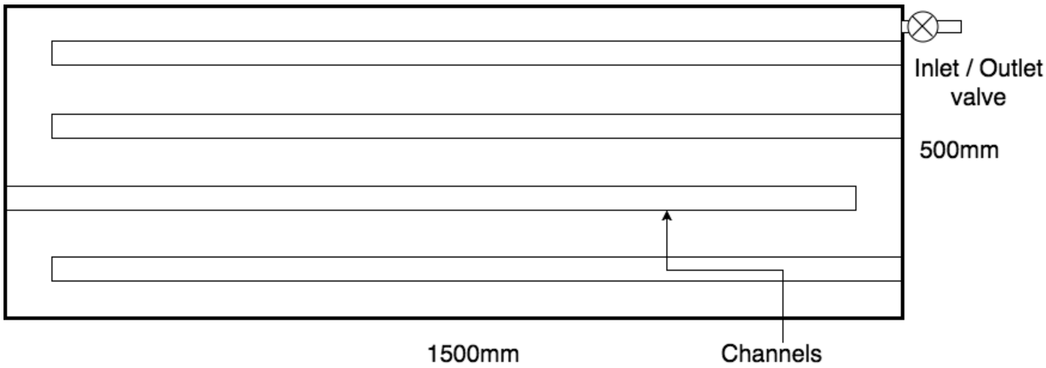

Figure 3.5: Bottom view of the container box

3.4 Data acquisition system

The basic parameters to be measured during the shake table experiment are acceleration and excess pore water pressure. These parameters are to be measured dynamically and stored during the experiment. Some of the off-shelf systems available are very expensive and hence a low cost data acquisition system with all the required components are designed and developed. Cost, availability of sensors, sampling rate and accuracy were the major considerations during the design. Any data acquisition system will have the following components – (1) sensors, for measuring the required parameters, (2) hardware module for acquiring data from sensors and (3) software for recording and manipulating data from the hardware (Fig.3.6).

3.4.1 Sensors

Two types of sensors are required for the system. Acceleration sensors and pore water pressure sensors. The most commonly available and cost effective sensors are Micro-Electro-Mechanical Systems, or MEMS. These sensors are essentially miniaturised mechanical and electromechanical elements which measure the parameters and give electrical signals as output. These devices when coupled with integrated circuits can give good performance and are very economical for

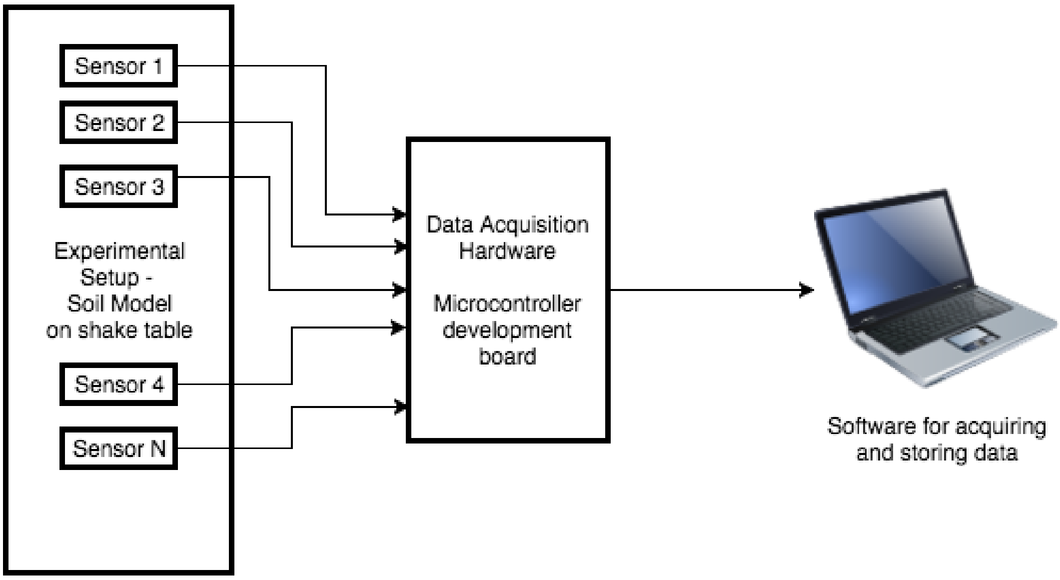

Figure 3.6: Data Acquisition System

developing measurement systems (Bhattacharya *et al.*, 2012). The advantages of using MEMS based sensors are

1. Low cost
2. Miniature size
3. Accuracy
4. Availability as integrated circuit boards

An additional criteria for selection of sensors is the sampling rate. Since the frequency of vibration of the designed shake table was 1Hz, a minimum of ten times the frequency, that is 10Hz, should be the minimum sampling rate of the sensors. Most of the MEMS based sensors are capable of much higher sampling rates.

3.4.1.1 Acceleration Sensors

As the name implies, acceleration sensors are devices which can measure acceleration of moving objects. Depending on the number of axes on which the measurements are made, these sensors are classified as 1-axis, 2-axis and 3-axis

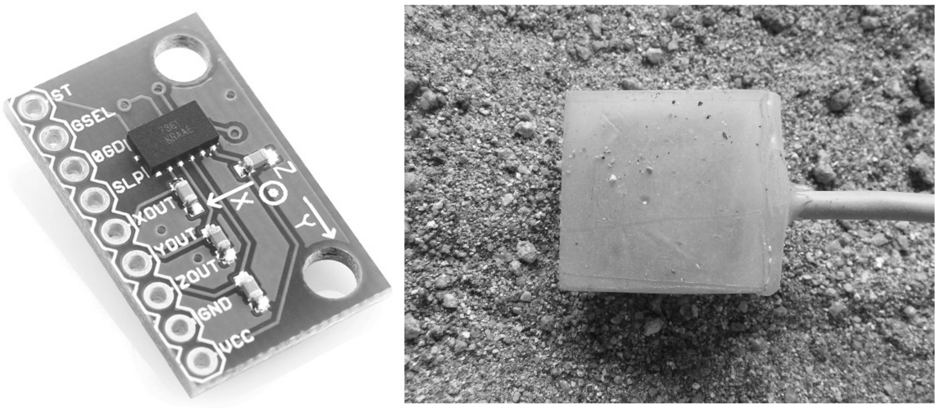

Figure 3.7: MMA7361 acceleration sensor breakout board & sensor embedded in glue

sensors. The measurement range of the acceleration sensors should be above the expected acceleration, $0.5g$. MMA7361, a three axis analog sensor was selected for the measurement(Fig.3.7). Though sensor is capable of measuring acceleration in two ranges $\pm 1.5g$ & $\pm 6.0g$, the former was selected in the present design. The sensor was covered with glue to prevent damage from getting in contact with water. The output voltage was measured and converted suitably to calculate the acceleration values.

3.4.1.2 Pore water pressure sensors

A simple piezometer can be used to measure pore water pressure. But the disadvantage is that the measurements will have to be manually taken and this method has its own limitations. Standard pore water pressure sensors are piezoresistive devices that convert pore water pressure to an output signal proportional to the measured value through a diaphragm. The sensor end will be covered with a filter to prevent soil from entering it. A small reservoir of fluid between the diaphragm and filter transfers the fluid pressure. There are also sensors based on vibrating wire technology. Here, a vibrating wire converts the fluid pressure into equivalent frequency signals that can be measured. In both these types, the electronic components also are kept inside the soil. This necessitates the

Figure 3.8: MPXV7007 Differential pressure sensor

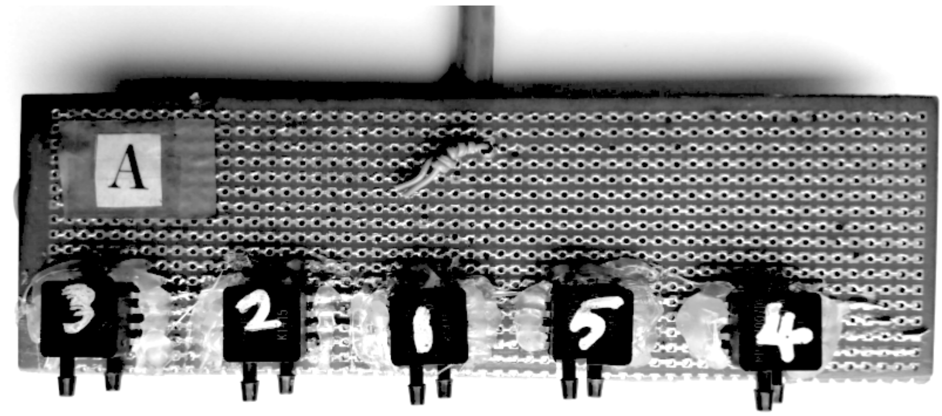

Figure 3.9: Pressure sensor unit - differential pressure sensors soldered on common board

sensor unit to be made water tight.

Since making a water tight sensor unit is challenging, an innovative technique had to be devised. The motivation was the pressure measurement systems used in process control. MPXV7007, an integrated silicon differential pressure sensor is used to measure pressure from pitot tubes in process control systems(Fig.3.8). Fig. 3.9 shows five differential pressure sensors soldered on single common board.

The advantage of this system is that the sensor does not get into contact with the fluid directly. A 2.5 mm diameter tube is used to connect probe to the sensor. The variation of the pressure in the air column between the fluid and the sensor is used for the measurement. This sensor is temperature compensated and calibrated to measure values between -7 to 7 kPa. To measure the pore water pressure inside soil, a probe with wide end made of high quality plastic is used. (Fig.3.10). The end of

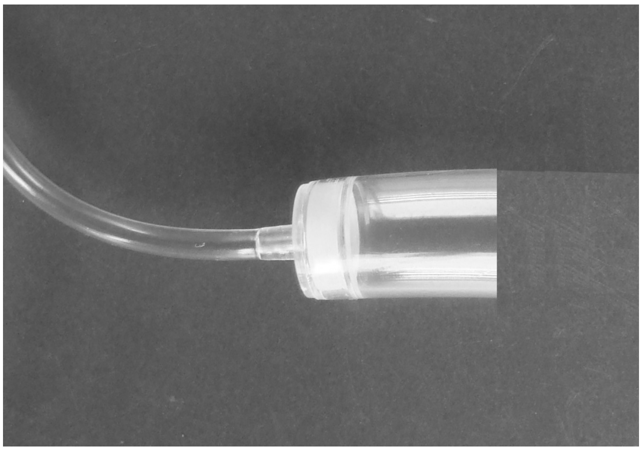

Figure 3.10: Probe for measuring pore water pressure

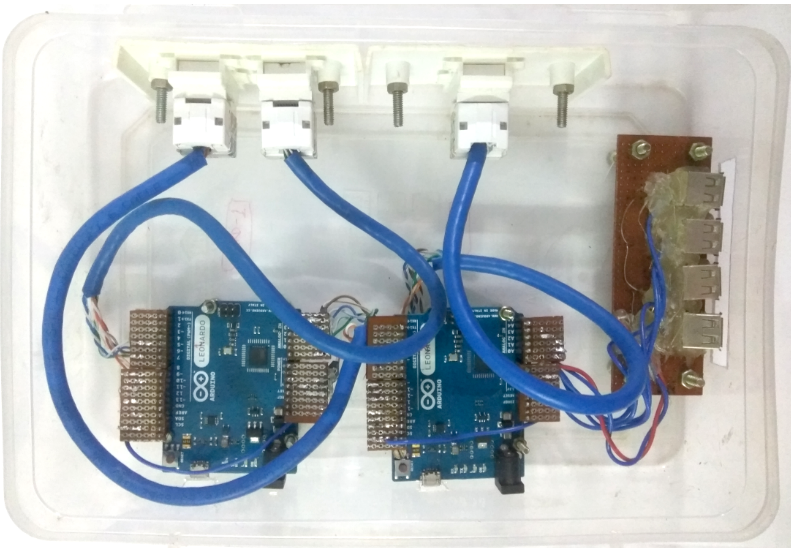

Figure 3.11: Data acquisition hardware

the probe is covered with fabric filter.

3.4.2 Hardware

A microcontroller is required for acquiring data from the sensors. A commonly available microcontroller development board manufactured by Arduino named Leonardo is used. The developed system with boards is shown in Fig.3.11.

The microcontroller used in this development board is a 8-bit ATmega32u4 controller with a clock speed of 16 MHz. The board has 20 digital input/output pins.

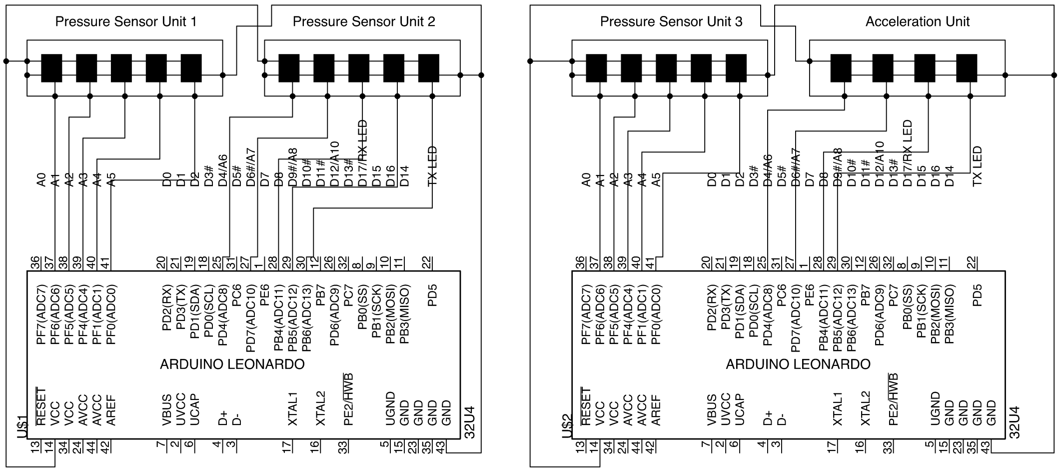

Figure 3.12: Circuit diagram of developed data acquisition system

The board features a built-in USB communication that helps it to be connected to the USB (Universal Serial Bus) port of a computer. Arduino also provides a software for writing and uploading program into the microcontroller.

The output of the sensors are connected to the input pins of the microcontroller board and the program in the microcontroller reads the sensor voltages and writes the data on communication port (USB). The circuit diagram is shown in Fig. 3.12. The program used to capture the sensor readings are given in Appendix A.

3.4.3 Software

To capture the data from the microcontroller board, a program is written using Python. One of the basic features of the program is a graphical user interface. The sensors can be initialised and data can be recorded using the interactive buttons provided in the user interface. A screenshot of the user interface is given in Fig. 3.13 and the source code of the program is included in Appendix A.

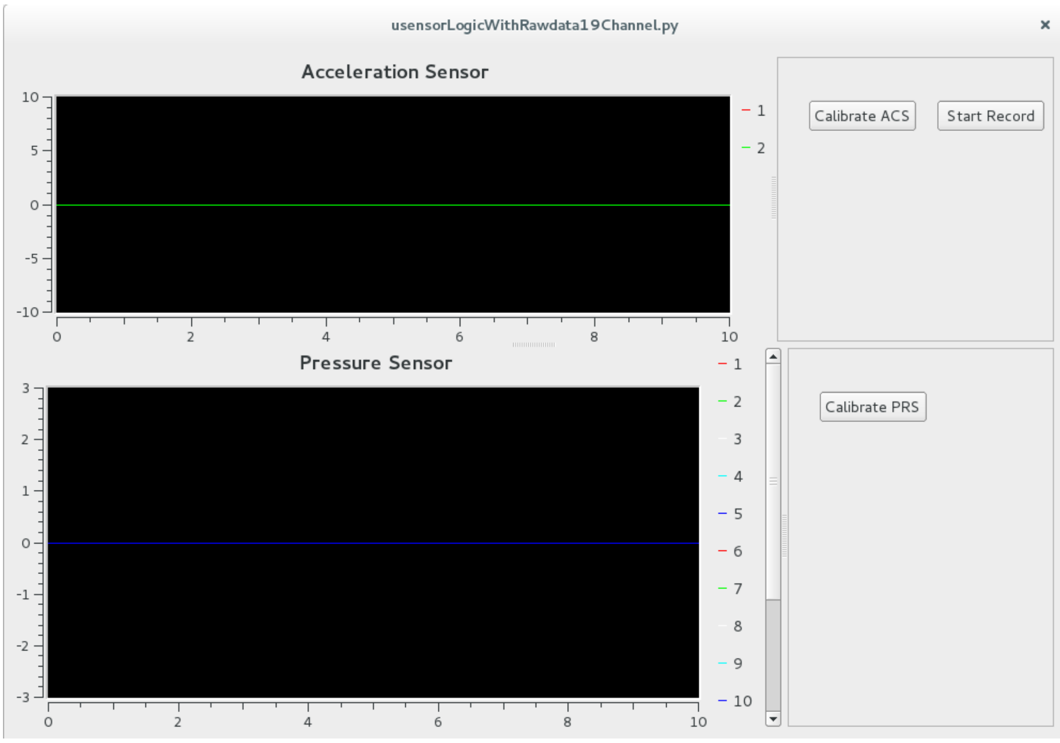

Figure 3.13: Data acquisition software interface

3.5 System performance

Several trials had to be conducted to calibrate the system. The performance of the shaking system can be established by monitoring the input acceleration measurements and the pore water pressure measurements. A test bed of depth 400 mm and a dry density of 15 kN/m^3 is used to check the performance of the set-up. Fig.3.14 shows the location of sensors in the typical experiment conducted. The details of the model preparation is described in the Section 4.3.

3.5.1 Acceleration measurements

Acceleration was measured at two locations and pore water pressure at fifteen locations in the sand bed. The system behaves satisfactorily; the sinusoidal input motion was 0.2g, and the acceleration measurements match well with the actual value as shown in Fig.3.15.

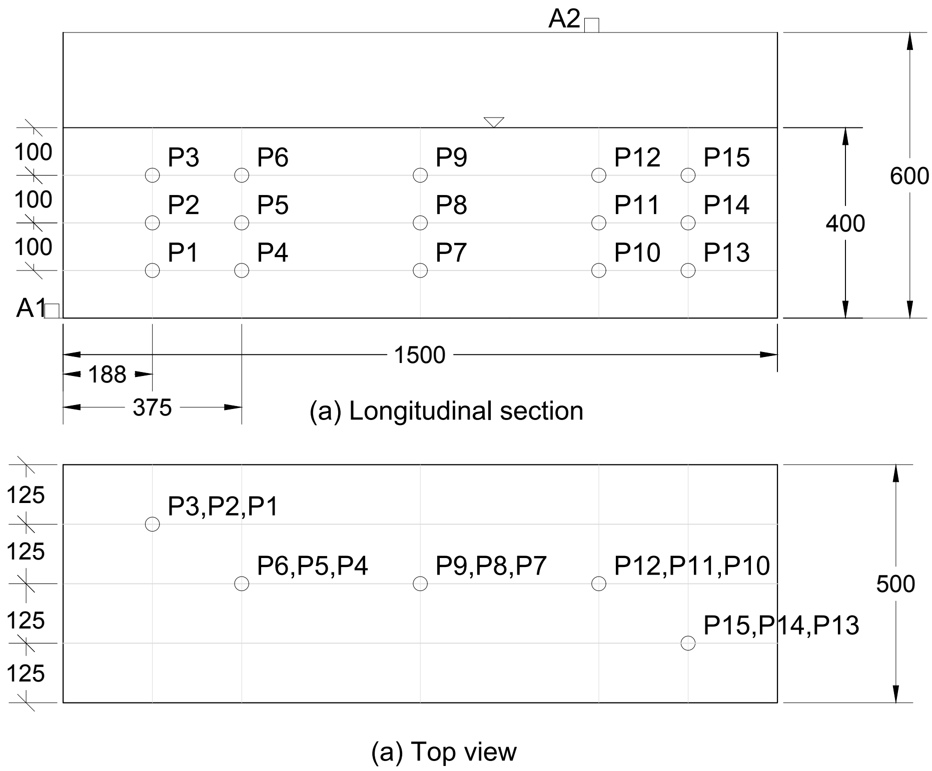

Figure 3.14: Location of sensors (dimensions in mm)

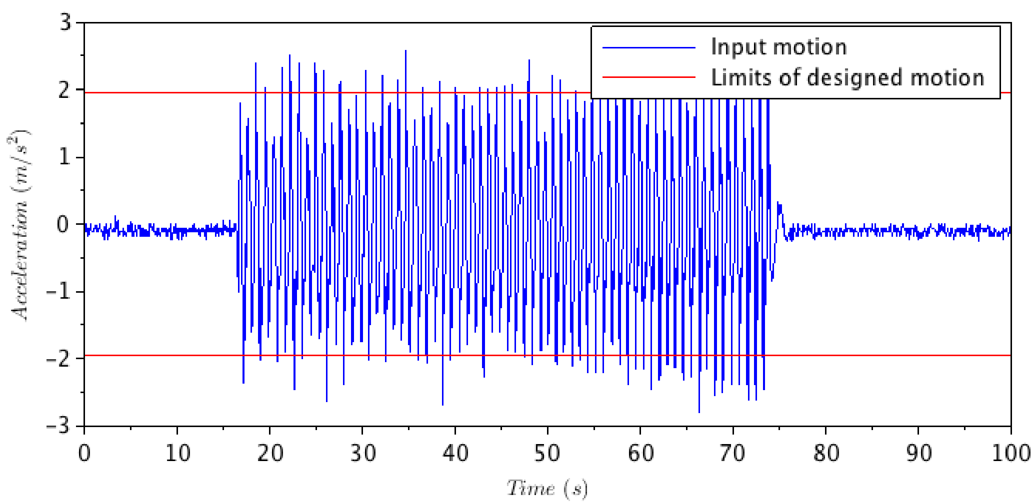

Figure 3.15: Acceleration sensors readings

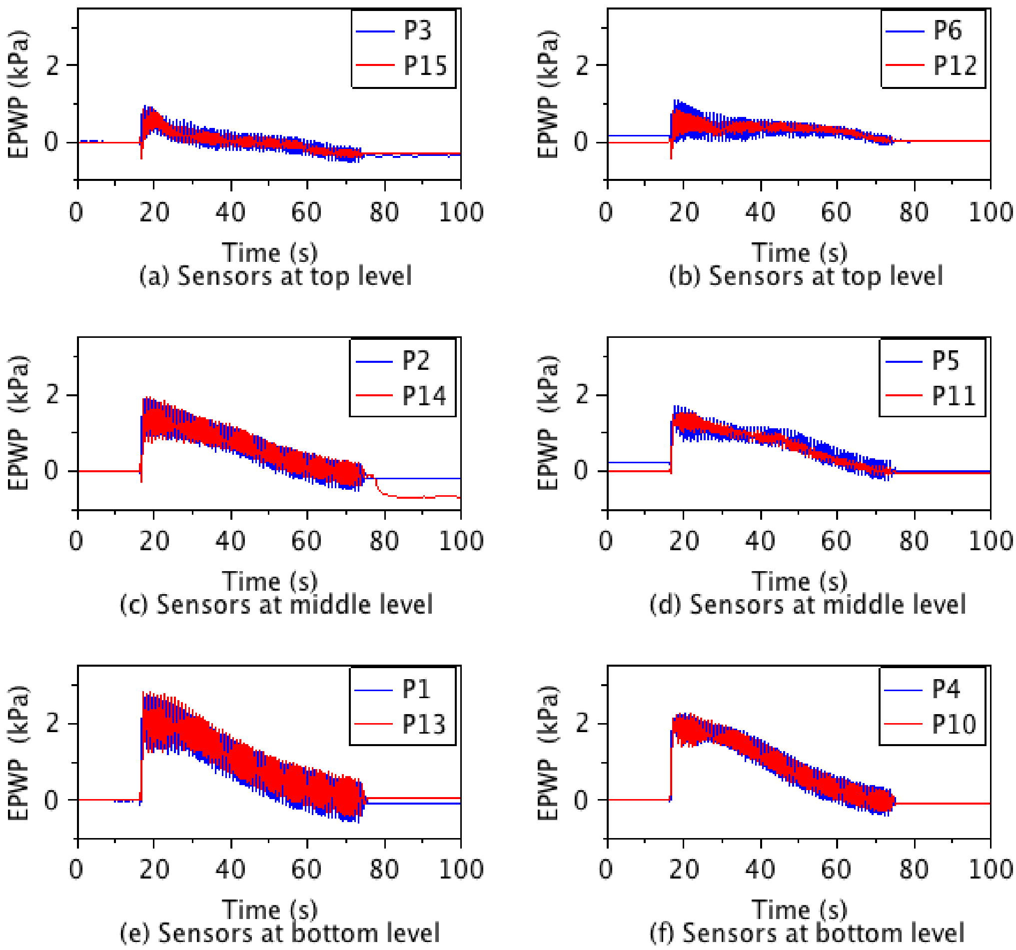

Figure 3.16: Excess pore water pressure measurements from symmetrically placed sensors

3.5.2 Symmetry of pore water pressure buildup

The symmetric behaviour of the system was established by comparing the pore water pressure measurements at symmetrically placed sensors in the sand bed. Fig.3.16 shows the plot of the pore pressure measured at symmetrically placed sensors at top, middle and bottom level.

To compare the measurements of pore pressure build up, the average of the difference between the pore pressure measurements of the sensors kept symmetrically i.e. P3 & P15 and P6 & P12 at top level, P2 & P14 and P5 & P11 at mid level and P1 & P13 and P4 & P10 at bottom level during shaking is

Table 3.6: Comparison of pore pressure values in symmetrically placed sensors

Level	Sensors	Average difference (kPa) (upto 50 s)	%Difference
Top	P3 & P15	0.029	5.27
Top	P6 & P12	-0.013	2.60
Middle	P2 & P14	0.022	1.57
Middle	P5 & P11	- 0.035	2.92
Bottom	P1 & P13	-0.072	3.60
Bottom	P4 & P10	-0.005	0.28

calculated. Table 3.6 shows the comparison of computed average of the difference in pore pressure values at three different levels. The maximum deviation is observed at bottom level, -0.072 kPa, which is within acceptable limits.

3.5.3 End effects

In the free field, the excess pore pressure developed is expected to remain equal at same depth. In the experimental model, the excess pore water pressure measurements along the longitudinal direction is compared to evaluate the end effects. Figure 3.17 shows the plot of measured values of excess pore water pressure at 188 mm (1/8 L), 375mm (1/4 L) and at 750 mm (mid point) from the box boundary.

Table 3.7 shows the average difference in the pore pressure values measured at same level. The pore pressure readings of the middle sensors (1/2 L) are compared with the measured values of sensors kept at the 1/4 L and 1/8 L from the edge of the container box. The average difference in values between the sensors kept at 1/2 L and 1/4 L are not considerable and it can be reasonably assumed that the measurements at the centre of the model are not affected by the boundaries.

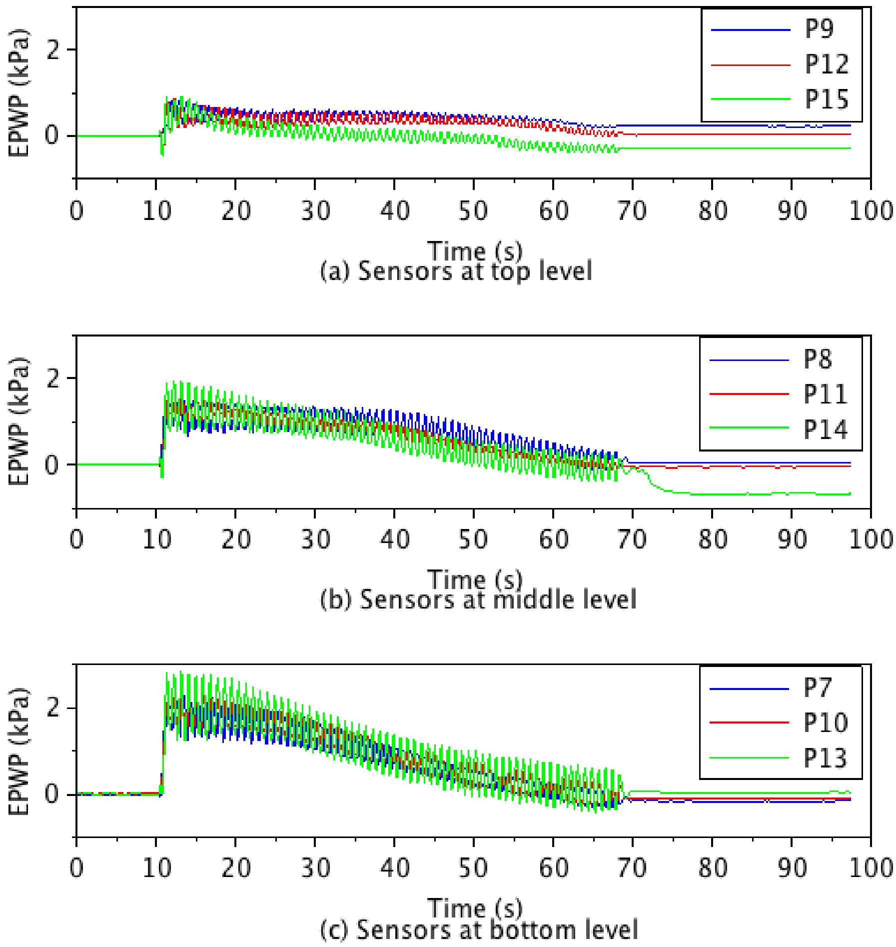

Figure 3.17: Excess pore water pressure measurements in the longitudinal direction

Table 3.7: Average deviation of pore pressure (kPa) from the values at middle

Level/Location	1/4 L	1/8 L
Top	0.074	0.0223
Middle	0.003	0.010
Bottom	0.002	0.097

Table 3.8: Comparison of results (EPWP at centre of model)

Researchers	Acc. (in g)	Freq. (Hz)	Dry density (kN/m3)	Relative density (%)	Depth* (mm)	EPWP (kPa)
Prasad *et al.* (2004)	0.50	2	14.64	56.9	20.0	2.00
Varghese and Latha (2014)	0.15	1	15.65	43	30.0	2.80
Maheshwari *et al.* (2012)	0.20	5	14.97	25	24.0	1.94
Wang *et al.* (2013)	0.20	3	14.46	35-45	22.5	1.90
Gupta (1977)	0.20	5	15.16	40	25.0	2.10
Present Study	0.20	1	15.00	30	20.0	1.50
					30.0	2.25

* Depth of observation from surface

3.6 Comparison with previous studies

To evaluate the performance of the system, the excess pore water pressure values observed at the centre of the model in the present study are compared with reported values in literature. Table 3.8 shows the results of the current study in comparison to similar studies conducted by researchers. One of the limitations in the comparison is the differences in the properties of sand and the size of the model which previous researchers have used. It is to be noted that the excess pore water pressure also depends on the input acceleration, frequency of shaking and relative density at which the model is prepared. *The values of excess pore water pressure lie within the range of values reported in the literature*. The pattern of build-up and dissipation of excess pore water pressure is also comparable.

3.7 Summary

This chapter detailed the development of the medium sized shake table and the data acquisition system suitable for studying liquefaction and related phenomenon in laboratory. The results of a typical experiment was used to evaluate the performance of the set-up. It is found that the system behaved symmetrically and the ends effects are minimal at the center of the model. The system performance was satisfactory as observed from the measurements obtained.

CHAPTER 4

LIQUEFACTION STUDIES ON SAND

4.1 Introduction

At the micro level, soil can be thought of as an assemblage of individual particles of varying size. Depending on the type of soil, the behaviour varies extensively, and it also depends on many parameters including cohesion between the particles, friction, density, saturation, confinement and drainage. In the case of cohesionless soil, the strength behaviour is mainly attributed to the inter-particular frictional forces. Here, the presence of water plays a significant role in determining the behaviour under loading. The most interesting behaviour is observed when the loading is dynamic, like in the case of an earthquake. Saturated sand deposits, when subjected to dynamic loading is known to have behaved like a viscous liquid with little shear strength and caused widespread damages to structures. This distinguishing feature during dynamic loading whenever soil loses its shear strength and flows like a liquid is called as liquefaction.

Several methods have been used by researchers for studying this phenomenon in the laboratory. In this research, shake table studies are used to investigate the behaviour of sands collected from three different locations in the central region of the state of *Kerala* and the susceptibility to liquefaction is evaluated. The sands are collected from *Aluva*, *Cherthala* and *Puthu Vypin*. Sufficient quantity of sand for the experiment was collected and transported to the laboratory. The investigations focus on the pore water pressure buildup in these sands under sinusoidal dynamic loading for different relative densities and fines content. Visual observations and excess pore water pressure ratio (r_u) are used to identify the initiation of liquefaction during the experiments. The present chapter discusses the properties of sand, the methodology for sample preparation and conducting the experiment, and the results obtained.

4.2 Properties of sand samples from different sources

The soil samples were tested as per the relevant IS Codes to obtain the basic properties and are presented in Table 4.1.

4.2.1 *Cherthala* Sand

Cherthala is sandwiched between the Arabian sea and *Vembanad* lake. The characterising feature of *Cherthala* sand is the presence of high silica content which makes it whitish in colour. This sand is extensively used in glass and cement industries. The region is also low lying with water table near the ground surface.

4.2.2 *Aluva Sand*

The sand deposit is *Aluva* sand thought to be riverine in origin. River *Periar* flows through the region and many sand deposits exist in the river belt.

4.2.3 *Puthu Vypin* Sand

Puthu Vypin is located near the Arabian Sea, and the region has sand deposits of varying depths. The sand samples were collected close to the beach. Traces of salt was present in the sample.

The particle size distribution of all the three sands fall under the liquefiable zones proposed by Tsuchida (1970) (Fig.4.1). In addition to the basic properties, the permeability values of the sands at different relative densities were also found out.

Table 4.1: Properties of sand samples

Property	*Cherthala*	*Aluva*	*Puthu Vypin*
Specific Gravity	2.63	2.60	2.64
% Sand	99.8	99.2	99.9
% Silt	0.2	0.8	0.1
% clay	0.0	0.0	0.0
% D_{10}	0.18	0.2	0.23
% D_{30}	0.21	0.41	0.30
% D_{50}	0.29	0.65	0.32
% D_{60}	0.32	0.75	0.34
e_{max}	0.78	0.87	0.88
e_{min}	0.50	0.51	0.57
C_u	1.78	3.75	1.48
C_c	0.77	1.12	1.15
IS Classification	SP	SP	SP

Table 4.2: Permeability of sand samples

Sand type	Relative Density(%)	Permeability (m/s)
Cherthala Sand	30	1.328×10^{-5}
Cherthala Sand	40	1.107×10^{-5}
Cherthala Sand	50	0.966×10^{-5}
Aluva Sand	30	3.712×10^{-5}
Aluva Sand	40	1.951×10^{-5}
Aluva Sand	50	1.392×10^{-5}
Puthu Vypin Sand	30	2.418×10^{-5}
Puthu Vypin Sand	40	1.729×10^{-5}
Puthu Vypin Sand	50	1.341×10^{-5}

Permeability is a basic parameter which determines the drainage potential of the soil and hence has a direct influence on the liquefaction behaviour. Falling head test was used to calculate the permeability and the values obtained are shown in Table 4.2. The variation of permeability with respect to relative density for all the three sands are shown in Fig. 4.2. It can be seen that *Aluva* sand is more permeable and *Cherthala* sand is the least, among the three. The permeability decreases with relative density. But, here, these differences are not much significant as all the permeability ranges are within $1 \times 10^{-5} m/s$ and $4 \times 10^{-5} m/s$.

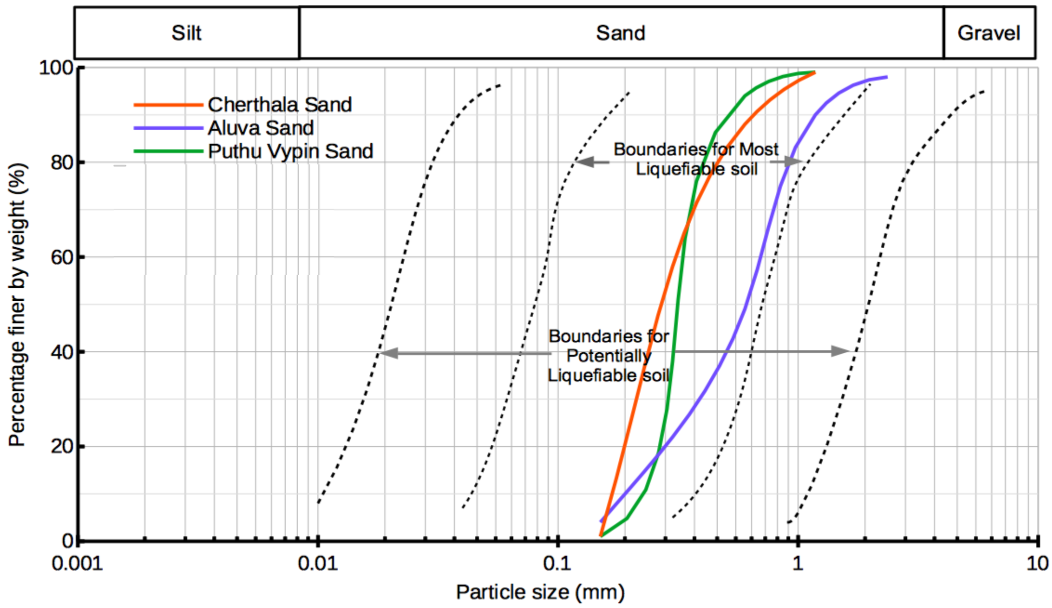

Figure 4.1: Particle Size Distribution of sands super imposed over curves defined by Tsuchida (1970)

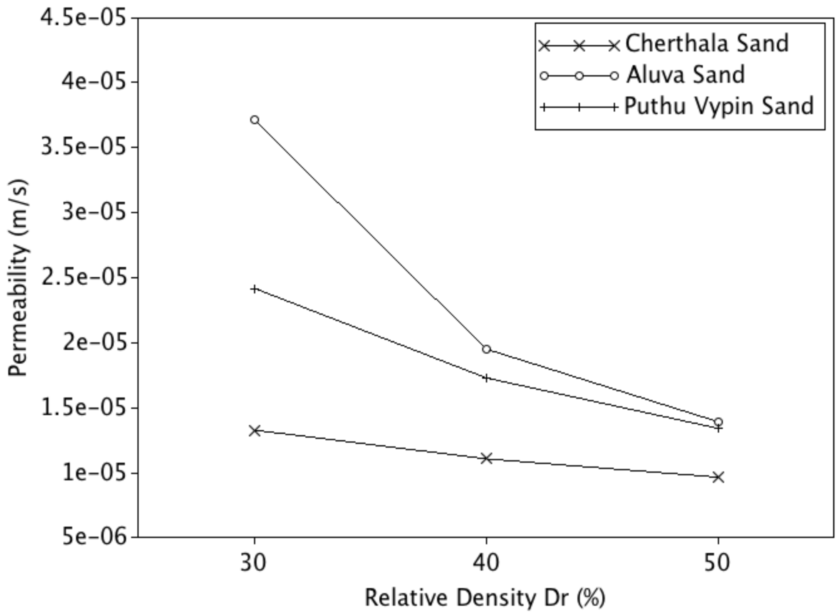

Figure 4.2: Permeability of tested sands

4.3 Shake table experiments conducted

Nine experiments were conducted to investigate the effect of relative density on pore water pressure generation, keeping the acceleration of shaking as $0.24g$ at 1Hz using the shake table. This value corresponds to maximum ground motion acceleration expected in Zone IV according to IS 1893: 2002. Moreover, it is reported that Pathanamthitta, Kottayam, Alappuzha and Ernakulam districts showed the highest value of peak ground acceleration ranging from $0.234g$ to $0.278g$ indicating that these regions are susceptible to high magnitude earthquakes (Sajudeen and Latheswary, 2012).

Many researchers seem to have preferred air pluviation technique for preparing the sample for conducting shake table experiments because of its simplicity (Dungca *et al.*, 2006; Belkhatir *et al.*, 2014; Yamamoto *et al.*, 2009) and hence the models in the present study were prepared following the same method. The total depth of the model, 400 mm, was filled in four layers of 100 mm each. Air-dried sample of required weight for each layer was deposited using a funnel. The drop height required was arrived at by trial and error method. For achieving 30% relative density, the drop height was kept very low. The height of fall was adjusted so that 40% and 50% can be achieved. The pore water pressure sensor probes are held in position using thin strings tied to the top and bottom frame of the container box. This was to prevent the sensors from dislocating during shaking. After filling the sand up to the required level, water was introduced from the bottom of the container at a slow pace. The head of flow was kept very low so that soil saturates slowly, from the bottom. The total time required for saturation was four hours on an average. As the soil fully saturates, a very thin layer of water formed at the top surface. The water level in the pore water pressure probes is noted to ascertain that full saturation is achieved. On full saturation, the level of water in the probe will be at the top level of the sand bed. The amplitude of the shake table was set to produce an acceleration of $0.24g$ at 1Hz and experiments were conducted. Recording of the acceleration and pore water pressure measurements from the sensors were started before switching on the shake table. The shaking of the table was continued for each experiment till the soil stratum achieve a stable state visually. The sensor measurements were continued till no further change in readings were observed.

4.4 Effect of relative density of soil

A total of nine experiments were conducted corresponding to three relative densities in each of the different sand types used for the study. The values of relative densities chosen for the study are 30%, 40% and 50% (loose to medium density states). The values lie in the range of densities of sand in its natural state. The objective was to evaluate the liquefaction potential in these range of relative densities, keeping the acceleration as constant.

Fig. 4.3, 4.4 and 4.5 shows the excess pore water pressure build up at the center of the model when it is subjected to a sinusoidal acceleration of $0.24g$ at 1Hz frequency, corresponding to *Cherthala*, *Aluva* and *Puthu Vypin* sand respectively. Fig. 4.6, 4.7 and 4.8 depicts the excess pore water pressure ratio (r_u) for the respective cases.

The pore water pressure builds up immediately on shaking and dissipates as sand moves to a closer configuration due to shaking. In all the test cases, the excess pore water pressure measured at the bottom was more than that at the top level. This indicates that a vertical hydraulic gradient exists with higher values at higher depths. This behaviour can be expected, since, the only drainage path available for the excess pore water generated during shaking is in the upward direction through the top surface. While the pore water pressure formed at the top gets dissipated fast, the excess water generated at higher depths will need to travel a longer path to reach the top.

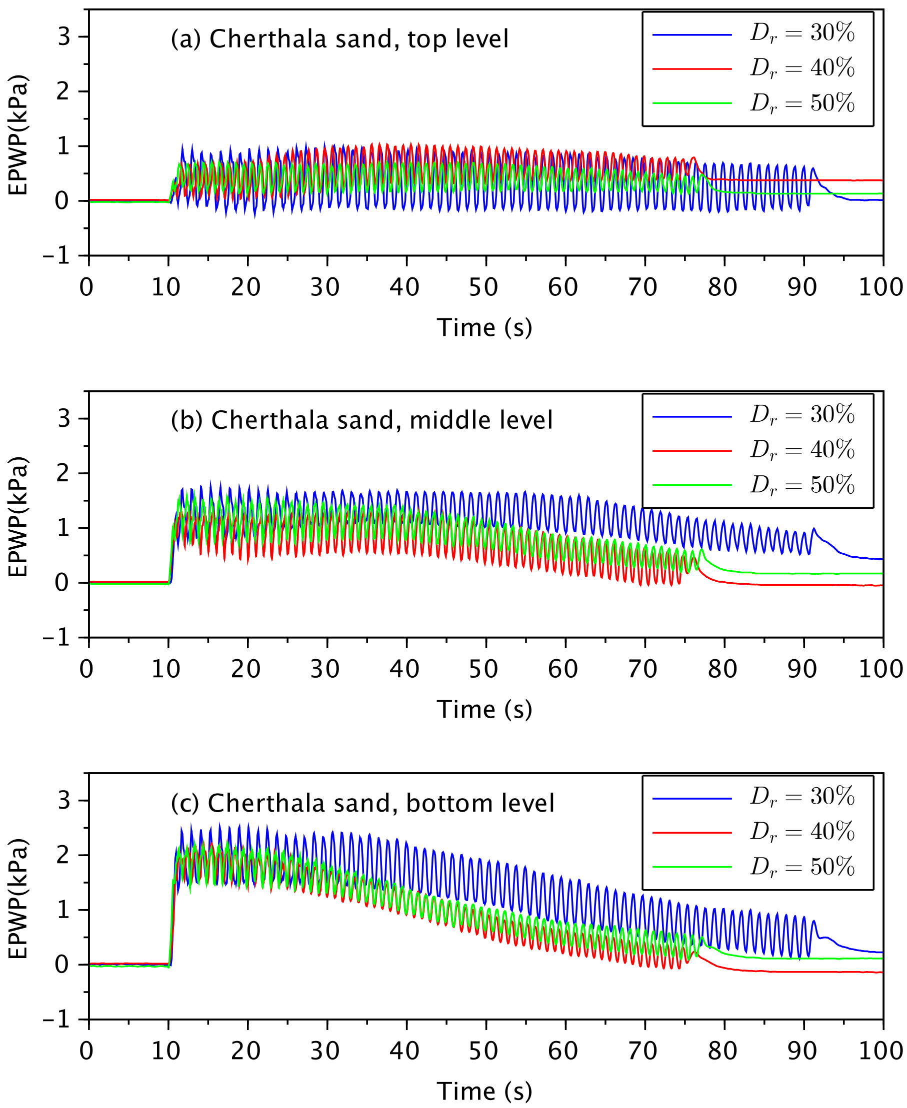

Figure 4.3: Excess porewater pressure at center of the model - *Cherthala* Sand

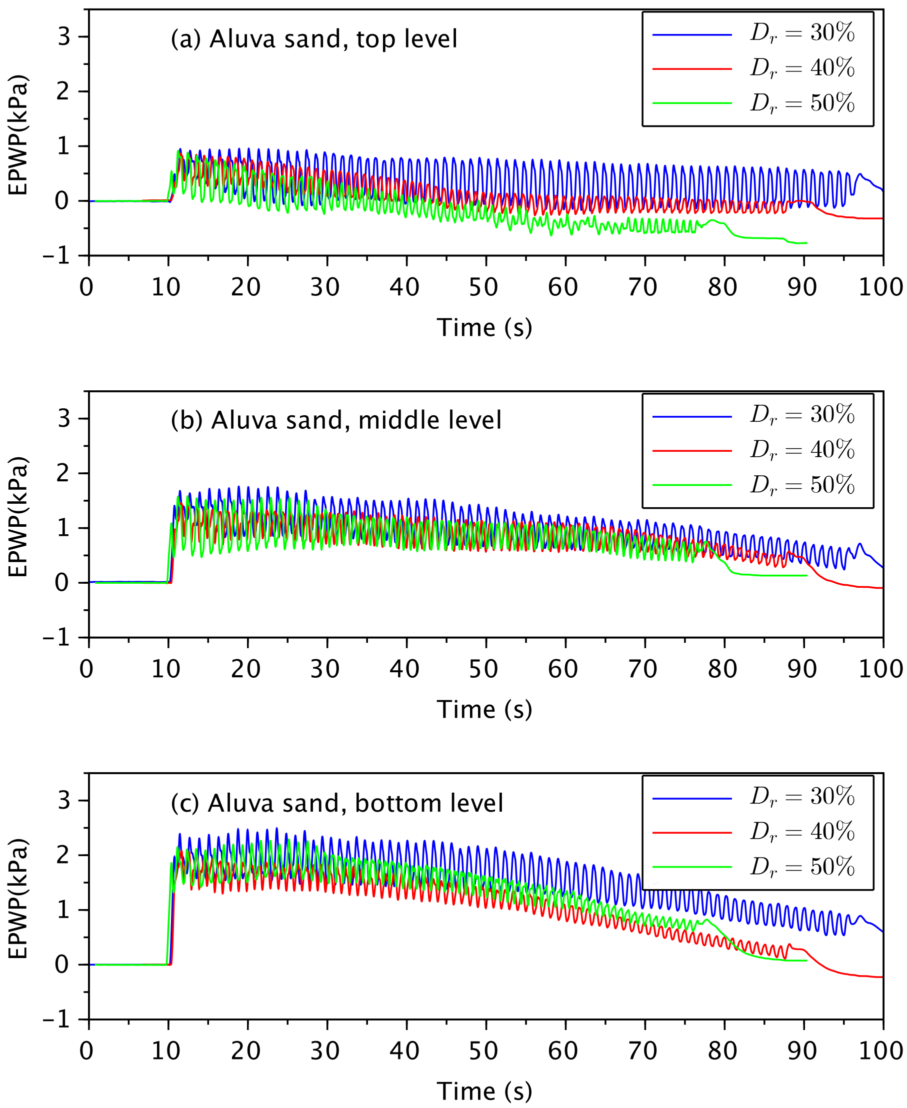

Figure 4.4: Excess porewater pressure at center of the model - *Aluva* Sand

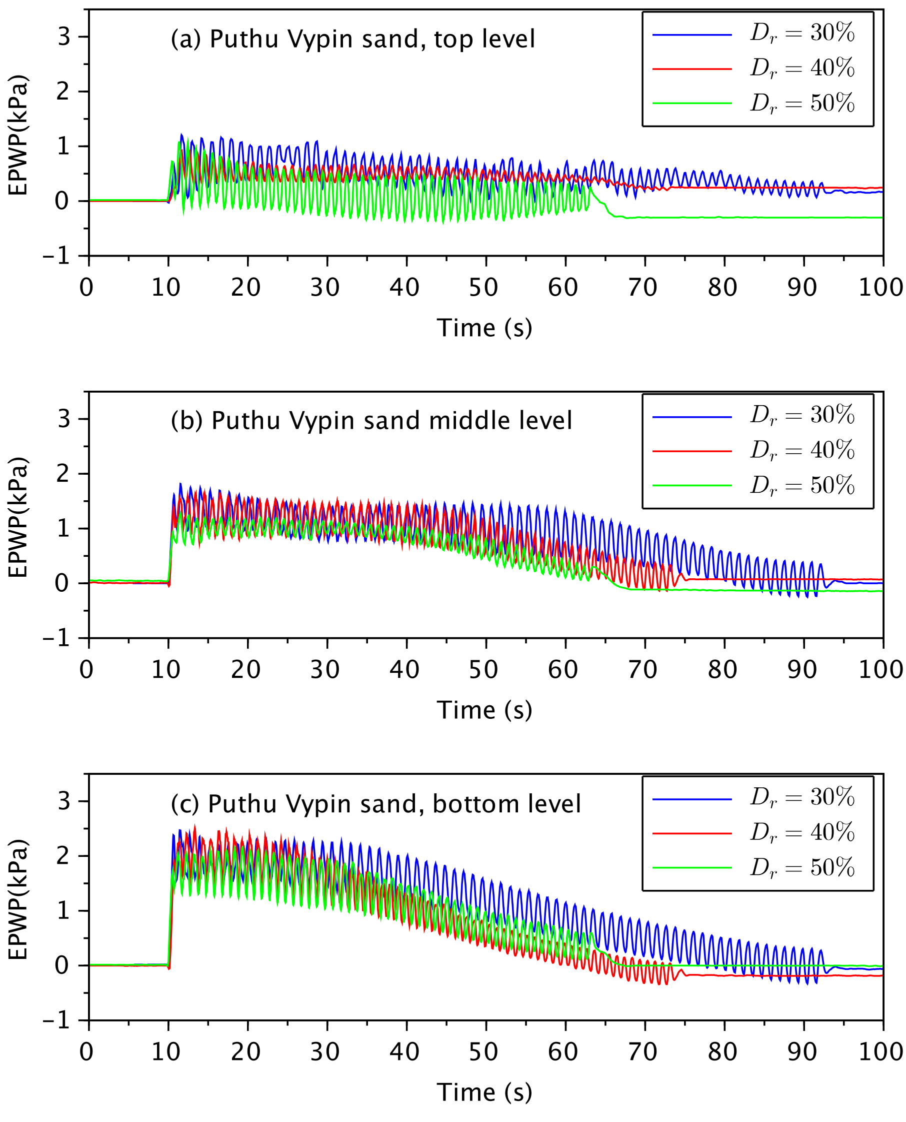

Figure 4.5: Excess porewater pressure at center of the model - *Puthu Vypin* Sand

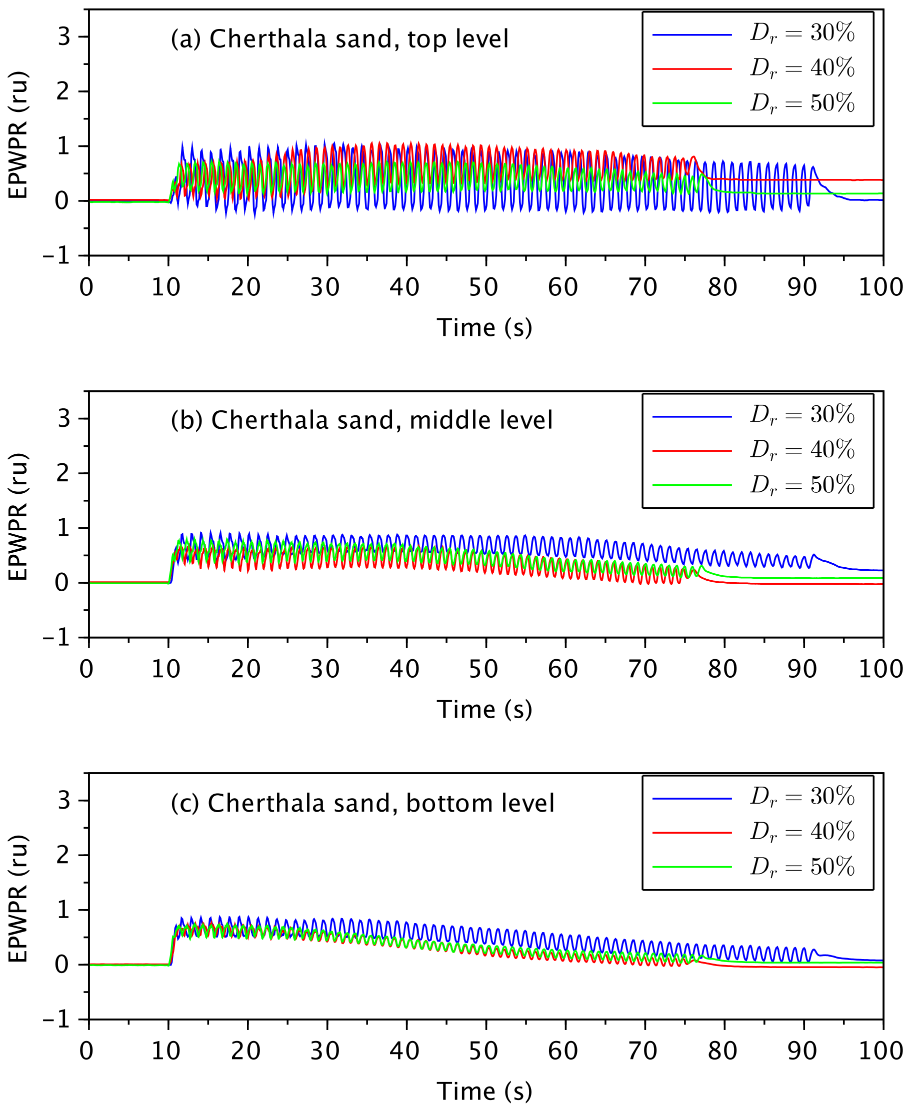

Figure 4.6: Excess porewater pressure raio at center of the model - *Cherthala* Sand

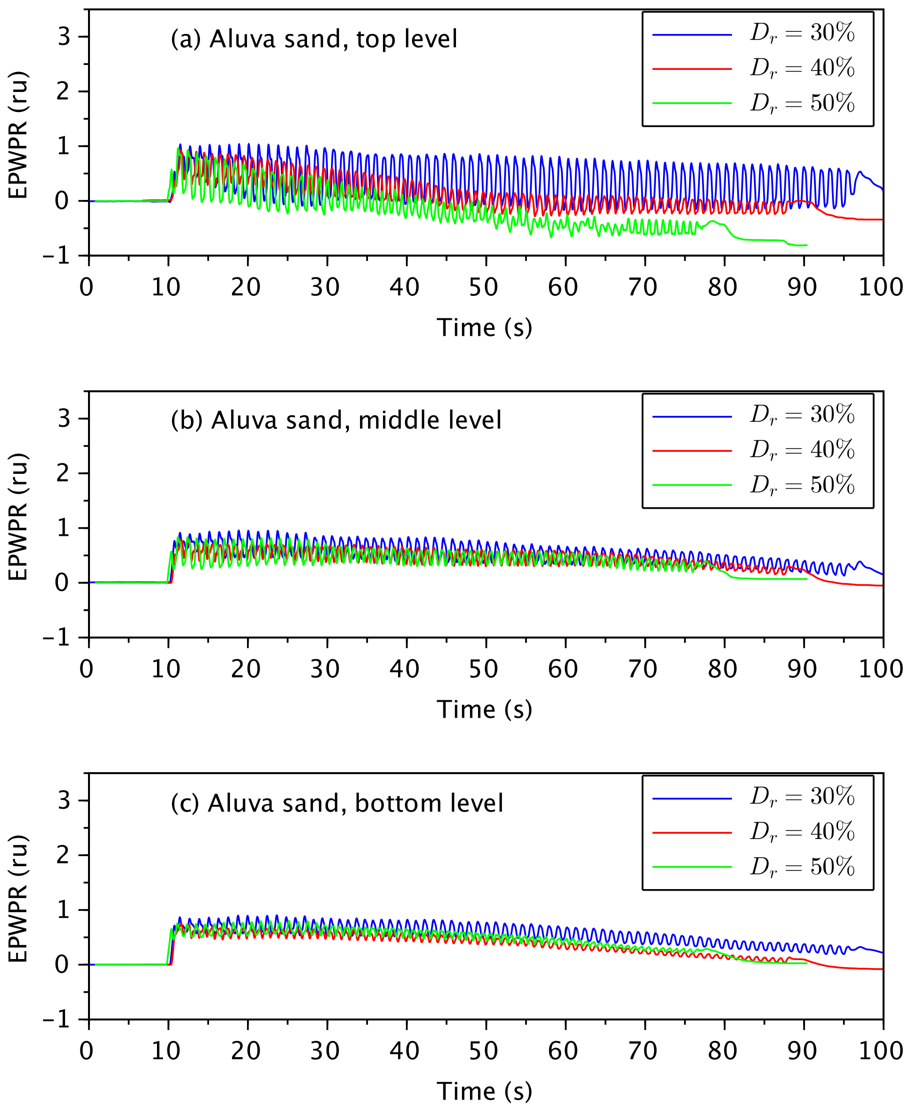

Figure 4.7: Excess porewater pressure raio at center of the model - *Aluva* Sand

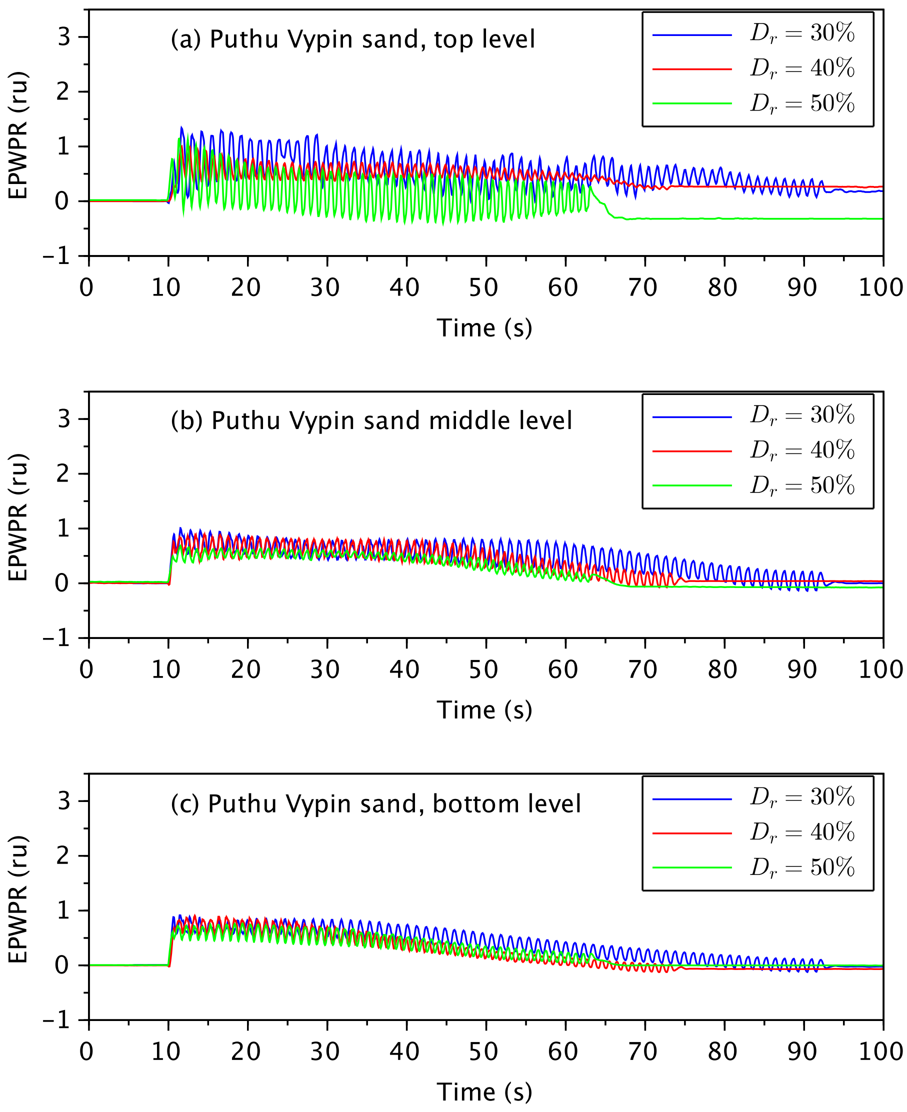

Figure 4.8: Excess porewater pressure raio at center of the model - *Puthu Vypin* Sand

It is generally understood that the possibility of liquefaction is less at higher relative densities due to higher effective stress and lower densities, the soil is more prone to liquefaction.

Even though it is observed that the excess pore water pressure values are more when the relative density is 30%, a clear relationship could not be derived between the relative density and the development of excess pore water pressure. There is no marked difference in the maximum value of pore pressure recorded at 40% and 50% relative density. It can be inferred from the plots of r_u that when the relative density is 30%, the r_u values are consistently higher that that observed at 40% and 50% relative density. There is no much marked difference between the values of r_u observed between 40% and 50% relative density.

It should be noted that if a sand stratum is liquefiable for a typical dynamic loading, irrespective of the relative density, the maximum value of excess pore water pressure generated is limited to the value which corresponds to the state where the excess porewater pressure ratio becomes one. Now, since all the three sands liquefied (at least partially) in the range of densities tested, the maximum value of excess pore water pressure will be almost the same. The variations observed are minimal as seen from the plots.

The excess porewater pressure developed is a function of relative density, but, the relationship is highly non-linear. The study by Varghese and Latha (2014) has reported a similar behaviour, where, a reduction in excess porewater pressure is observed only at very high relative densities (67%) and not much for relative densities 43% and 58%.

Table 4.3: Sand gradation

Sand type	% Fine sand size (0.075mm-0.425mm)	% Medium sand size (0.425mm-2.0mm)	% Coarse sand size (2.0mm-4.75mm)
Cherthala	77	33	0
Aluva	32	66	2
Puthu Vypin	83	17	0

4.5 Effect of sand type

Excess pore water pressure ratio (r_u) is the parameter used to detect the initiation of liquefaction in saturated sand during dynamic loading. Fig. 4.9, 4.10 and 4.11 show the excess pore water pressure ratio at the centre of the model for 30%, 40% and 50% relative densities respectively for the three different sand samples studied.

Table 4.4 shows the status of liquefaction among all the experiments conducted. L indicates that excess porewater pressure ratio reached a value of 1.0 and liquefaction has occurred. NL shows that the soil bed has not liquefied and excess pore water pressure ratio is less than the critical value, 1.0. From the measurements, it is observed that the liquefaction resistance improved when the relative density is more. All the three different sands liquefied to full depth at 30% relative density. At 40% relative density, *Puthu Vypin* sand exhibited liquefaction at all depths and the top layers liquefied for the other two sands. Also, the middle layer in *Cherthala* sand liquefied. At 50% relative density, liquefaction was observed only in the top layer in *Puthu Vypin* sand but the middle and bottom layers remained non-liquefied. These observations are consistent with the visual feedback during the experiments.

It can be observed from the Table 4.3 that *Puthu Vypin* sand has 83% finer content (0.075mm-0.425) which might be the reason for its highly liquefiable behaviour compared with the other two sands. *Cherthala* sand which has 77% fine sand showed slightly more resistance and *Aluva* with 66% showed greater resistance to liquefaction during experiments. It may be concluded that the percentage of finer

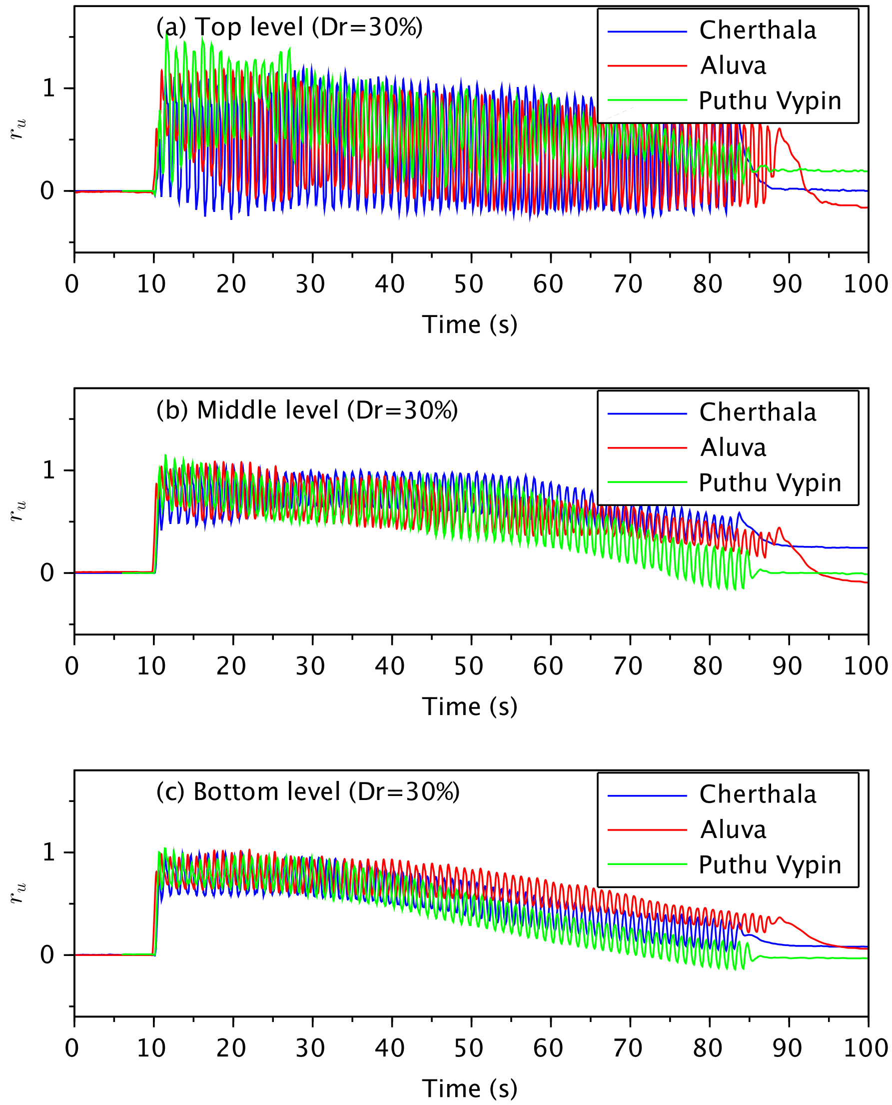

Figure 4.9: Excess porewater pressure ratio at center of the model D_r 30%

Table 4.4: Liquefaction observed in experiments conducted

Sand type \ D_r	$D_r = 30\%$			$D_r = 40\%$			$D_r = 50\%$		
	T	M	B	T	M	B	T	M	B
Cherthala Sand	L	L	L	L	L	NL	NL	NL	NL
Aluva Sand	L	L	L	L	NL	NL	NL	NL	NL
Puthu Vypin Sand	L	L	L	L	L	L	L	NL	NL
T - Top, M - Middle, B - Bottom, L - Liquefied, NL - Not Liquefied									

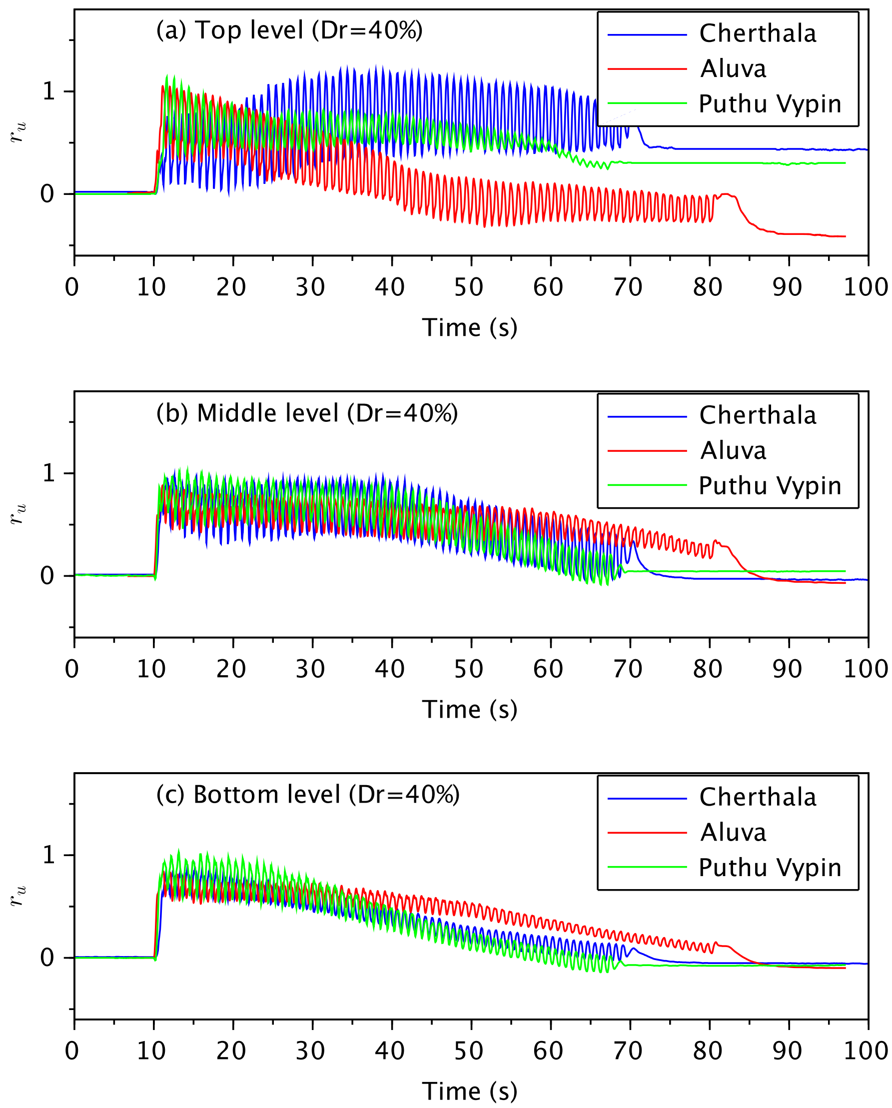

Figure 4.10: Excess porewater pressure ratio at center of the model D_r 40%

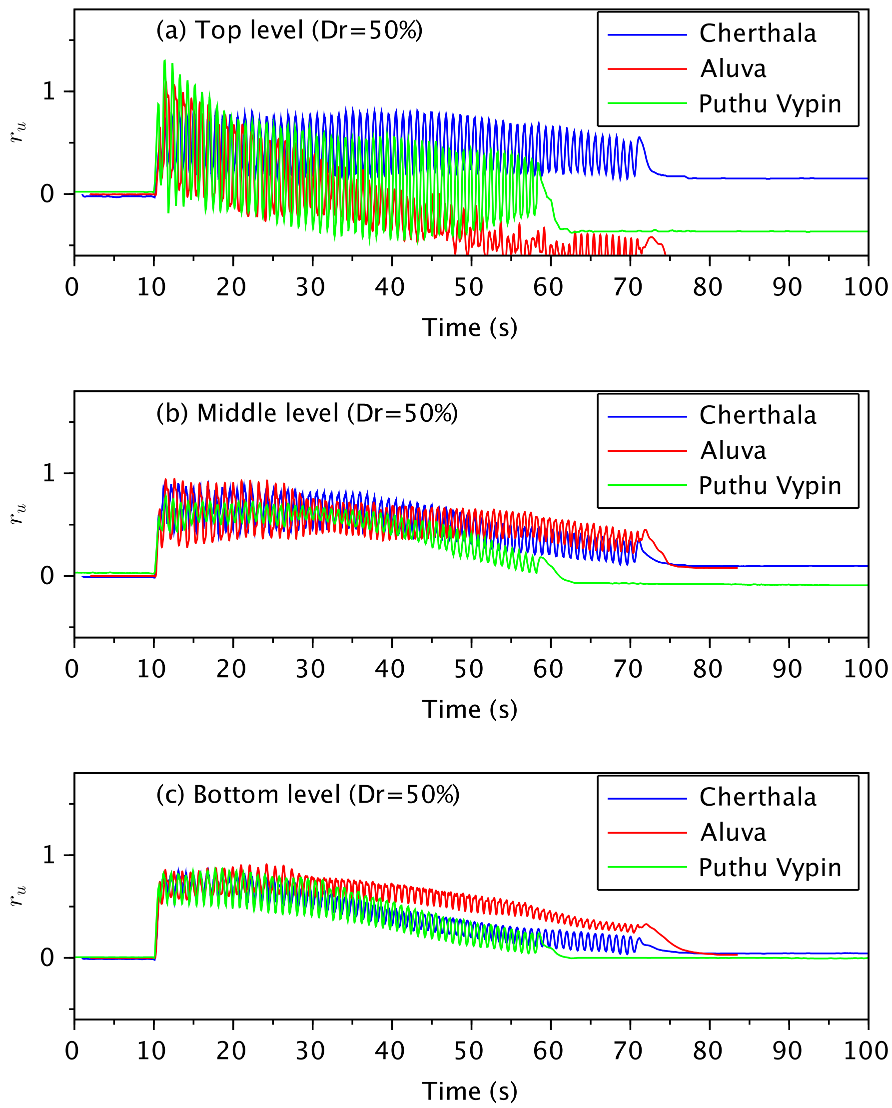

Figure 4.11: Excess porewater pressure ratio at center of the model D_r 50%

Table 4.5: Properties of non-plastic fines

Specific gravity	2.71
Liquid Limit (%)	34
% Silt size	99
% Clay size	1

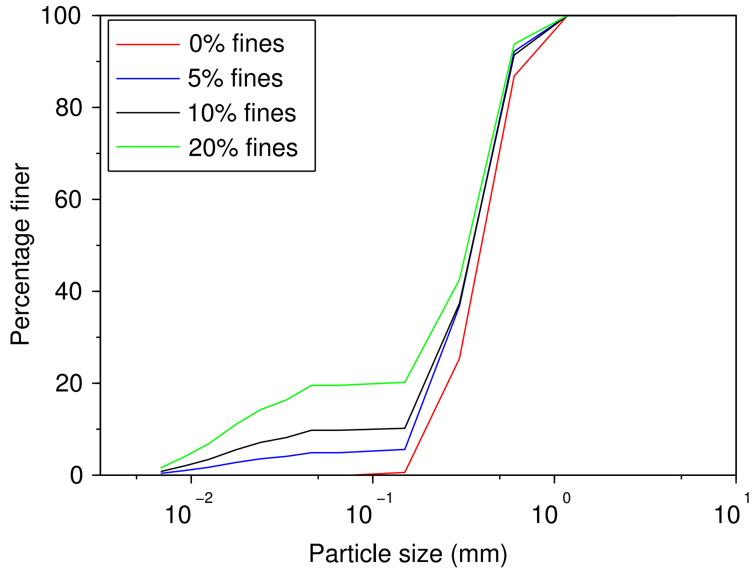

Figure 4.12: Particle size distribution of sand with fines

sands has an adverse effect on the liquefaction behaviour of sands.

4.6 Effect of non-plastic fines content

Cherthala sand was used to study the effect of non-plastic fines in the liquefaction behaviour. The sand was sieved, and fines less than 75μm sizes were removed. Non-plastic fines were added in varying percentages (5%, 10% and 20%) and four shake table experiments were conducted. The fines selected were the by-product of rock crushing and of silt size. The properties of added fines are given in Table 4.5.

The grain size distribution curves of sand mixed with fines are shown in Fig.4.12.

The relative density and the input acceleration is kept constant values as 30% and

Table 4.6: Properties of sand with fines

Fines content	0%	5%	10%	20%
G	2.671	2.675	2.680	2.686
e_{max}	0.765	0.753	0.746	0.735
e_{min}	0.539	0.474	0.432	0.382
e for D_r=30%	0.697	0.669	0.652	0.629
Permeability(m/s)	1.12×10^{-4}	0.903×10^{-4}	0.753×10^{-4}	0.471×10^{-4}
Bulk Density (kg/m^3)	1573	1603	1622	1649

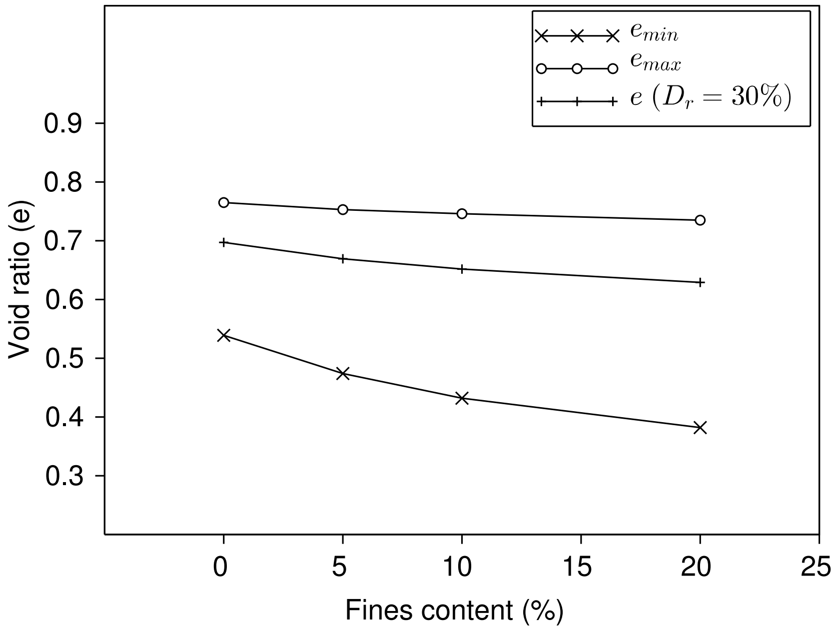

Figure 4.13: Variation of e_{max} and e_{min} with fines content

$0.24g$ respectively for all the experiments. Table 4.6 consolidates the properties of sand mixed with fines used for conducting the shake table experiments. The variation of e_{max} and e_{min} are shown in Fig.4.13. The shaking of the table is continued for each experiment till the soil stratum achieve a stable state visually.

To analyse the development of pore pressure during shaking, the value of excess pore pressure ratio at the centre of the model at three different levels (top, middle and bottom) were plotted as shown in Fig.4.14. Liquefaction was observed in all the four cases studied. This is indicated by the value of r_u in all the three cases. The top layer of sand liquefied completely during the experiments with large deformations

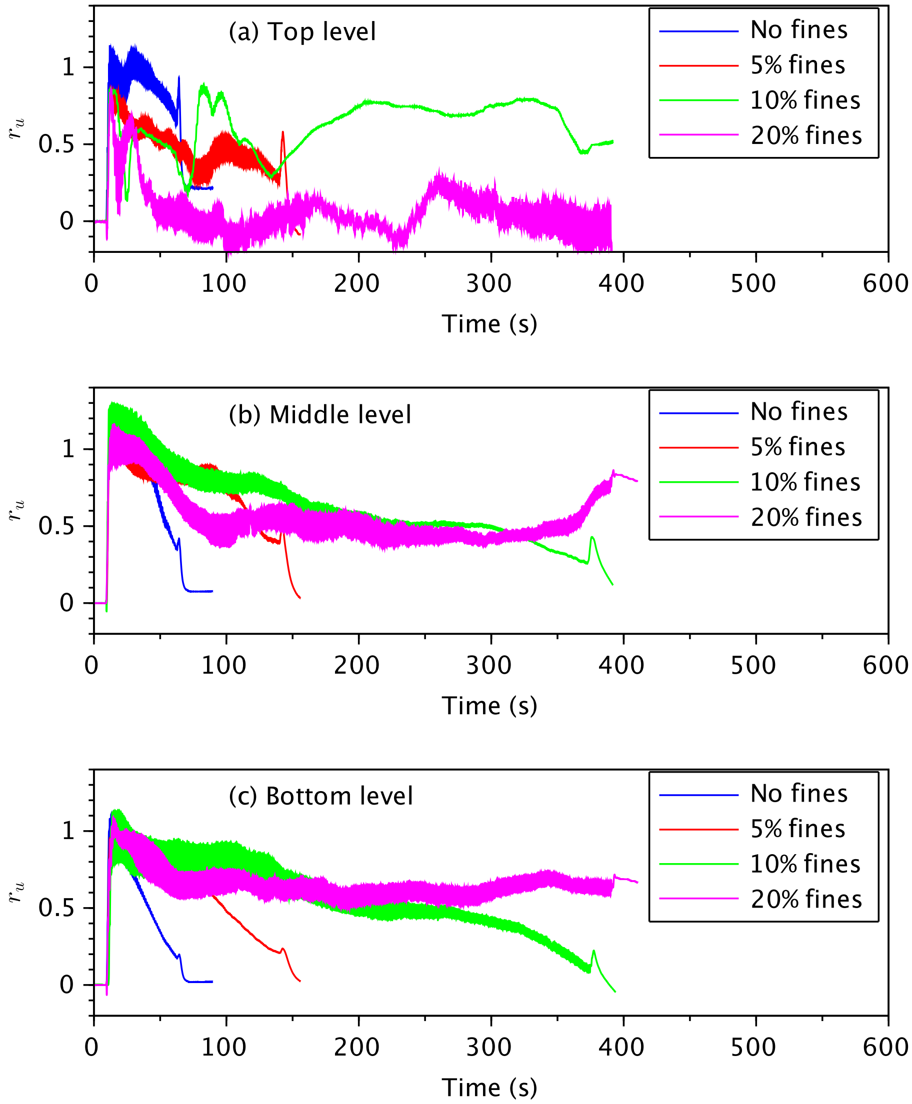

Figure 4.14: Excess pore water pressure ratio with different fines content

and this lead to inconsistent readings from the sensors kept at the top level.

In the event of liquefaction, at a particular depth, the excess pore pressure builds up to a level where the value of r_u becomes 1.0. At that instant, the soil would completely liquefy and behave like a viscous fluid. This is a critical state which the system can attain, and no further pore pressure build-up is possible. This phenomenon was observed in all the cases studied as observed in Fig.4.14.

The build-up of excess pore water pressure during the experiment can be viewed in terms of liquefaction resistance as small build-up of excess pore water pressure

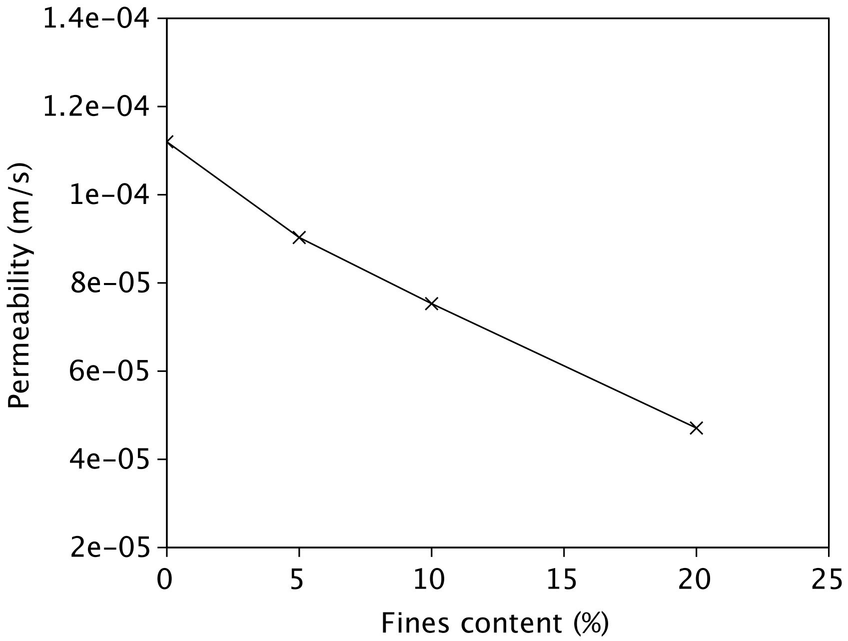

Figure 4.15: Variation of permeability with fines content

denotes the more resistance to liquefaction. It was observed that the effect of increase of percentage of non-plastic fines content on the build-up of excess pore water pressure is minimal. The liquefaction resistance is not affected by the presence of non-plastic fines for a typical relative density of the sample. This observation is consistent with the observations made by Polito and Martin II (2001) while studying the cyclic resistance of sand using the cyclic triaxial tests.

Even though the change in fines content has not affected the pore pressure build-up, it seems to have considerable effects on its dissipation. When the fines content is 0%, the soil settles to a stable state in 53 seconds or 53 cycles of loading during the shaking process. This behaviour could be attributed to the fact that soil particles are moving to a closer configuration during dynamic loading. In the course of this reconfiguration, the water held in the pores are expelled thereby increasing the relative density and decreasing the void ratio. The expelled water could be seen on the top of the soil bed during shaking. The soil eventually reaches the maximum density state. This reconfiguration process may impair any further pore pressure

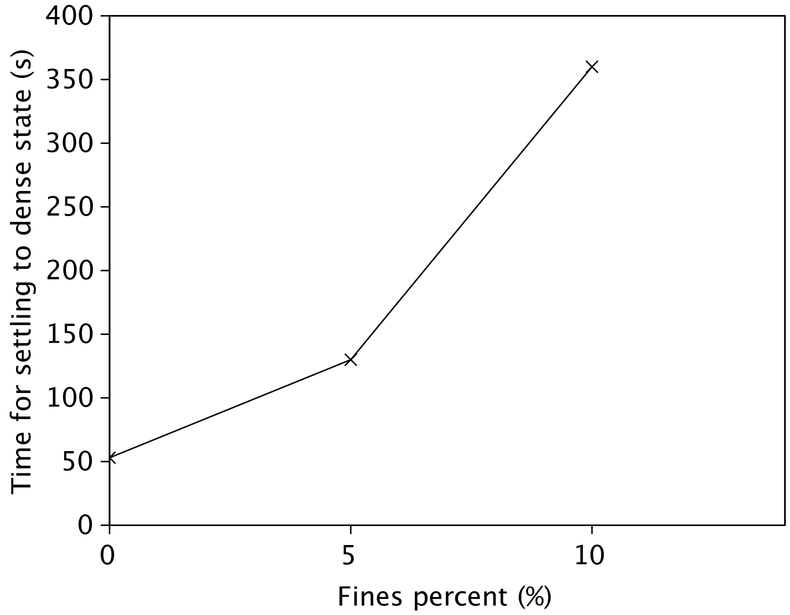

Figure 4.16: Variation of time for final settling with fines content

build-up during shaking. When non-plastic fines is added to sand, it occupies the voids between the sand particles, decreasing the void ratio (for same D_r) as seen from Fig.4.13. The permeability of sand also decreases with the inclusion of fines as seen in Fig.4.15. From the Table 4.6 it can be inferred that the reduction in permeability is more than 50%. These two factors will prevent the pore water from dissipating during shaking and keeps the soil in the liquefied state for a longer period. At 5% fines content, it took 130 seconds for the soil to settle, almost 1.6 times the time taken without fines. As the fines content is increased to 10%, soil stayed liquefied longer and settled in 360 seconds. Further increase in fines to 20% created a very similar behaviour, with soil not showing any signs of settlement in 380 seconds and remaining in a steady liquefied state. It is inferred that when the fines content goes beyond a limit, in this case, 20%, almost all the voids are completely filled with fines, and it may prevent the soil from settling to a stable dense state. Fig. 4.16 shows the time required for final settling with varying fines content. It may be noted that for 20% fines no final settling was observed and hence the point is not plotted in the figure.

4.7 Summary

A detailed discussion about the observations and results obtained from the shake table tests with different types of sand and density are presented in this chapter. An attempt was made to study the similarity in the behaviour of the three types of sands, the effect of relative density and also the effect of non-plastic fines. The following conclusions could be derived from the experiments conducted.

1. The relationship between relative density and excess pore water pressure buildup is not direct. But, it is certain that sand at lower packing density is more prone to liquefaction.

2. The different sands tested are identified to be prone to liquefaction at 30% relative density under a ground motion acceleration of $0.24g$.

3. It is observed that when the percentage of fine sands size (0.075mm - 0.425mm) is more, liquefaction resistance decreases. Out of the three sands tested, *Puthu Vypin* sand had 83% finer content (0.075 mm-0.425 mm) and showed highly liquefiable behaviour while *Cherthala* sand, which has 77% finer sand showed slightly more resistance and *Aluva* sand with 66% showed greater resistance to liquefaction during experiments.

4. Non-plastic fines content seem to have a predominant effect on the dissipation and settling time to final dense state due to shaking for a constant relative density. At the same time, it is observed that fines content has a minimal effect on the pore pressure build up and liquefaction resistance. When the fines content goes beyond a limit (20%), almost all the voids are completely filled with fines, and it may prevent the soil from settling to a stable dense state.

CHAPTER 5

LIQUEFACTION MITIGATION USING STONE COLUMNS

5.1 Introduction

Stone columns (SC) have been traditionally used as a ground improvement technique in soft soil (Najjar *et al.*, 2010; Murugesan and Rajagopal, 2009). In addition to the enhancement of the bearing capacity, stone columns also work as drainage paths due to its high hydraulic conductivity. High permeability makes stone columns a suitable mitigation method in soil prone to liquefaction. It can drain out pore water pressure as soon as it is generated during dynamic loading if designed properly. An attempt is made here to study the effectiveness of stone columns in mitigating liquefaction, using shake table experiments.

In the present chapter, the results of an experimental investigation conducted on sand beds with stone columns using the shake table developed are presented. The experiments were conducted on saturated sand beds with and without the stone column to understand the behaviour under sinusoidal shaking. The study focus on the effect of the diameter of the stone column on the liquefaction response. In addition to this, to understand the effect of the encasement, an experiment was conducted with geotextile wrapped stone column. The excess pore pressure developed in the model during shaking is measured at various locations and used to compute the excess pore water pressure ratio, the value of which can indicate the initiation of liquefaction.

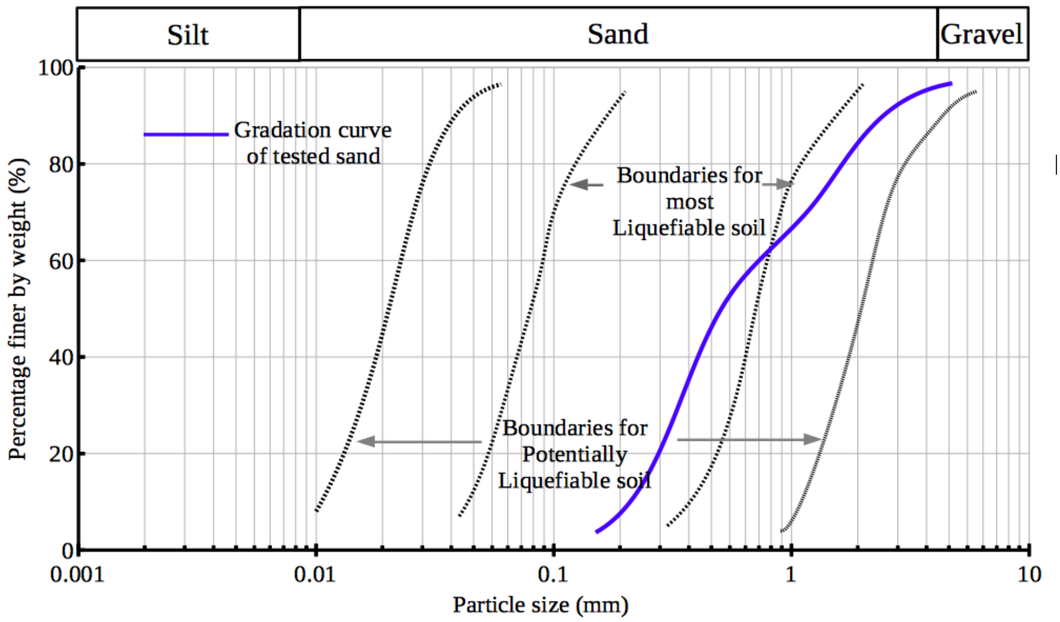

Figure 5.1: Particle size distribution of sand superimposed on proposed graph by Tsuchida (1970)

5.2 Properties of sand and stone columns

River sand procured from *Kalady* is used for conducting the study. The properties of sand and stone used for forming the stone columns are presented in Table 5.1 and Table 5.2. The particle size distribution of sand lies within the liquefiable ranges proposed by Tsuchida (1970) as shown in (Fig.5.1). The properties of geotextile used for wrapping is given in Table 5.3.

5.3 Details of experiments conducted

Initially, an experiment was conducted on saturated sand bed without the stone column. From the trial run, it is observed that the sand bend liquefied at $0.15g$ itself. Hence for further studies, the same acceleration and frequency are maintained. Further, in other experiments, stone columns are introduced at the centre of the model with diameter 50 mm and also 100 mm. Another investigation was conducted

Table 5.1: Properties of sand

Type	Poorly Graded Fine Sand
Sp. Gravity	2.59
D_{10} (mm)	0.21
D_{30} (mm)	0.36
D_{50} (mm)	0.50
D_{60} (mm)	0.70
C_u	3.33
C_c	0.882
Permeability (m/s)	$1.36 x 10^{-6}$
e_{max}	0.933
e_{min}	0.585

Table 5.2: Properties of stones used for stone column

Properties	for 50mm dia column	for 100mm dia column
Effective Size (mm)	6	14
Sp. Gravity	2.8	2.8
Fineness Modulus	6.46	3.71
C_u	1.33	1.22
C_c	1.08	1.11
Permeability (m/s)	$2.4 x 10^{-4}$	$2.5 x 10^{-4}$

Table 5.3: Properties of coir geotextile

Type	Non woven lined (NWL)
Mass per Area (GSM)	740
Thickness at 2 kPa (mm)	11.35
Wide tensile strength in machine direction (kN/m)	3.49

with 50 mm stone column encased in coir geotextile. This geotextile can provide the confining effect to the stone chips to keep it in position and minimise kinking during shaking. The relative density of sand is maintained at 45% (Medium dense state), and the intensity of shaking was kept constant at $0.15g$ for all the experiments. The sand bed is formed in four equal layers, each layer accommodating the required weight of soil. This helps to have greater control over density. While forming the model with the stone column, PVC pipe of required diameter is kept in position. After completing one layer of the sand bed, stone chips of 1/6 to 1/8 diameter of columns are introduced, compacted by tamping as recommended by Nayak (1983). The pipe is withdrawn slowly intermittently without disturbing the sand bed after completing each layer. Fig. 5.2 (a) shows the formation of a stone column using PVC pipe and (b) the stone column after forming the soil bed.

Pore water pressure sensor probes are placed in the desired position during the formation of the model. Fig.5.3 shows model dimensions and the sensor locations for the experiments conducted. The total height of the model was 400 mm. The model was then saturated from the bottom at a slow pace.

5.4 Results and discussion

The excess pore water pressure generated was monitored at three levels, top (at 100 mm depth), middle (at 200 mm depth) and bottom (at 300 mm depth). The sensors were kept close to the stone columns to monitor the excess pore water pressure at the boundary. Fig.5.4 shows the development and dissipation of excess pore water pressure during the experiment.

It is observed that the excess pore water pressure builds up immediately after the shaking. The values of r_u are 1.0 at a depth of 100 mm and 200 mm below the top surface and stay almost the same till the end of shaking when there are no columnar inclusions in the soil bed. Significant liquefaction was observed in this case at the

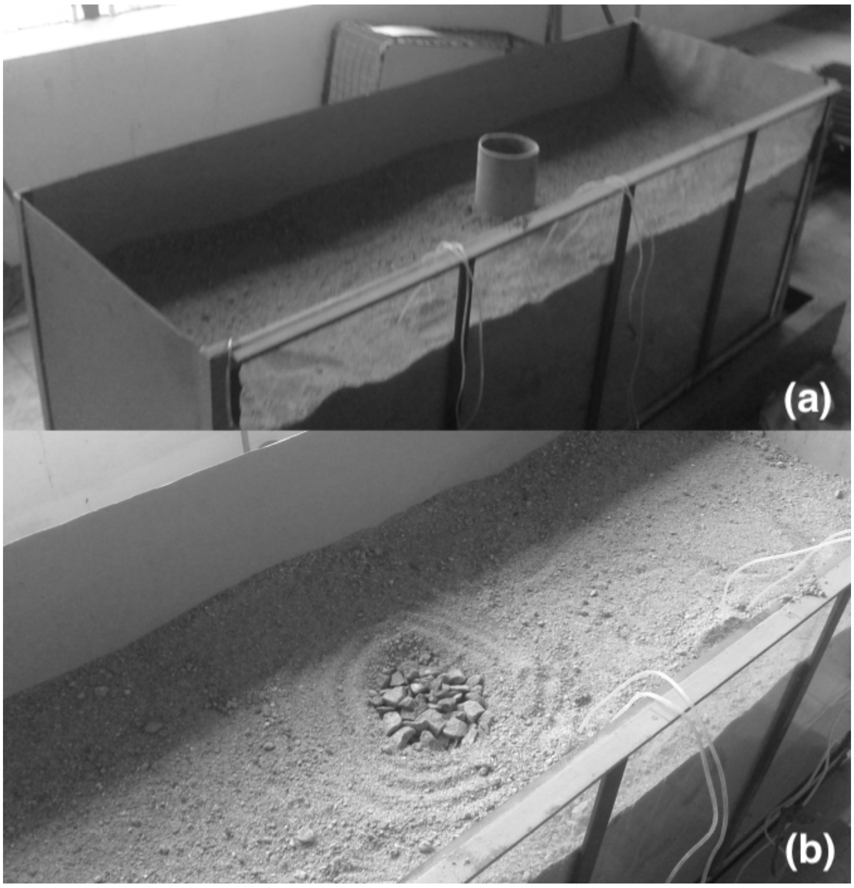

Figure 5.2: Formation of stone columns

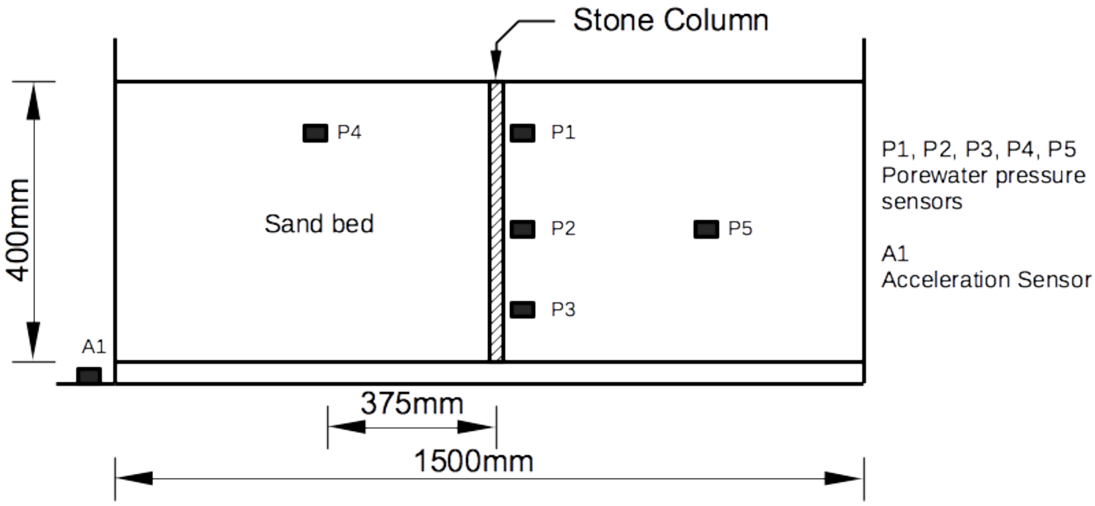

Figure 5.3: Location of sensors

top and middle layers. At 300 mm depth, the r_u value was 0.85.

r_u builds up to 0.85 at 100 mm depth when the stone column of 50 mm diameter was introduced. At 200 mm depth, the pore pressure ratio is 0.7, slightly lower than the value at the top. This value remains almost the same till the end of the shaking. This decrease in the pore pressure ratio is the result of dissipation of excess pore water pressure generated, through the stone column in the vertical direction.

During the experiment, it is visually observed that the soil in the topmost layer (approximately up to 30 mm) was liquefied. Even then, the sand bed was relatively stable, and the deformations were very small beyond a depth of about 100 mm. When the diameter of the stone column is 100 mm, the excess pore water pressure ratio initially builds up 0.6 at 100 mm depth, but immediately, approximately within 10 seconds, decreases to near zero values even when the shaking was present. No liquefaction was observed in this case. The sand bed was stable, and no water layer formed at the top surface.

The geotextile wrapped column of 50 mm diameter showed a similar build-up and dissipation behaviour as that of the 100 mm diameter column, but with a slightly higher value of r_u. No liquefaction was observed in this case. It may be noted that with a 50 mm stone column with two layers of geotextile wrapping results in an increase in the diameter of the inclusion to nearly 90 mm.

The maximum excess pore water pressure ratio at all depths was observed to be less when the stone column is introduced as seen in Fig. 5.5, indicating improved drainage. At 100 mm depth, 15% reduction in r_u is observed with the introduction of 50 mm diameter column whereas 40% reduction is observed when the diameter of the column is 100 mm. The percentage reduction obtained with geotextile wrapped column is 20%. At mid-depth, the reduction in r_u is 20%, 60% and 40% with the stone column of diameter 50 mm, 100 mm and 50 mm geotextile wrapped column respectively. At the bottom layer (300 mm depth), nearly 28% reduction in r_u is observed when the stone column diameter is 50 mm. The reduction in r_u

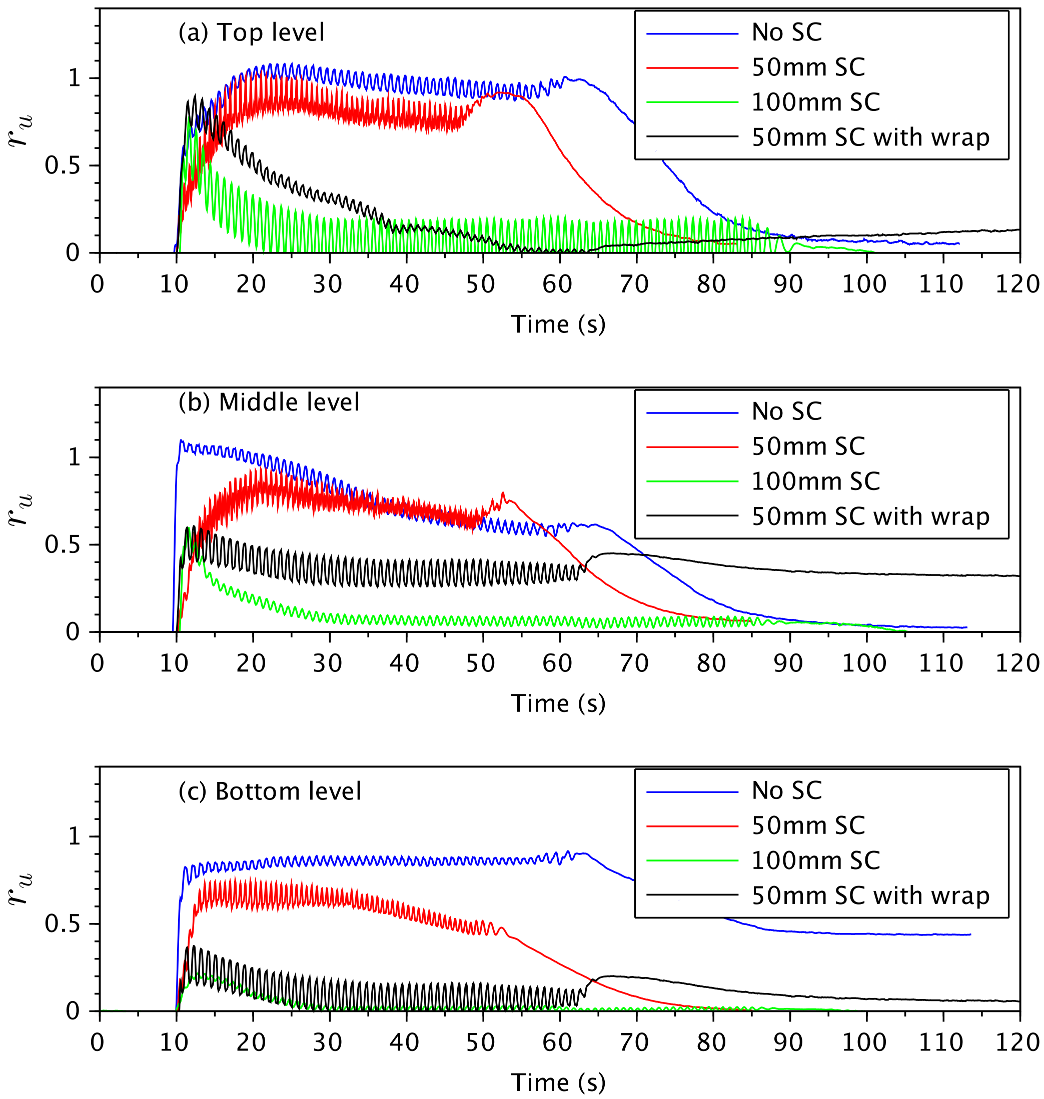

Figure 5.4: Excess pore pressure ratio with and without stone columns

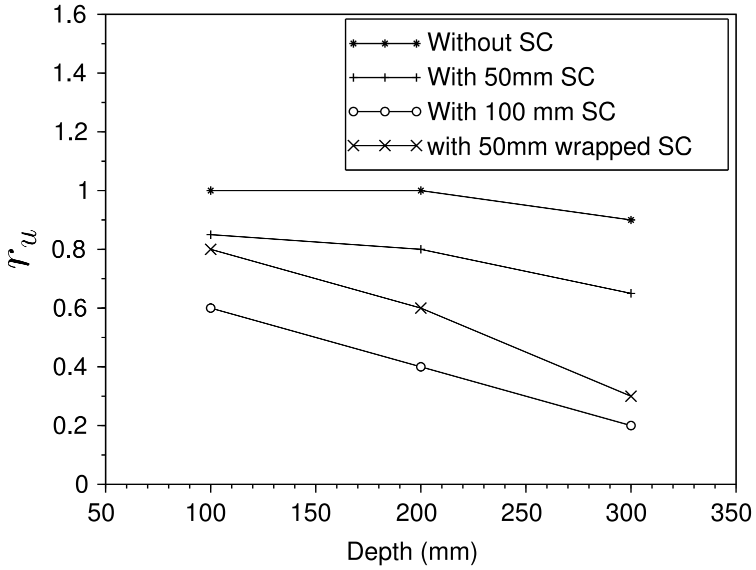

Figure 5.5: Maximum excess pore pressure ratio with and without stone columns

Table 5.4: Depth of liquefaction observed in experiments

Case	Observed depth to which soil liquefied (approximate)
Without stone column	350 mm (almost full depth)
With 50 mm stone column	30 mm
With 100 mm stone column	0 (no liquefaction)
with 50 mm wrapped stone column	0 (no liquefaction)

for 100 mm column is very high and nearly 78%. The wrapped column resulted in a reduction of 67%.

During the experiments, the depth of sand layer which is taking part in the process of liquefaction can be observed visually. Markings are made on the transparent side of the box and the values observed are tabulated in Table 5.4 for the different models studied.

5.5 Summary

The performance of stone columns as a liquefaction mitigation measure was presented in this chapter. Experimental investigations suggest that a considerable reduction in the development of excess pore water pressure during shaking can be achieved as a result of easy and fast drainage created by installing stone columns. The average reduction in r_u obtained with 50 mm diameter column is 21%, 100 mm column is 59%, and 50 mm geotextile wrapped column is 42%. The effectiveness of the stone column increased with an increase in diameter of the column. A geotextile wrapping around the column increases its efficiency by keeping the stones intact within the column. It is ascertained that stone columns are a suitable method for mitigating liquefaction due to the additional drainage created.

CHAPTER 6

NUMERICAL MODELLING AND VALIDATION

6.1 Introduction

Numerical modelling provides a feasible solution when conducting a large number of experiments or testing large sized models are practically difficult. But, one of the limitations of numerical modelling is arriving at the most appropriate model for simulating the behaviour of the materials. Soil often present a huge challenge in modelling due to the inherent uncertainties in the behaviour as well as non-linearity in the stress-strain relationship. In the case of liquefaction studies, modelling pore pressure build-up also requires special modelling techniques. In the present chapter, the development of a finite element model using *OpenSees* platform is described and the model is validated using the experimental results obtained from the shake table tests.

6.2 Opensees

The software platform *OpenSees* was chosen because of two major reasons, viz., its advanced simulation capabilities with specific models for liquefaction modelling, and it is free and open-source. There is also no constraint on the size of the model that can be analysed. This software is an interpreter and can be run from the command line interface and can read text files written in the Tool Command Language (TCL). Initially, the software source code was downloaded from the website and compiled in a local computer for conducting the analysis. To perform the analysis, input files had to be created using the *OpenSees* commands in TCL.

This input file consists of three essential components (1) the model details – material properties, nodes, elements, loads and boundary conditions etc., (2) The analysis options – time steps, algorithm, convergence criteria etc. and (3) the output recorders – details of output required, like, displacements, stresses, strains, pore pressure, temperature etc.. This file is created using the standard text editor and saved with an extension *.tcl*. For easy file management, the details of nodes, elements and boundary conditions are created and saved separately and invoked in the input file. The output recorder files are specified for displacements and pore water pressure at all nodes for all time steps and the stresses and strains for all the elements for all time steps. The input file is shown in Appendix B.

6.3 Validation of model

The experiment was modelled as a two-dimensional Finite Element Analysis plane strain model using the *OpenSees* platform. Permeability matching method was used to convert the problem to a plane strain model in line with the suggestions of Tan *et al.* (2008). The soil is modelled using four node elements with coupled u-p formulation (Elgamal *et al.*, 2009), which can simulate pore water pressure build and dissipation due to dynamic loading. The unknowns in this formulation are displacement of the solid phase (u_{xy}) and pore fluid pressure (p_u). The basic equation of the formulation is as follows:

$$M\ddot{U} + \int_v B^T \sigma' dV - QP - f^{(s)} = 0 \tag{6.1}$$

$$Q^T \ddot{U} + HP + S\dot{P} - f^{(p)} = 0 \tag{6.2}$$

Where M is the mass matrix, U is the solid displacement vector, B is the strain-displacement matrix, σ' is the effective stress tensor Q indicates the discrete

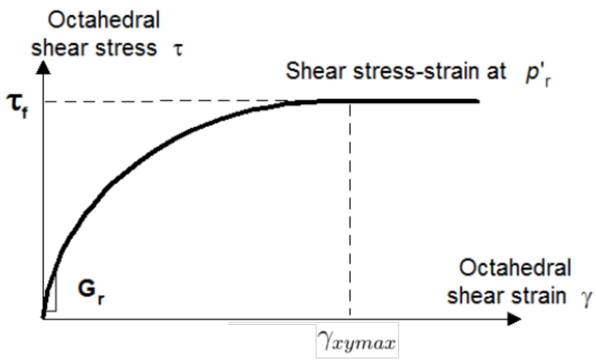

Figure 6.1: Stress strain characteristics used for soil modelling

gradient operator coupling the motion and flow equations, P is the pore pressure vector, S is the compressibility matrix and H is the permeability matrix. The vector $f^{(s)}$ include the effects of body forces and external loads and $f^{(p)}$ includes fluid fluxes. The material is modelled as Pressure Dependent Multi Yield model (PDMY), which include characteristics like dilatancy, cyclic mobility, etc.. The stress-strain response is linearly elastic during gravity load and elastic-plastic during the dynamic loading phase. The yield surfaces are of Drucker Prager type as shown in Fig. 6.1. G_r and γ_{xymax} are the low-strain shear modulus and maximum shear strain specified at a reference mean effective confining pressure p_r. Both sand and stone column were modelled using the same element formulation.

The discretised model has a regular grid of variable size elements with 171 nodes and 144 quadratic elements and the same dimensions of the experimental set up with denser mesh at the location of the stone column. Each element node has two displacement degrees of freedom and one additional degree of freedom for pore water pressure. The nodes at the bottom were fixed in x and y directions, and the boundary end nodes were constrained in the x-direction. The drainage condition was constrained at the bottom and freed at the top. The discretised model is shown in Fig. 6.2.

A sinusoidal base excitation, representing the input acceleration is applied in the model. The major input parameters used in the model are shown in Table 6.1. The mass density, friction angle and permeability of the soil and stone column are

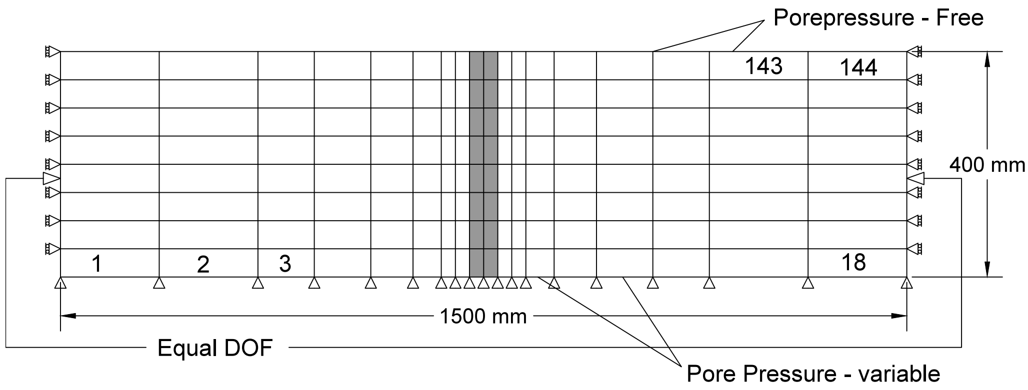

Figure 6.2: Finite Element Model of the shake table experiment

Table 6.1: Input parameters of FEA model (Yang *et al.*, 2003)

Parameter	Sand	Stone Column
Mass Density (kg/m^3)	1930	2100
Permeability (m/s)	1.36×10^{-6}	2.5×10^{-4}
Shear Moduls in MPa (80kPa confinement)	75.0	130.0
Friction Angle	33	40
Peak shear strain	10%	0
Phase Transformation Angle	27	27
Contraction parameter	0.2	0.03
Dilation parameter-1	0.4	0.8
Dilation parameter-2	2.0	5
Liquefaction parameter-1	10.0	0.0

obtained from laboratory experiments. Based on that values it can be assumed that the soil is medium dense state. The other model parameters are chosen based on the recommended values for medium dense sand recommended by Yang *et al.* (2003).

In the analysis, the excess pore pressure at every node and stresses and stains in all elements were recorded for all the time steps.

In order to validate the formulation, the experimental data and FEA results of excess pore water pressure ratio are plotted together in Fig. 6.3, 6.4 and 6.5, corresponding to top, middle and bottom level respectively. It can be seen that the Finite Element analysis provided a very good prediction of the measured excess pore water pressure

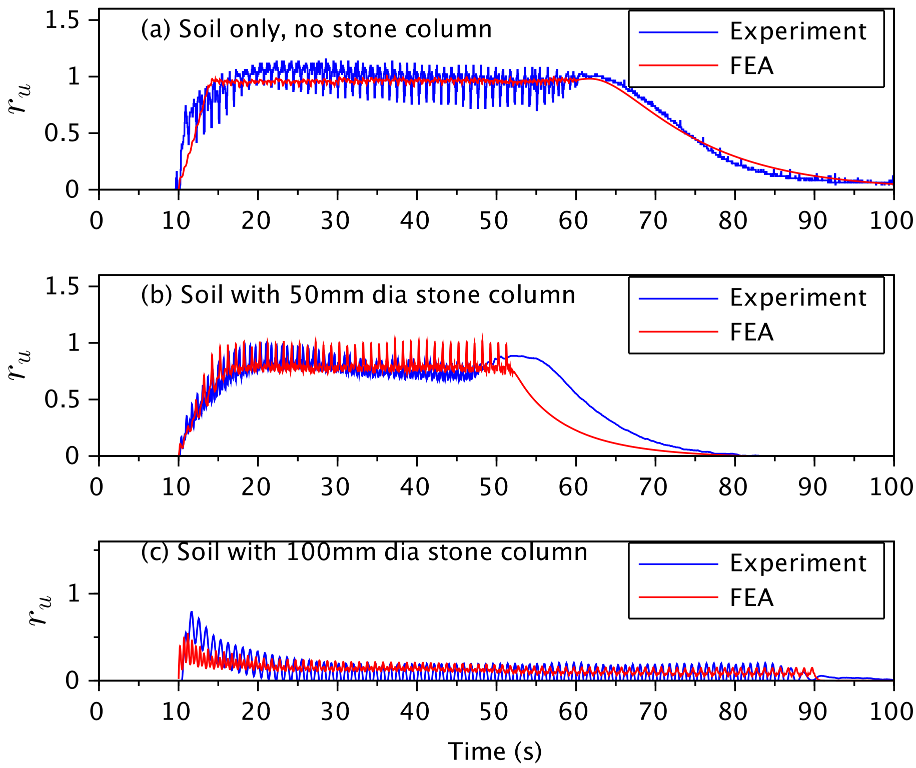

Figure 6.3: Comparison of excess pore water pressure ratio at top (P1)

ratio at the different levels (P1, P2 & P3), which were monitored with sensors.

Figure 6.6 shows the comparison of the maximum excess pore water pressure ratio observed during experiments and FEA. At the top level, i.e., 100 mm depth, the difference between the maximum excess pore water pressure obtained from FEA and experiments are 0.02 kPa, 0.05 kPa and 0.1 kPa for sand bed along with no stone column, with 50 mm and 100 mm stone columns respectively. At the middle level, the corresponding differences are 0.2 kPa, 0.0 kPa and 0.05 kPa respectively. At the bottom level, the differences are 0.1 kPa, 0.2 kPa and 0.02 kPa for the same cases. The differences are reasonably within limits, and it can be concluded that the FEA model can satisfactorily predict the excess pore water pressure due to dynamic loading.

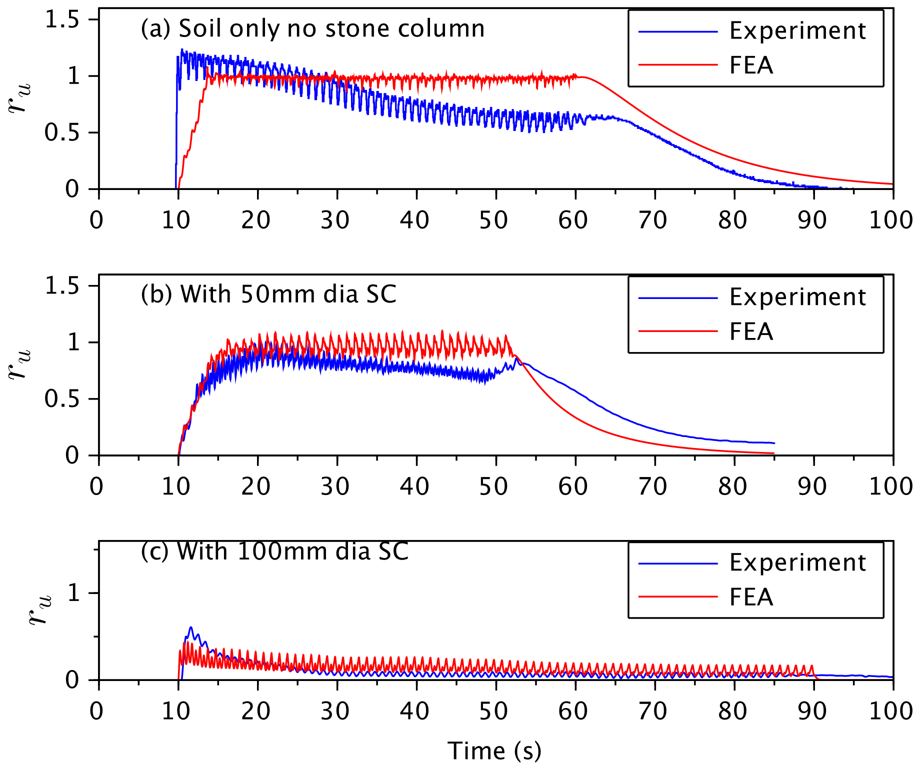

Figure 6.4: Comparison of excess pore water pressure ratio at middle (P2)

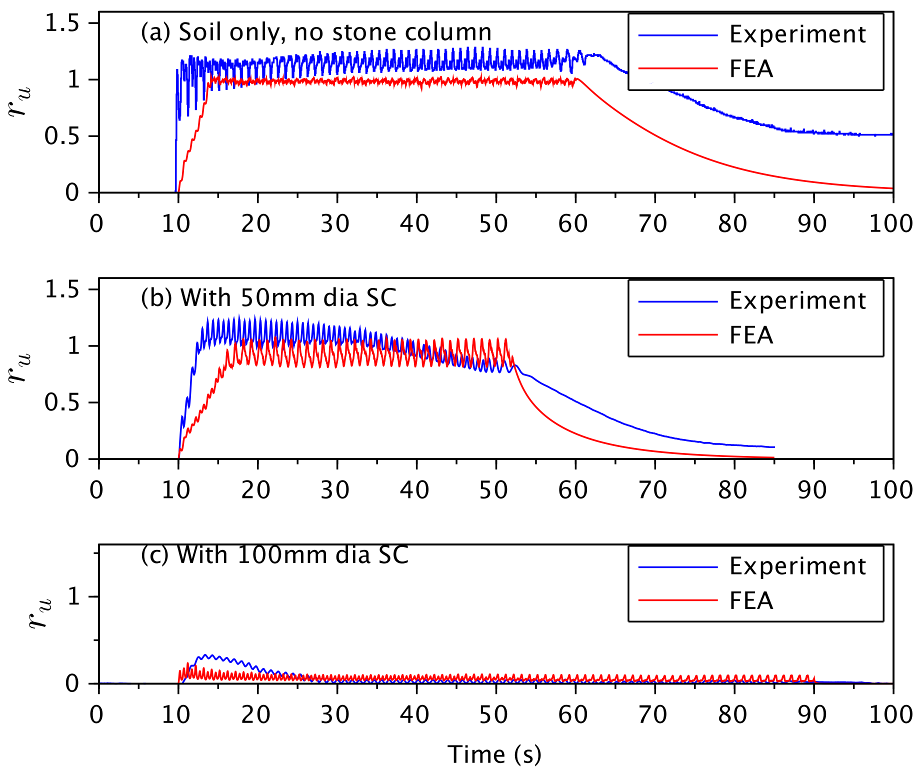

Figure 6.5: Comparison of excess pore water pressure ratio at bottom (P3)

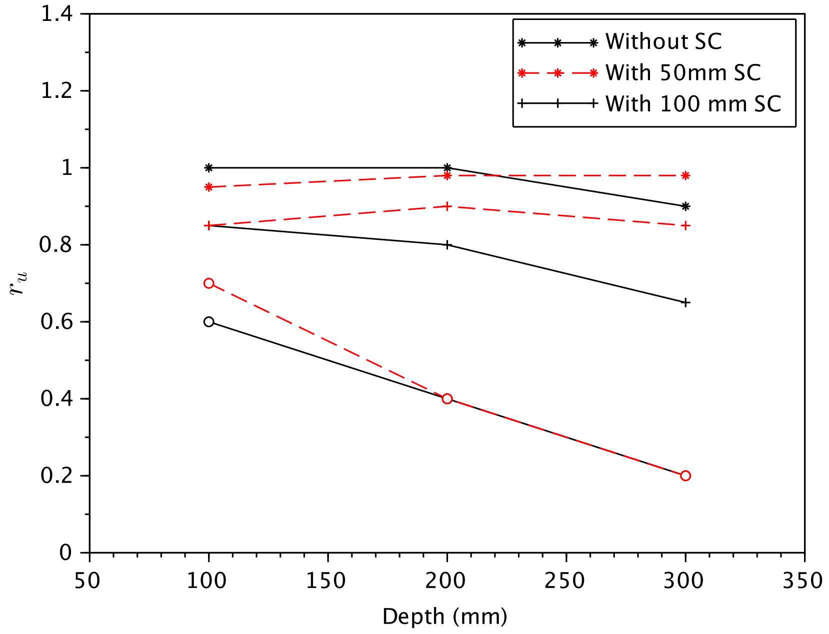

Figure 6.6: Comparison of maximum excess pore water pressure from FEA and experimental results

6.4 Pore pressure distribution and end effects

Figure 6.7 shows the pore pressure distribution contours in the FEA model immediately after the shaking is started (0.01 s). It is observed the contours are almost horizontal indicating that the pore water pressure is almost the same along a particular depth. The pore pressure increases as depth increases and the maximum value is seen at the bottom of the model. It is also observed that the build-up of pore pressure is less when the stone column is present. This is because of the drainage provided by the stone column.

Figure 6.8 shows the contours after 1.0 s, and the influence of the stone column is more distinguishable. The pore pressure values are clearly lower – reduces approximately from 2.5 kPa for soil only to 1.9 kPa and to 1.6 kPa at the mid-depth for 50 mm and 100mm dia column respectively. A dip in the shape of the contour is observed at the centre of the model, where the stone column is present.

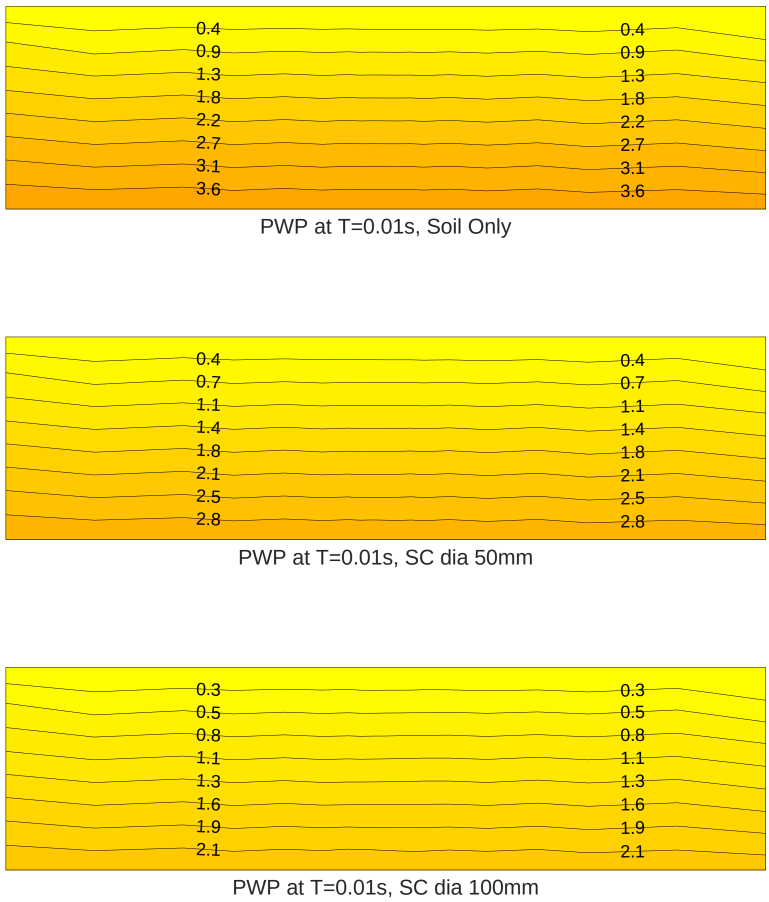

Figure 6.7: Pore water pressure in FEA model at start

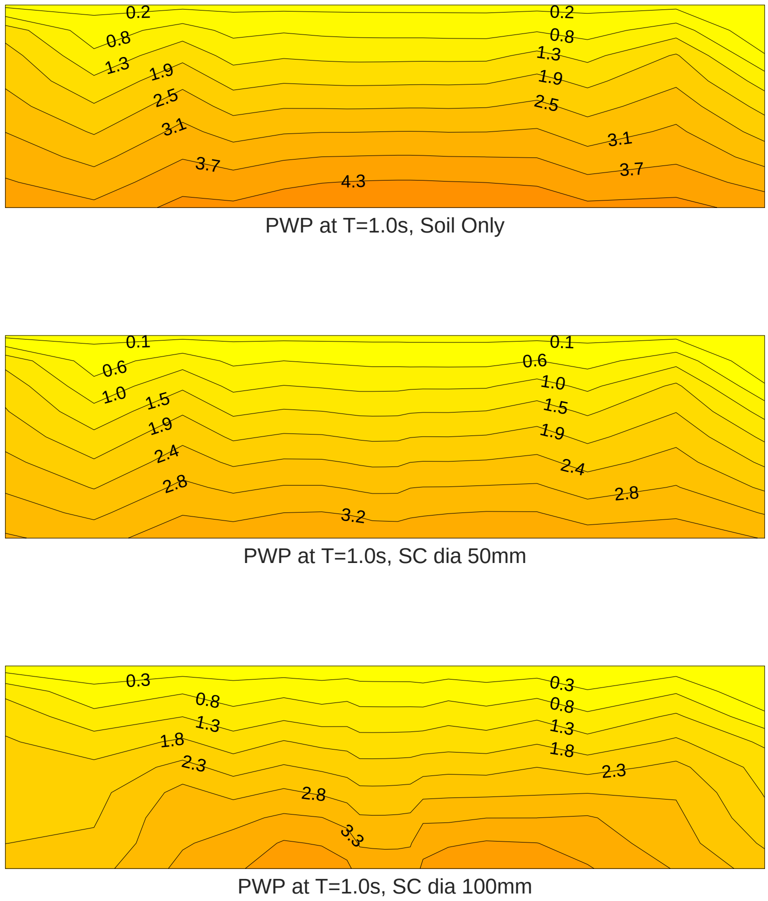

Figure 6.8: Pore water pressure in FEA model at 1.0 s

This is due to the influence of radial drainage of water into the stone column and a resulting decrease in the pressure around it.

Further, at 10 s, in Fig. 6.9, the reduction in pore water pressure in the periphery of the stone column is more evident. The reduction is approximately from 3.9 kPa for soil only to 3.1 kPa and 2.4 kPa at the mid-depth for 50 mm and 100mm dia column respectively. Also, the drainage provided by the stone column seems to have reduced the pore pressure in the entire model.

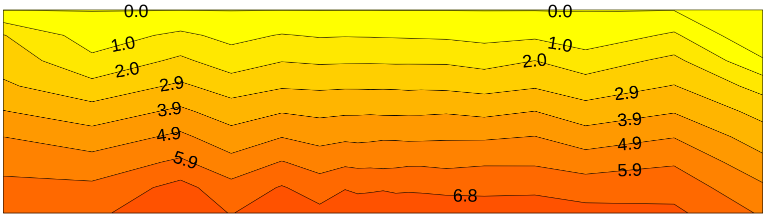

PWP at T=10.0s, Soil Only

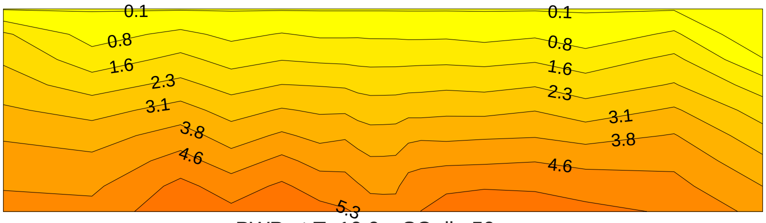

PWP at T=10.0s, SC dia 50mm

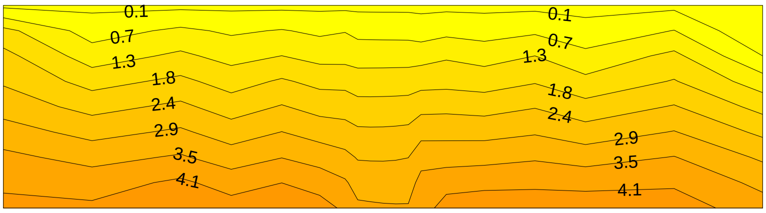

PWP at T=10.0s, SC dia 100mm

Figure 6.9: Pore water pressure in FEA model at 10.0 s

As the shaking take place, the saturated soil within the container move towards one boundary of the box, and at the same time instant, move away from the boundary on the opposite side. This can lead to an increase in the pore pressure at the forward boundary and a reduction in the other side. This pattern can be clearly observed from the contours in Fig. 6.7, 6.8 and 6.9 in the form of a heave at one end and a dip at the other end for the same contour. This change in pressure near the ends of the model is because of the presence of the rigid boundary. This phenomenon is seen approximately at a distance of 1/8 L consistently in all cases.

6.5 Stress strain behaviour

Figure 6.10 (a), (b) & (c) shows the development of shear strain in the soil at the mid-depth of the model, during shaking, for soil without the stone column and with stone columns of diameter 50 mm and 100 mm respectively. A reduction in shear modulus due to the buildup of pore water pressure can be seen in the case with no stone column (Figure 6.10 (a)), which can be observed from the increase in the slope of the curves with each cycle of loading. Here, the excess pore water pressure buildup was sufficient to induce liquefaction in the model. The presence of stone column decreases the reduction in shear modulus as can be observed from the steeper curves in Fig. 6.10 (b). This may be due to the dissipation of pore water pressure owing to the higher permeability of the stone column. In the case of 100 mm diameter column (Figure 6.10 (c)), the pore pressure build-up is not sufficient to create a reduction in shear modulus, but a build up of shear strain is observed. The observation of greater shear strains with the granular column is consistent with the findings of Goughnour and Pestana (1998) and can be attributed to the actual deformation mechanism not being pure simple shear when the granular column is present.

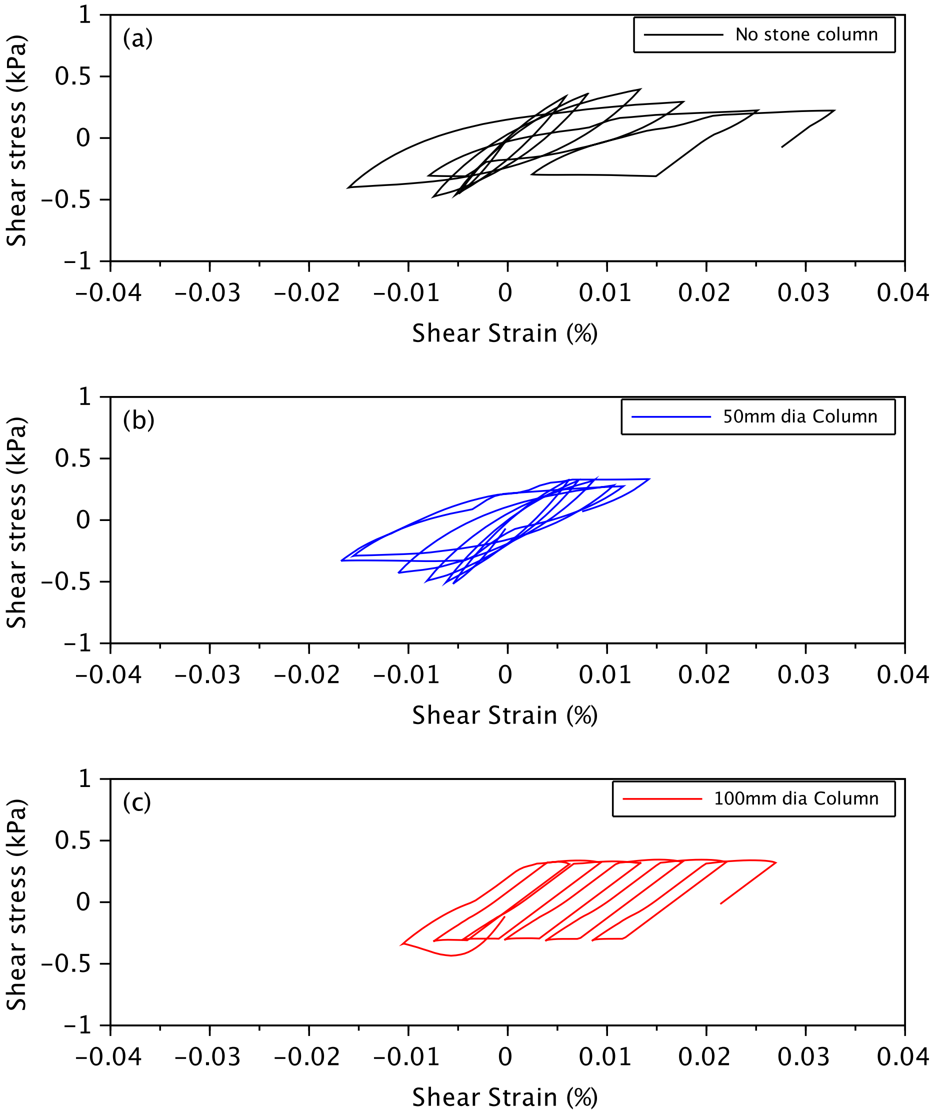

Figure 6.10: Shear stress vs shear strain in improved soil at at mid depth

6.6 Summary

The finite element model developed using *OpenSess* was found to predict the excess pore water pressure value which compares well with the experimental results. The percentage deviation of predicted excess pore water pressure from the observed value is approximately 6%. The FEA model also helped to understand the behaviour of the complete system and, it is observed that the end effects are present till 1/8 times the length of the box. The stress-strain behaviour indicated that the reduction in shear modulus of the soil due to build up of pore water pressure is less when the stone column is present.

CHAPTER 7

PARAMETRIC STUDY USING FEA

7.1 Introduction

In the previous chapter, it was shown that the 2D finite element models developed on *OpenSees* platform can satisfactorily predict the excess pore water pressure buildup and dissipation in problems involving saturated sands with stone columns subjected to sinusoidal shaking.

The literature survey has revealed that many experimental and numerical studies have been conducted on stone columns on liquefiable sands, but, researchers have not attempted the behaviour of partially penetrating stone columns in liquefiable deposits. Such a study has relevance, since, the economy of the ground improvement method depends on the depth of the stone column used. Hence, a detailed parametric study has been attempted here to understand the behaviour of liquefiable ground, modified with partially penetrating stone columns. A larger system is chosen for the parametric study to represent the real-life field application.

The current chapter discusses the results of this parametric study conducted to understand the effect of depth of penetration and diameter of stone columns in the pore water pressure buildup for soils with different permeability, density and subjected to different ground motion acceleration. Since the parametric study involves numerous analysis cases, the parallel analysis option of *OpenSees*, *OpenSeesMP* is utilised.

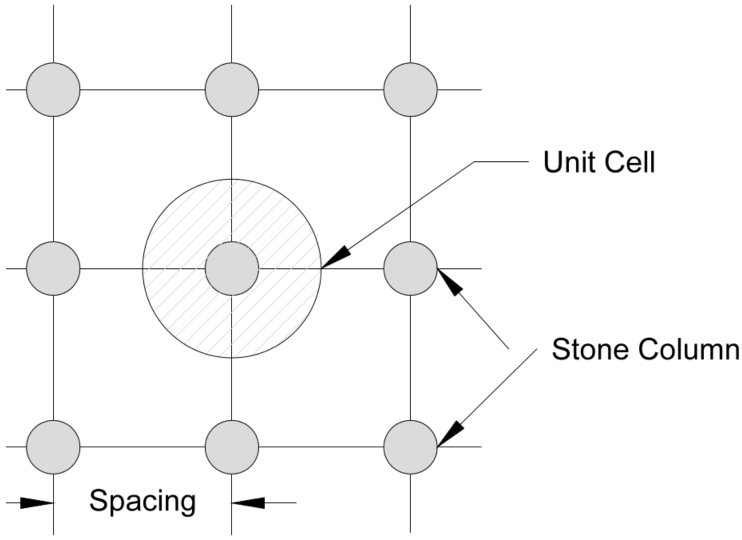

Figure 7.1: Unit cell used for FEA modelling

7.2 FEA Model

Stone columns are typically installed at a uniform spacing in grid form in the ground. A unit cell which represents the area of improved soil was used for the finite element modelling of soil and discrete columns. This modelling technique has been used by previous researchers Rayamajhi *et al.* (2013, 2016*a*,*b*). Fig. 7.1 shows the unit cell used for the study, which is axisymmetric in nature.

For the parametric study, to consider different area replacement ratios, the spacing is kept constant as 2.1 m, and the diameter of the column is varied. The depth of soil stratum that is being improved is also kept constant as 12 m. A two-dimensional plane strain model of the soil stratum is used for all the analysis. The permeability matching method was used to convert the problem to a plane strain model (Tan *et al.*, 2008; Howell, 2013). Fig. 7.2 shows the discretised model used for the study. A regular grid was used to discretise the model to make the analysis of the results of the parametric study simple, since, the data to be handled is of large volume.

Multiple analysis with different mesh configurations were conducted for mesh optimisation to arrive at the number of elements used for the study. The mesh size

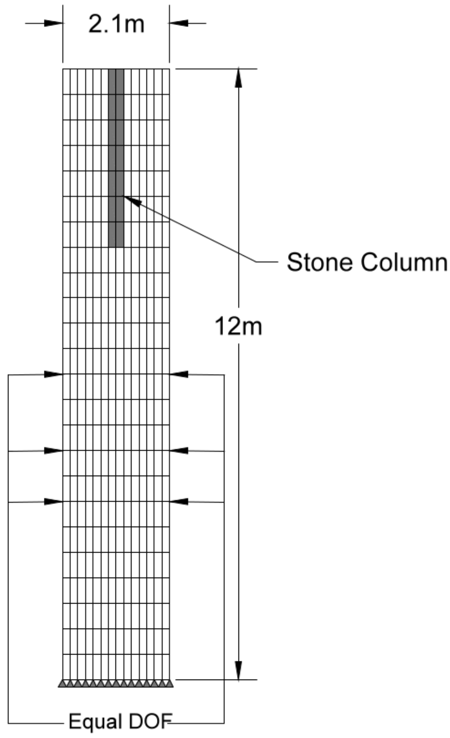

Figure 7.2: Discretised 2D plane strain FEA model of ground with stone column

which gives no further significant changes in the pore pressure value for further increase in mesh density was chosen for the analysis. The model used for the analysis has 375 nodes and 336 elements. The element model used was quadratic with four nodes. Each node has two displacement degrees of freedom in x and y directions and one additional degree of freedom for pore water pressure. Equal degree of freedom was imposed at the sides of the model to represent continuity at the unit cell boundary. The bottom nodes were fixed in both x and y directions, and the pore pressure boundary condition was constrained for no drainage. The pore water pressure boundary condition was freed at the top to simulate drainage. The nodes at the outer boundary at the same level were tied together in the direction of application of sinusoidal motion as recommended by Howell *et al.* (2014); Karamitros *et al.* (2012); Karimi and Dashti (2016).

The analyses were carried out for three different densities of soil - loose sand, medium sand and medium dense sand. The soil and stone column parameters used

Table 7.1: Parameters used for FEA adopted from Elgamal *et al.* (2009)

Parameters	Loose Sand (Dr 15%-35%)	Medium Sand (Dr 35%-65%)	Medium-dense Sand (Dr 65%-85%)	Stone Column
Saturated Density ($\rho kN/m^3$)	17.0	19.0	20.0	21.0
Shear Moduls (kPa)	5.5×10^4	7.5×10^4	1.0×10^5	1.3×10^5
Bulk Modulus (kPa)	1.5×10^5	2.0×10^5	3.0×10^5	3.9×10^5
Friction Angle	29	33	37	40
Peak Shear Strain	0.1	0.1	0.1	0.1
Pressure Dependence Coeff.	0.5	0.5	0.5	0.5
Phase Transformation Angle	29	27	27	27
Contraction Parameter	0.21	0.07	0.05	0.03
Dilatancy Parameter 1	0	0.4	0.6	0.8
Dilatancy Parameter 2	0	2	3	5
Liquefaction Parameter 1	10	10	5	0
Liquefaction Parameter 2	0.02	0.01	0.003	0
Liquefaction Parameter 3	1	1	1	0
Initial Void Ratio (e)	0.85	0.7	0.55	0.45

for the FEA are given in Table 7.1. The values were adopted from Elgamal *et al.* (2009).

7.3 Parameters chosen for study

A total of 1440 analysis with stone columns and 90 analysis without stone column were performed. The various parameters that are varied are given in Table 7.2.

The permeability of the stone column is kept constant as $1 \times 10^{-3} m/s$ and the frequency of shaking as 1 Hz for a time period of 10 seconds in all the analyses cases. A time of shaking of 10 seconds or 10 significant stress cycles can be considered equivalent to an earthquake magnitude of 7.0 (Seed and Idriss, 1971).

7.4 Analysis options chosen for the study

The analyses were conducted on a high-performance computing machine, which has 32 cores and 64GB of RAM. To run parametric studies, the parallel version

Table 7.2: Range of parameters chosen for study

Density	Diameter of SC (m)	Depth of SC (m)	Permeability of sand (m/s)	Acceleration in g	No. of analysis performed
Loose	0.3, 0.6, 0.9, 1.2	3.0, 6.0, 9.0, 12.0	5e-4, 1e-4, 5e-5, 1e-5, 5e-6, 1e-6	0.05, 0.10, 0.15, 0.20, 0.25	480
Medium	0.3, 0.6, 0.9, 1.2	3.0, 6.0, 9.0, 12.0	5e-4, 1e-4, 5e-5, 1e-5, 5e-6, 1e-6	0.05, 0.10, 0.15, 0.20, 0.25	480
Medium Dense	0.3, 0.6, 0.9, 1.2	3.0, 6.0, 9.0, 12.0	5e-4, 1e-4, 5e-5, 1e-5, 5e-6, 1e-6	0.05, 0.10, 0.15, 0.20, 0.25	480
Loose	-	-	5e-4, 1e-4, 5e-5, 1e-5, 5e-6, 1e-6	0.05, 0.10, 0.15, 0.20, 0.25	30
Medium	-	-	5e-4, 1e-4, 5e-5, 1e-5, 5e-6, 1e-6	0.05, 0.10, 0.15, 0.20, 0.25	30
Medium Dense	-	-	5e-4, 1e-4, 5e-5, 1e-5, 5e-6, 1e-6	0.05, 0.10, 0.15, 0.20, 0.25	30
				Total	1530

of the program, *OpenSeesMP* is used. In *OpenSeesMP*, multiple analyses can be run in parallel utilising all the cores of the system. This is facilitated by a program called "Message Passing Interface" (MPI). An input script was written to allocate 32 analysis jobs to each of the cores at the same time. The script will then allocate successive job as soon as any of the allotted analyses jobs are completed. The result files are written with different names which help to identify the analysis cases. This procedure helped in automating the parametric study. The program is run from the command line by invoking the command

```
nohup mpirun -np 32 OpenSessMP input.tcl &
```

Here, `nohup` is a program that prevents any hang-up while executing the program, `mpirun -np 32`, invokes 32 processess of *OpenSeesMP* in one instant and `&` is used to run the program in the background. The program used for performing the analysis is included in Appendix C. The total time required for conducting all the analysis could be reduced to 50 hours using this technique.

To run dynamic analysis in OpenSees, a few additional options are to be defined. The material properties are updated as nonlinear after the gravity analysis. The FE matrix equation is integrated using the Newmark's Method, and the solution for each time step is obtained using the Krylov-Newton algorithm. The stresses and strains at all integration points, displacements in both x and y directions and the pore water pressure at all nodes at all time steps are recorded in separate files during the analysis. These results are obtained in simple text format which was read using a program written using Python and Octave for post-processing and plotting.

7.5 Analysis of FEA results

The results obtained from the different analysis performed are classified and analysed to understand the factors affecting the development of excess pore water pressure in soil stratum improved with stone columns. The distribution of excess pore water pressure ratio (r_u) in the model is plotted as a colourmap to understand the behaviour. Though the analysis has been done for all the 1530 combinations, for the purpose of discussion of results, only typical cases are considered. While discussing the variation of a parameter, one typical system is considered, and all other parameters are kept constant.

7.5.1 Variation of excess porewater pressure ratio with respect to the diameter of stone column

Fig. 7.3 shows the distribution of r_u in the model when it is subjected to a sinusoidal acceleration of $0.10g$ for 10 s. The values at 1 s, 5 s and 10 s are shown for loose sand with a stone column of 6 m depth. The permeability of soil is $1 \times 10^{-4} m/s$ and that of stone column is $1 \times 10^{-3} m/s$.

It can be noted that the soil liquefied completely within 5 s indicated by a r_u value ≥ 1.0 when no stone column is present. When the stone column diameter is 0.3 m, there is a reduction in r_u, but this is effective only to the depth to which the stone column is present, and that too only during the initial time. Beyond this depth, r_u close to 1.0, indicating liquefaction. A similar behaviour is observed when the diameter of the stone column is 0.6 m, but with a slightly more reduction in r_u. When the diameter is 0.9 m and 1.2 m, the stone column could almost prevent the liquefaction with $r_u < 1.0$ to the depth to which it exists. Interestingly, the value of r_u below the stone column is ≥ 1.0, and the soil is liable to liquefaction.

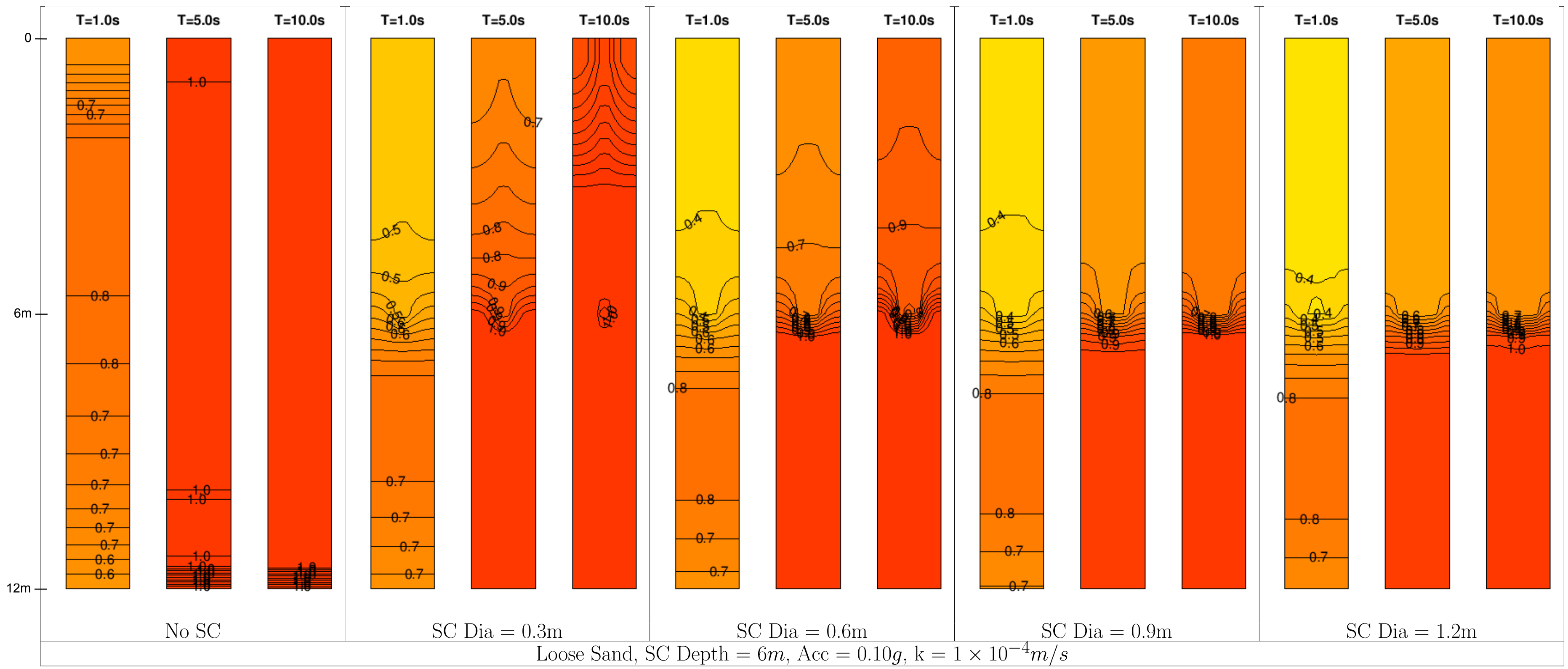

Figure 7.3: Variation of excess porewater pressure ratio with respect to diameter of stone column

Fig. 7.4 shows the variation of r_u at the boundary of the model, 1 m depth, with 6 m deep column subjected to $0.1g$ and k=$1 \times 10^{-4} m/s$ at 10 s. It can be observed that the r_u value decreases as the diameter of the column increases for loose, medium as well as medium dense sand. Increasing the diameter of the column improves the permeability around the stone column leading to a lesser value of r_u.

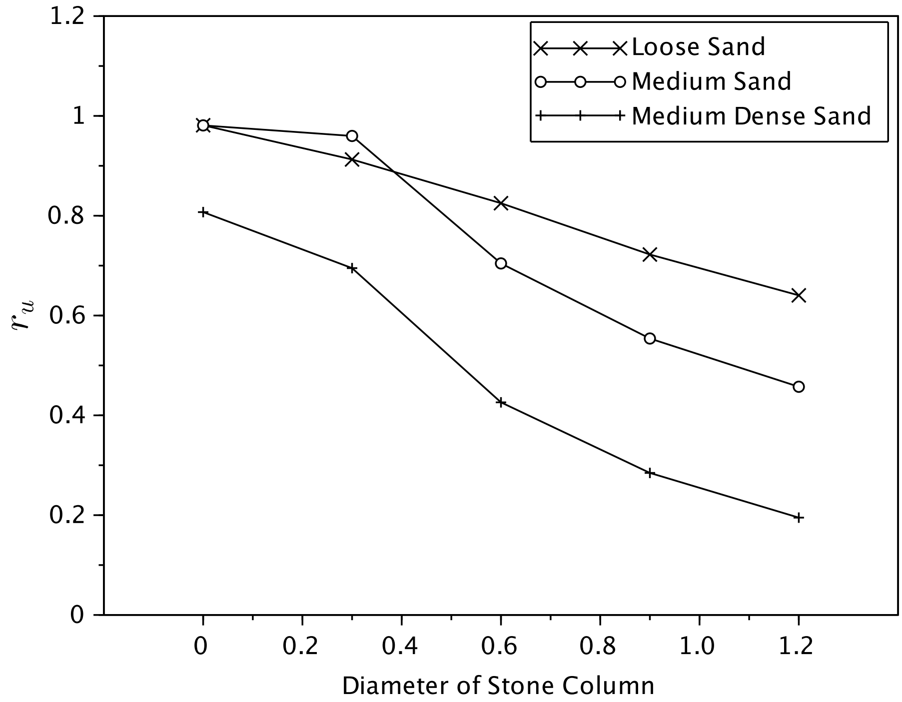

Figure 7.4: Variation of EPWPR at 1 m depth at boundary, with 6 m deep column, $0.1g$ and k=1×10^{-4} m/s at 10 s

7.5.2 Variation of excess porewater pressure ratio with respect to the depth of stone column

Fig. 7.5 shows the distribution of r_u, when the stone column depth is varied. The figure shows the distribution of r_u for the case with medium dense sand having permeability $1 \times 10^{-5} m/s$, with stone column diameter 0.6 m and subjected to a ground acceleration of $0.10g$ at 10 s. In all the analysis cases studied, it is observed that the stone column is effective in reducing the pore pressure build up around it, but, not beyond the depth of the column. This can be attributed to the improved drainage around the stone column and the resulting improvement in the dissipation of the pore water pressure developed due to shaking. Apparently, there is no improvement in the soil below the stone column depth, which can be seen clearly with r_u values ≥ 1.0. When the depth of the stone column is 12 m (total depth), liquefaction is completely eliminated as seen in the last image in Fig. 7.5, the values of r_u is well below 1.0.

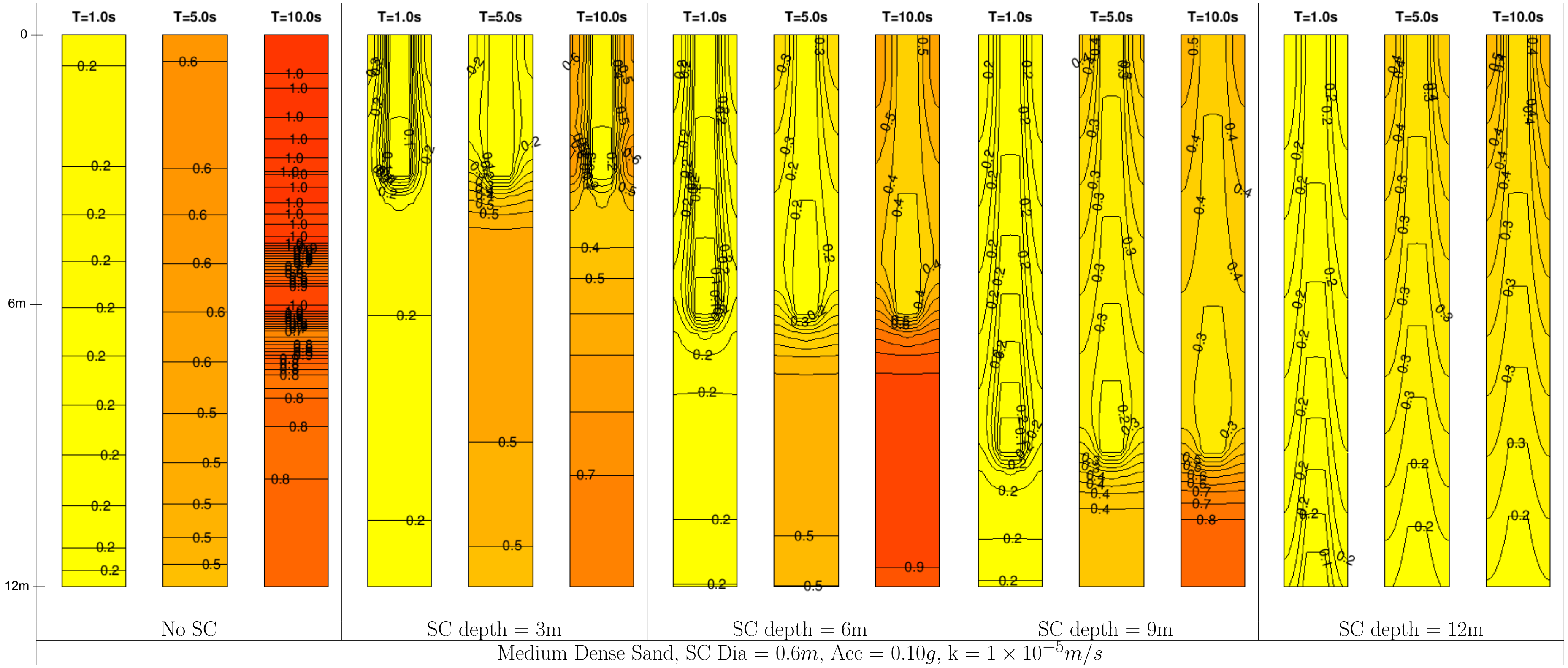

Figure 7.5: Variation of excess porewater pressure ratio with respect to depth of stone column

Fig. 7.6 depicts the variation of r_u at 1 m depth as the depth of stone column is varied for loose, medium and medium dense sand with the same permeability of 1×10^{-4} and subjected to $0.10g$ at 10 s. It can be observed that there is a reduction in r_u due to the presence of SC and r_u increases when the depth of the stone column is more.

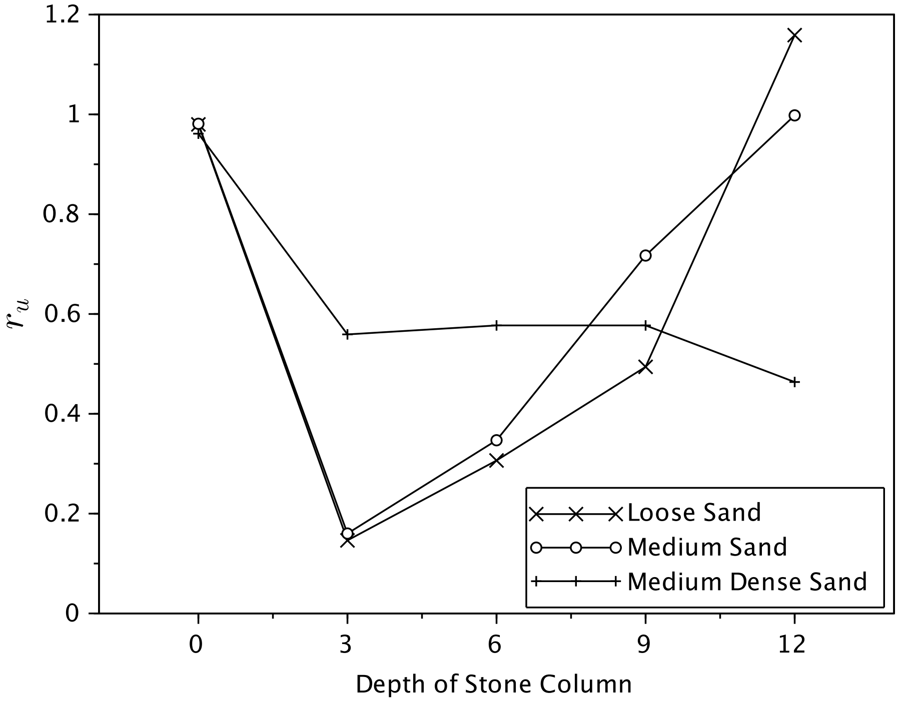

Figure 7.6: Variation of EPWPR at 1 m depth at boundary, with 0.6 m diameter column, $0.1g$ and k=1×10^{-4} m/s at 10 s

7.5.3 Variation of excess porewater pressure ratio with respect to the permeability of sand

To understand how permeability of sand affects the pore pressure buildup, the distribution of r_u in medium sand with stone column of diameter 0.3 m and depth 6 m subjected to a ground motion acceleration of $0.05g$ is compared for a range of permeability of sand $1 \times 10^{-4} m/s$ to $1 \times 10^{-6} m/s$ at 10 s as shown in Fig. 7.7. Normally, if the permeability of sand is less, the excess pore water pressure generated will take more time to dissipate, since, the velocity of flow depends on permeability. In the presence of a stone column, the radial flow of pore water towards the stone column will be influenced by the difference between the permeability of the stone column and sand. As expected, the value of r_u is lesser when the permeability is more, and the variation of r_u in the radial direction is less when the difference in permeability is less. Higher values of permeability lead to faster dissipation of excess pore water pressure and hence lower values for r_u as seen in Fig. 7.7.

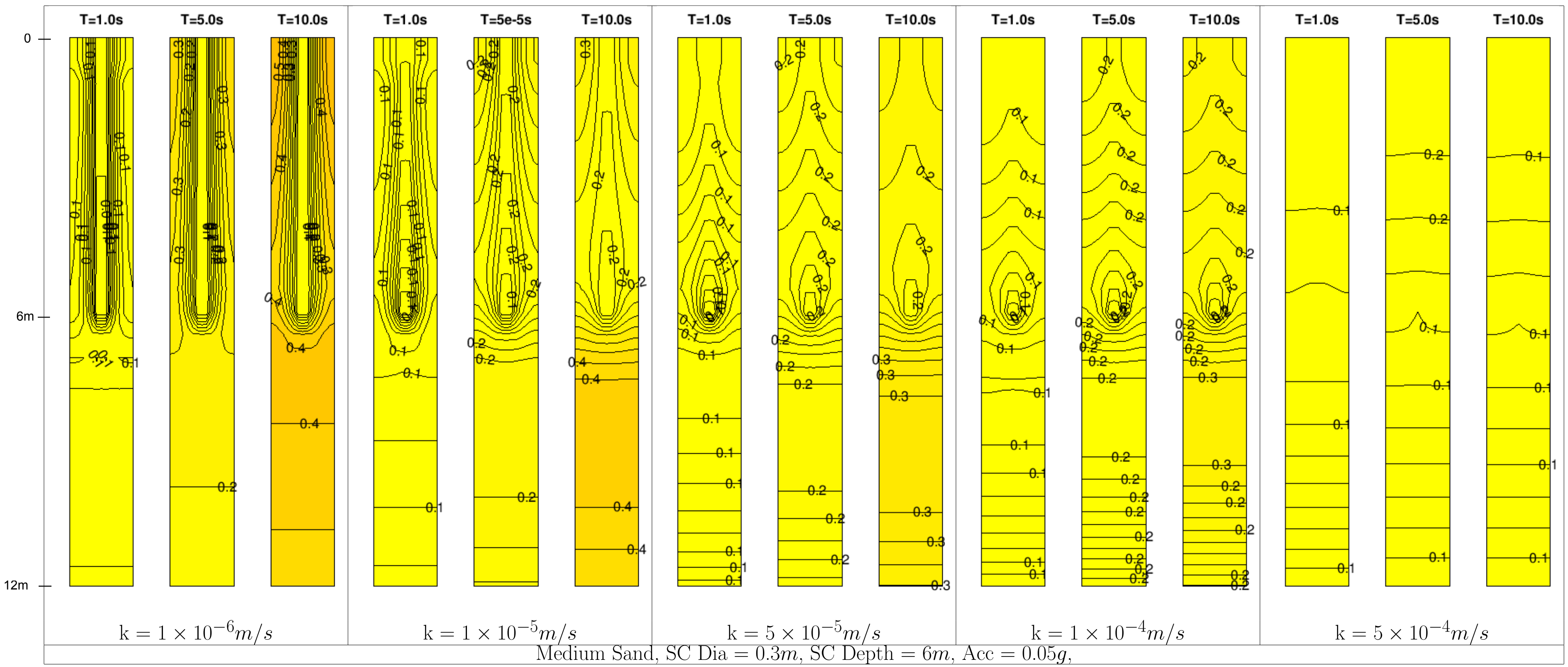

Figure 7.7: Variation of excess porewater pressure ratio with respect to permeability of sand

Fig. 7.8 shows the variation of r_u at 1 m depth at boundary, with 0.3 m diameter, 6 m deep column subjected to $0.05g$ acceleration. It can be observed that as the permeability improves, the value of r_u decreases, due to the improved drainage.

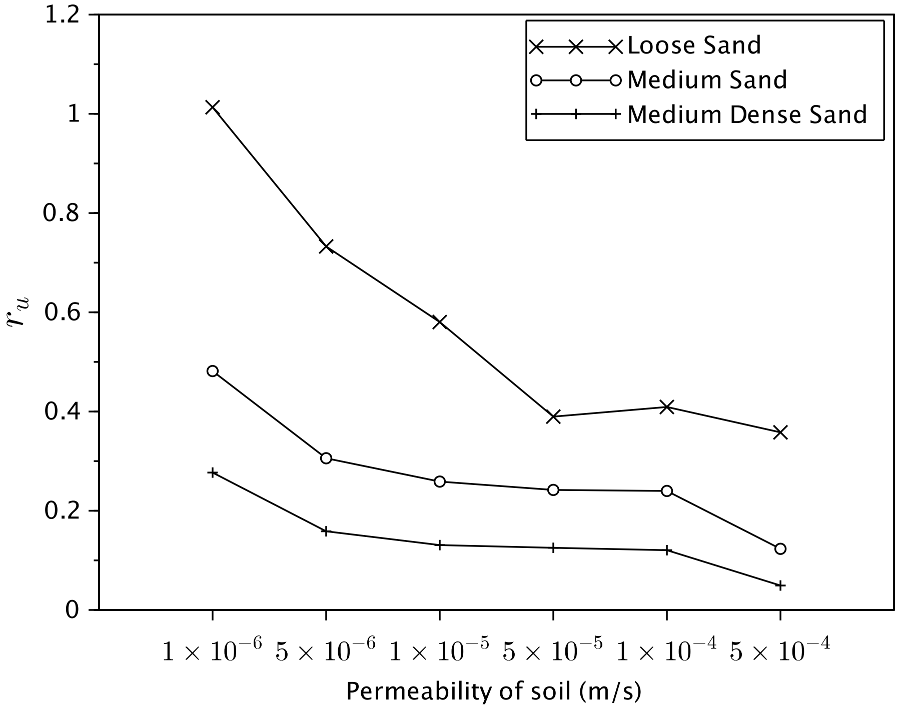

Figure 7.8: Variation of EPWPR at 1 m depth at boundary, with 0.3 m diameter, 6 m deep column, $0.05g$ at 10 s

7.5.4 Variation of excess porewater pressure ratio with respect to the intensity of shaking

The development of r_u with respect to the intensity of shaking is almost direct and very influential. As the ground motion acceleration increases, the excess pore water pressure also increases leading to higher values of r_u. Fig. 7.9 shows the variation of r_u when the acceleration increases from $0.05g$ to $0.25g$. The plot shows the distribution of r_u in the medium dense sand with the stone column of diameter 0.9 m having 9 m depth and permeability $5 \times 10^{-6} m/s$. It can be observed that the soil did not liquefy till 10 s, when the acceleration value is less than or equal to $0.10g$ since all values of r_u are < 1.0. When the acceleration value exceeds $0.10g$, r_u values build up and exceeds 1.0, indicating liquefied state.

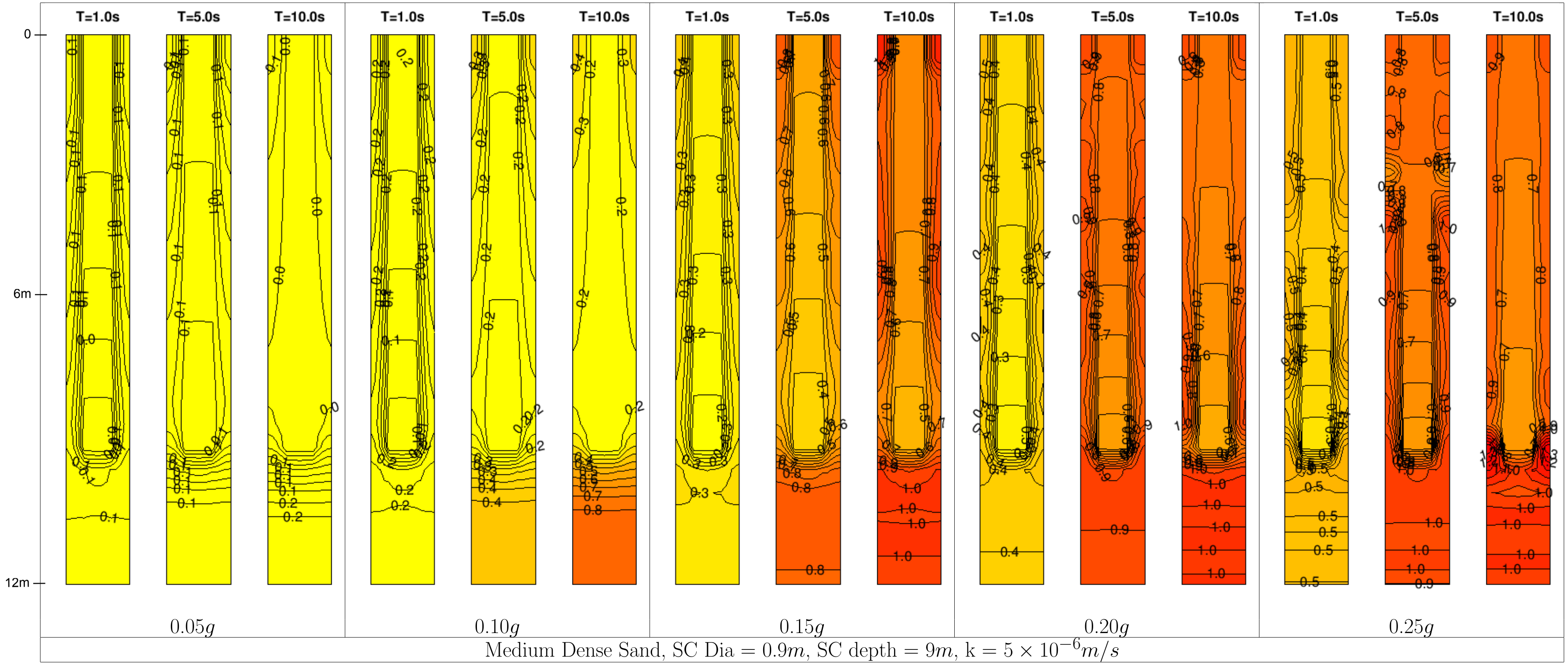

Figure 7.9: Variation of excess porewater pressure ratio with respect to intensity of shaking

Fig. 7.10 shows the variation of r_u at the boundary of the model at 10 s for the case with 0.9 m diameter, 9 m deep column, and k=5×10^{-5}m/s when the acceleration varies from $0.05g$ to $0.25g$. It can be observed that as the intensity of shaking increases, the r_u values increases.

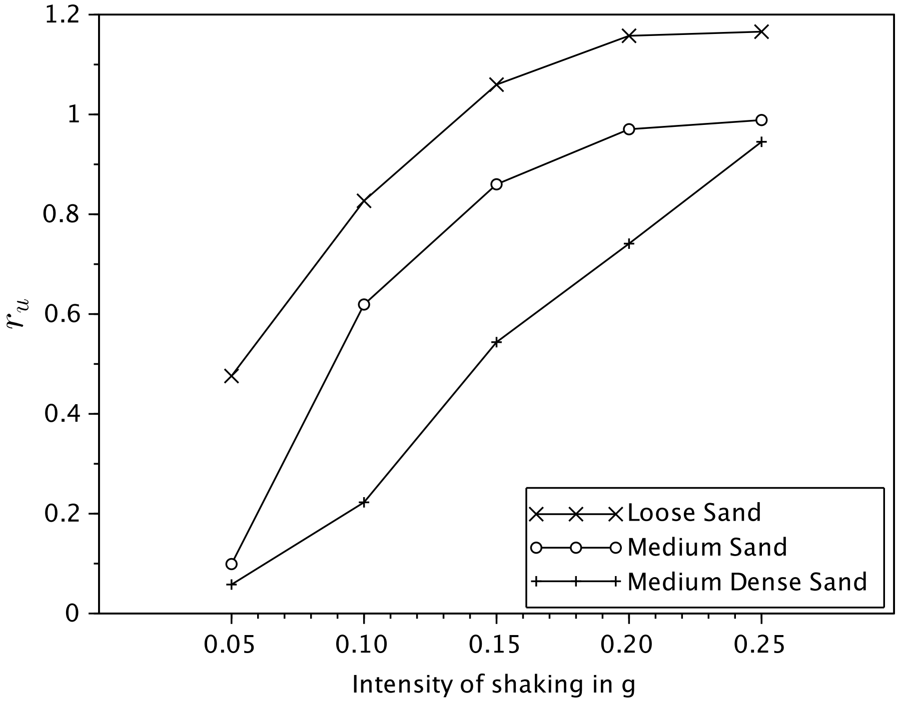

Figure 7.10: Variation of EPWPR at 1 m depth at boundary, with 0.9 m diameter 9 m deep column, and k=5×10^{-5} m/s at 10 s

7.5.5 Variation of excess porewater pressure ratio with respect to the density of sand

Relative density is one of the major factors affecting the liquefaction susceptibility of soil. Three different density states are compared in the present study, viz. Loose, Medium and Medium Dense. It is observed that as the relative density increases, the buildup of excess pore water pressure decreases due to lesser voids between the particles of sand. Higher total stress due to higher density also improves the liquefaction resistance reducing r_u. Fig. 7.11 shows the distribution of r_u in soil subjected to a ground motion acceleration of $0.10g$ and permeability of soil $1 \times 10^{-4} m/s$. It can be observed that the soil stratum liquefied in the loose and medium states and not in the medium dense state.

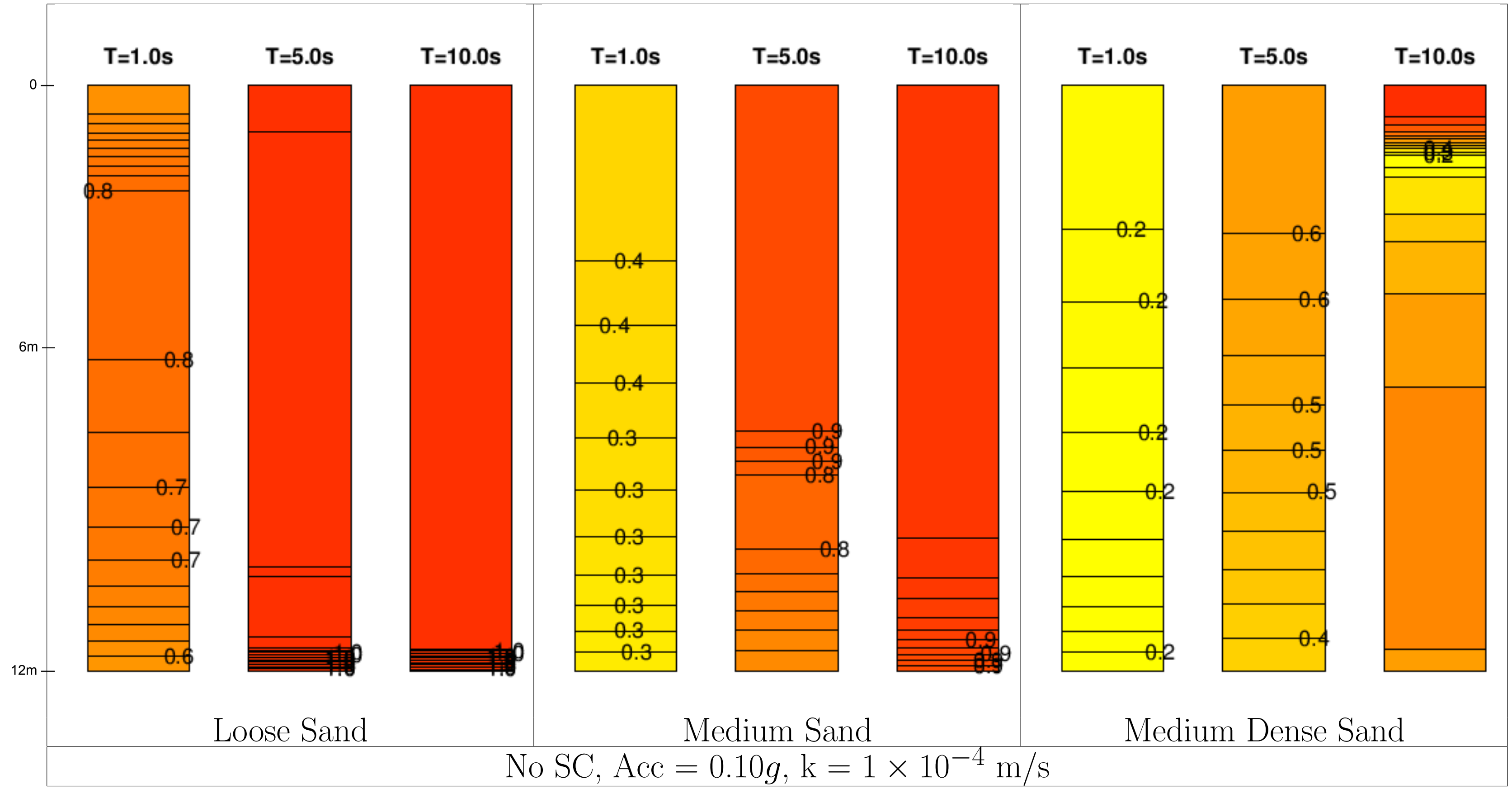

Figure 7.11: Variation of excess porewater pressure ratio with respect to relative density (soil alone)

Fig. 7.12 shows the distribution of r_u in soil improved with the stone column of diameter 0.9 m and depth 3 m, subjected to a sinusoidal acceleration of $0.10g$ for 10 s. The permeability of sand is 1×10^{-4} m/s. It is observed that the presence of a stone column reduces the excess pore water pressure ratio around it. The model exhibits similar behaviour to the case without stone columns, i.e. lesser r_u values when the relative density is high. It is clear that higher relative densities will lead to lesser build up of excess pore water pressure.

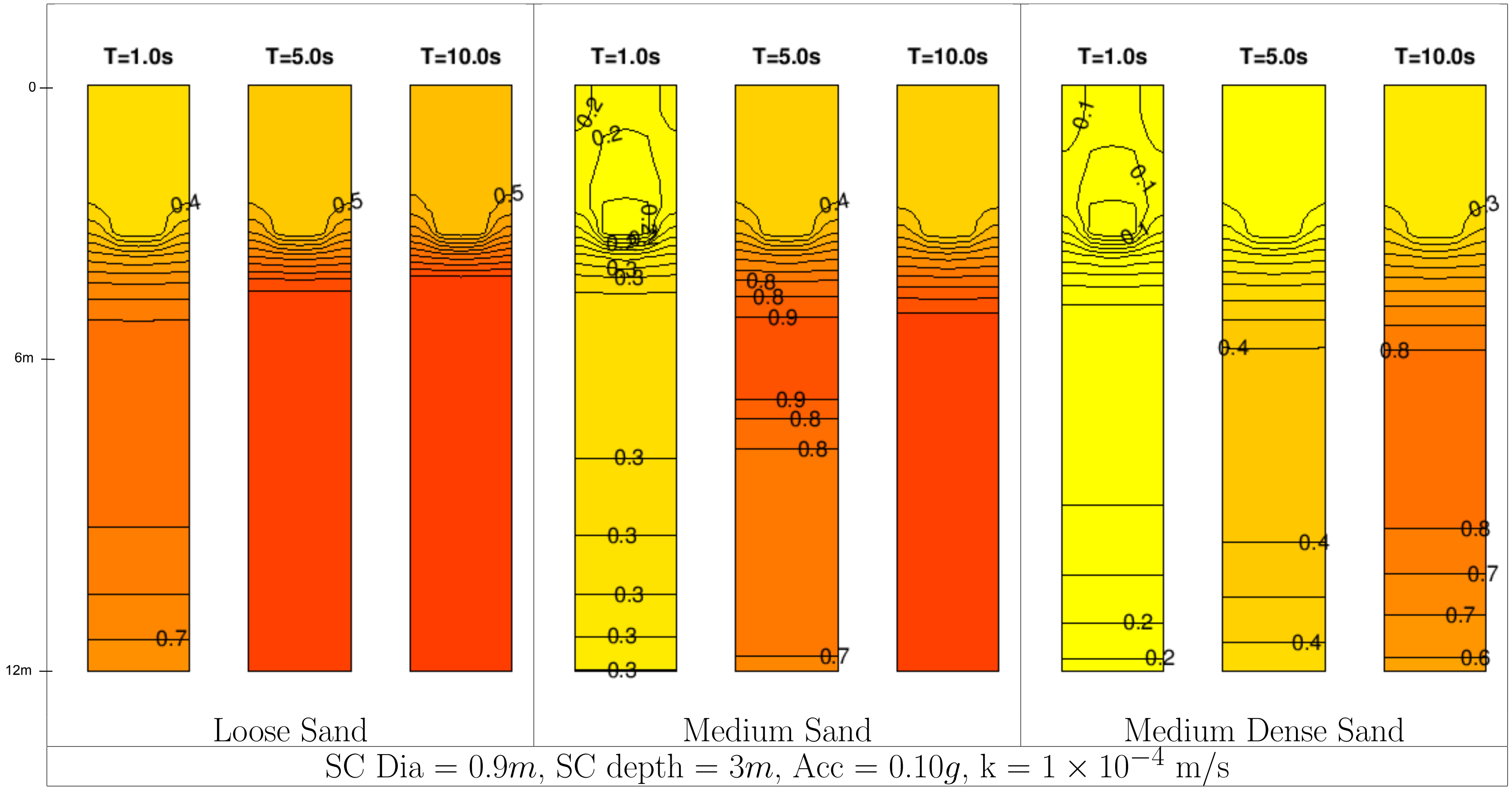

Figure 7.12: Variation of excess porewater pressure ratio with respect to relative density in the presence of stone column

Fig. 7.13 shows the variation of r_u when the model is subjected to $0.10g$ and having a permeability of 1×10^{-4}m/s with 3 m deep stone column at 10 s. The variation of r_u at a depth of 1 m at the boundary is plotted for this case with a stone column having diameter 0.3 m, 0.6 m, 0.9 m and 1.2 m along with the case without any stone column. It is clear from the figure that as the relative density of soil increases, the pore water pressure buildup decreases.

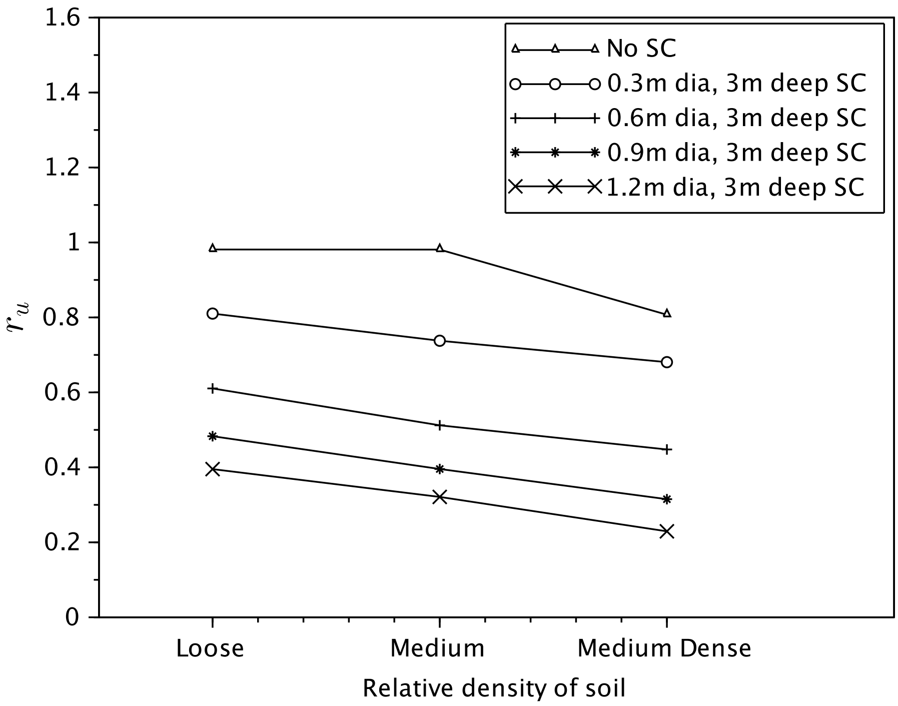

Figure 7.13: Variation of EPWPR at 1 m depth at boundary, 3 m deep column, $0.10g$ and k=1×10^{-4} m/s at 10 s

A detailed study into the results obtained reveals a few basic qualitative observations about the development of excess pore water pressure ratio when the different parameters vary.

1. The excess pore water pressure ratio decreases in the immediate vicinity of the stone column. This may be due to the improvement in drainage because of its high permeability.

2. As the diameter of the stone column increases, the area of influence improves. As a consequence, the pore water pressure ratio in the surrounding region of stone column decreases considerably.

3. As the depth of stone column increases, the depth of improvement – in terms of reduction of r_u is observed till the depth of penetration.

4. Higher pore water pressure ratios are observed below the stone column when the depth of penetration is partial. This implies that a partially penetrating stone column can be detrimental, since, the soil under the column will become more vulnerable to liquefaction due to impaired drainage and increased stress due to the presence of stone column.

5. The intensity of acceleration has a direct influence on the development of pore water pressure. As the intensity increases, r_u value also increases.

6. Higher density of sand leads to lesser build up of excess porewater pressure and is clearly observed in the cases studied, both with and without stone columns.

7.6 Excess Pore water pressure build up

To understand the effect of diameter and depth of stone column on the pore water pressure buildup, the value of excess pore water pressure at 10 s, at the boundary of the model was plotted for the various cases studied. Time = 10 s was chosen for plotting since the sinusoidal input motion exits till then. The boundary of the model represents the limiting zone of influence of a stone column in a grid pattern of field layout of the group of stone columns. Also, this is the section where the maximum pore water pressure is expected.

7.6.1 Effect of the diameter of the stone column on EPWP

Fig. 7.14 to Fig. 7.17 shows the Excess Pore Water Pressure (EPWP) for the different models having permeability $1 \times 10^{-4} m/s$, $1 \times 10^{-5} m/s$ and $1 \times 10^{-6} m/s$ with varying stone column diameter at the boundary at 10 s when it is subjected to a sinusoidal input motion of $0.10g$. Here, the comparison is made between stone columns of the same depth but with different diameters. Each of the figures is drawn for a specific stone column depth. Also, Fig. 7.18 to Fig. 7.21 shows the Excess Pore Water Pressure Ration (EPWPR) for the above mentioned cases. It can be observed that as the diameter of the column increases, the reduction of EPWP is more along the periphery of the stone column. This reduction in EPWP increases when the permeability of sand increases for same relative density. Also, the EPWP values decrease when the relative density increases. Below the stone column, the EPWP increases with an increase in diameter of the stone column and the EPWP values are close to or greater than the case without the stone column. This behaviour is more predominant in the case of loose soil. This may be due to the additional stresses in soil due to the presence of a larger stone column.

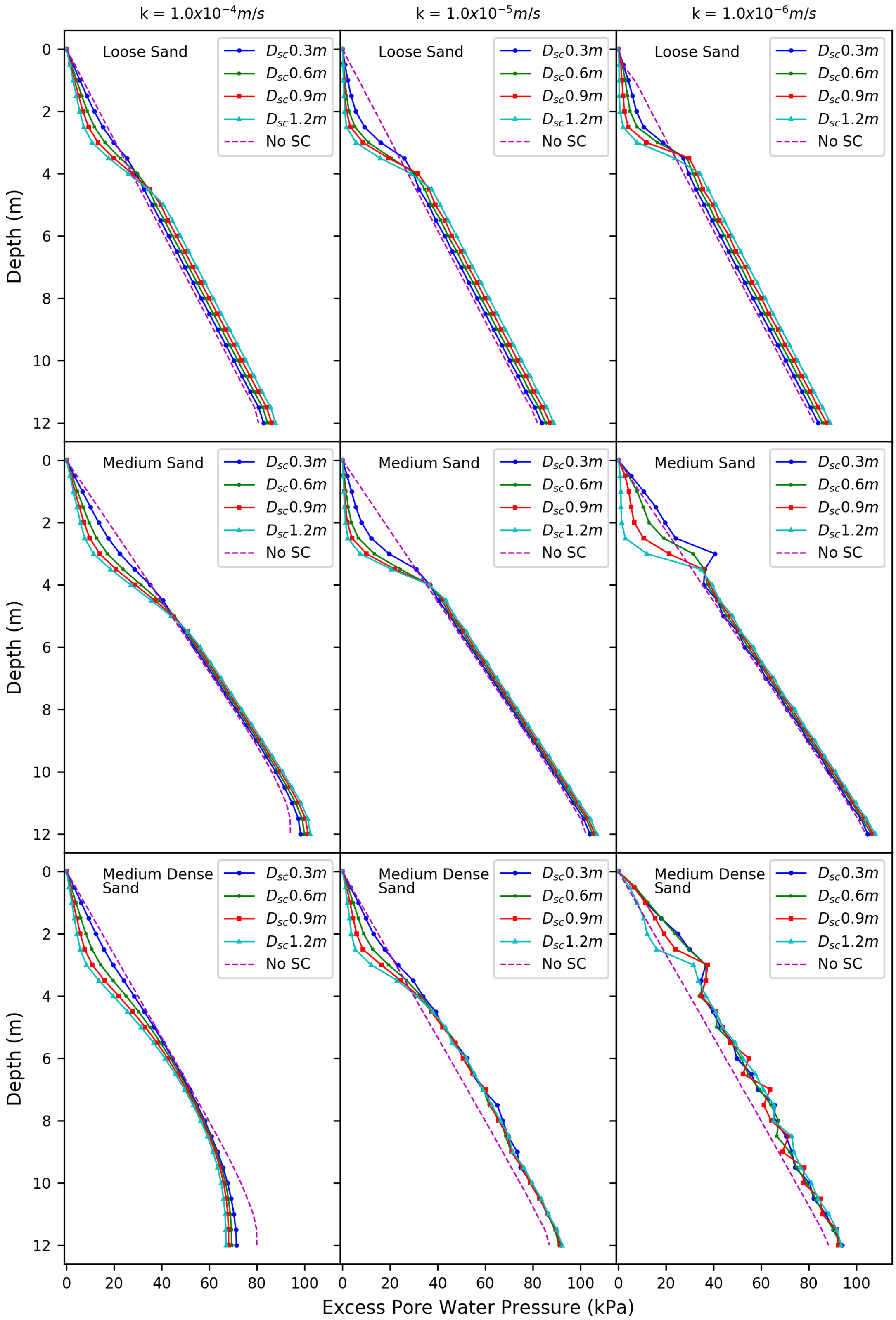

Figure 7.14: EPWP at the model boundary at $10s$ due to $0.10g$, SC depth = 3 m

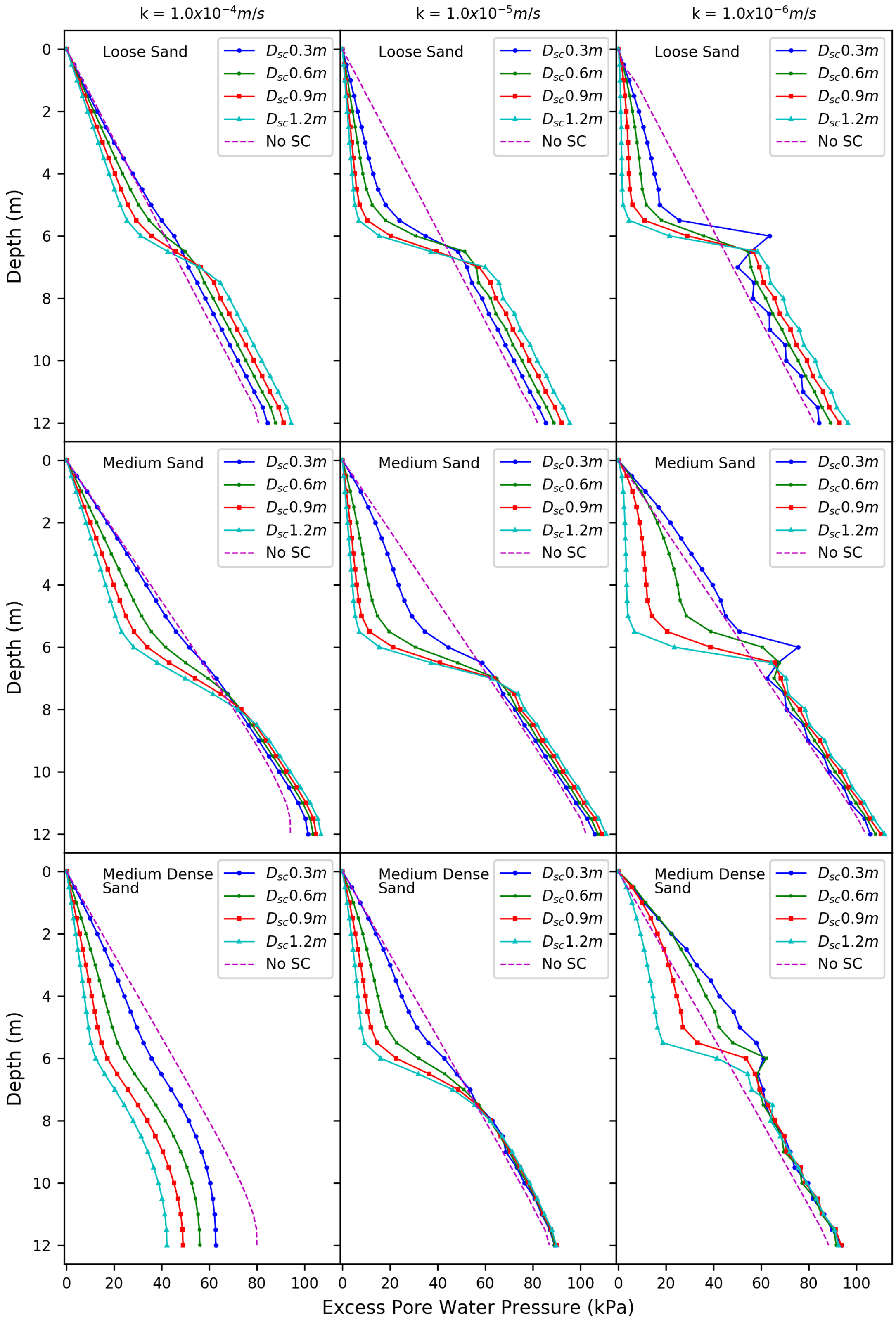

Figure 7.15: EPWP at the model boundary at $10s$ due to $0.10g$, SC depth = 6 m

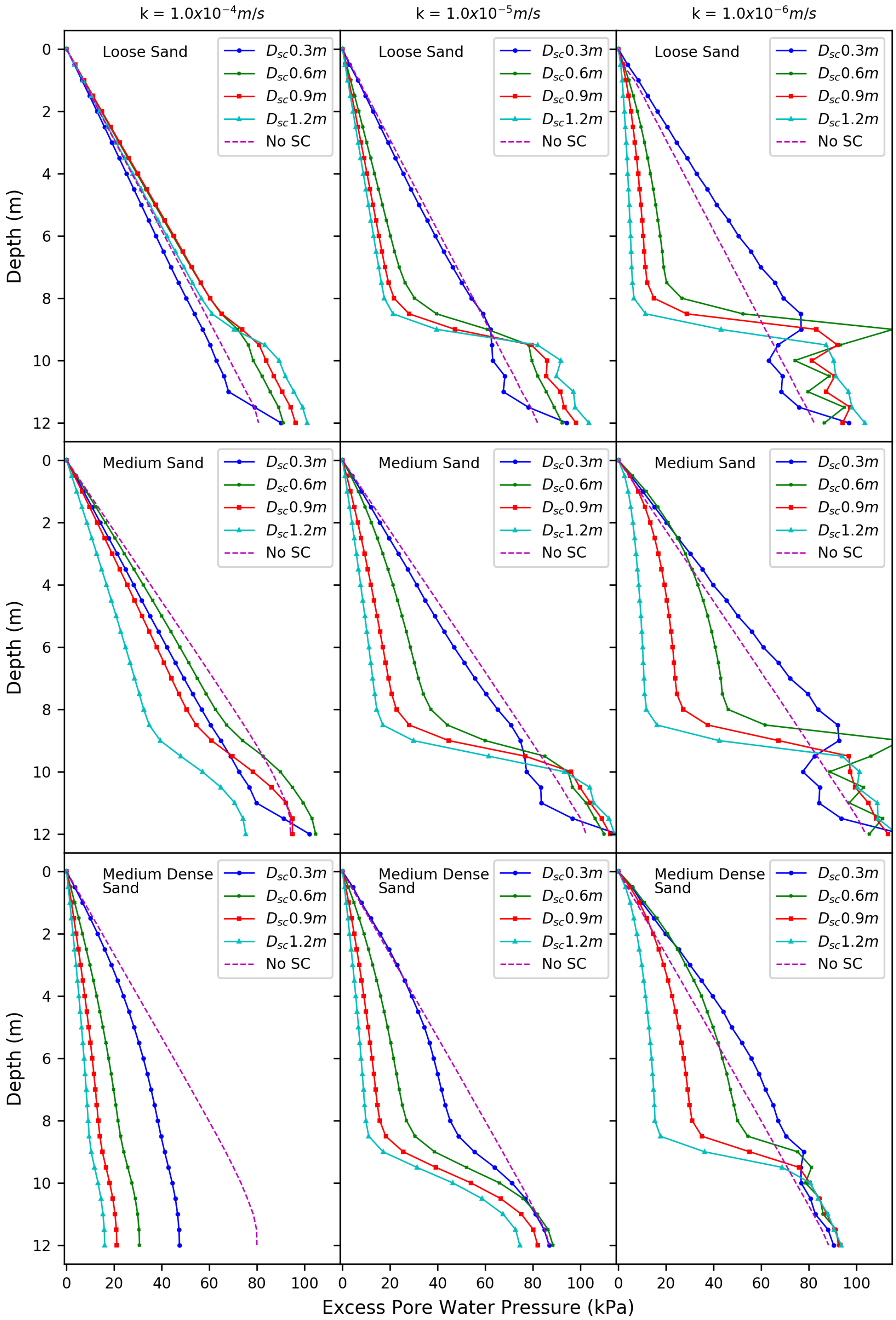

Figure 7.16: EPWP at the model boundary at $10s$ due to $0.10g$, SC depth = 9 m

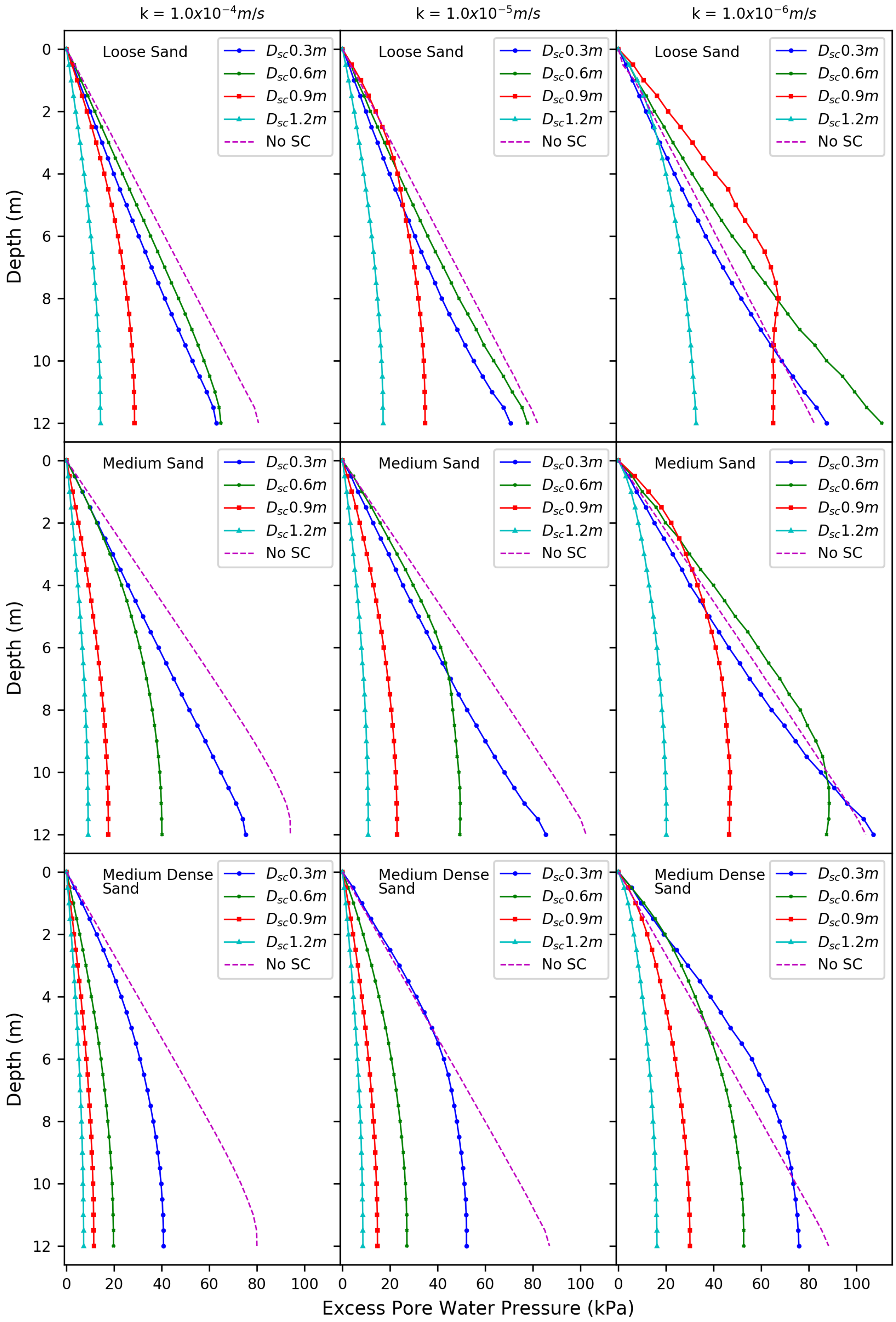

Figure 7.17: EPWP at the model boundary at $10s$ due to $0.10g$, SC depth = 12 m

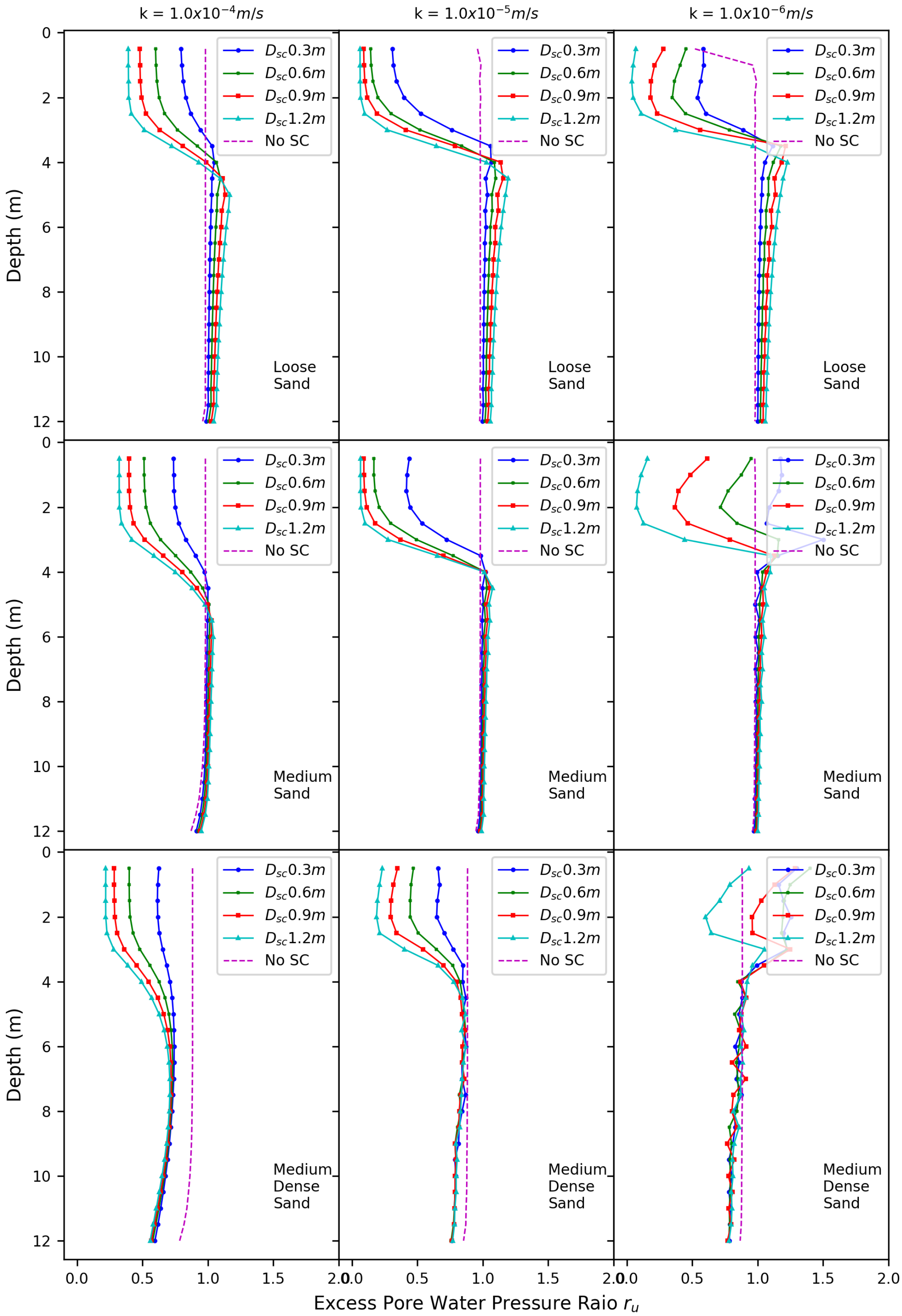

Figure 7.18: EPWPR at the model boundary at $10s$ due to $0.10g$, SC depth = 3 m

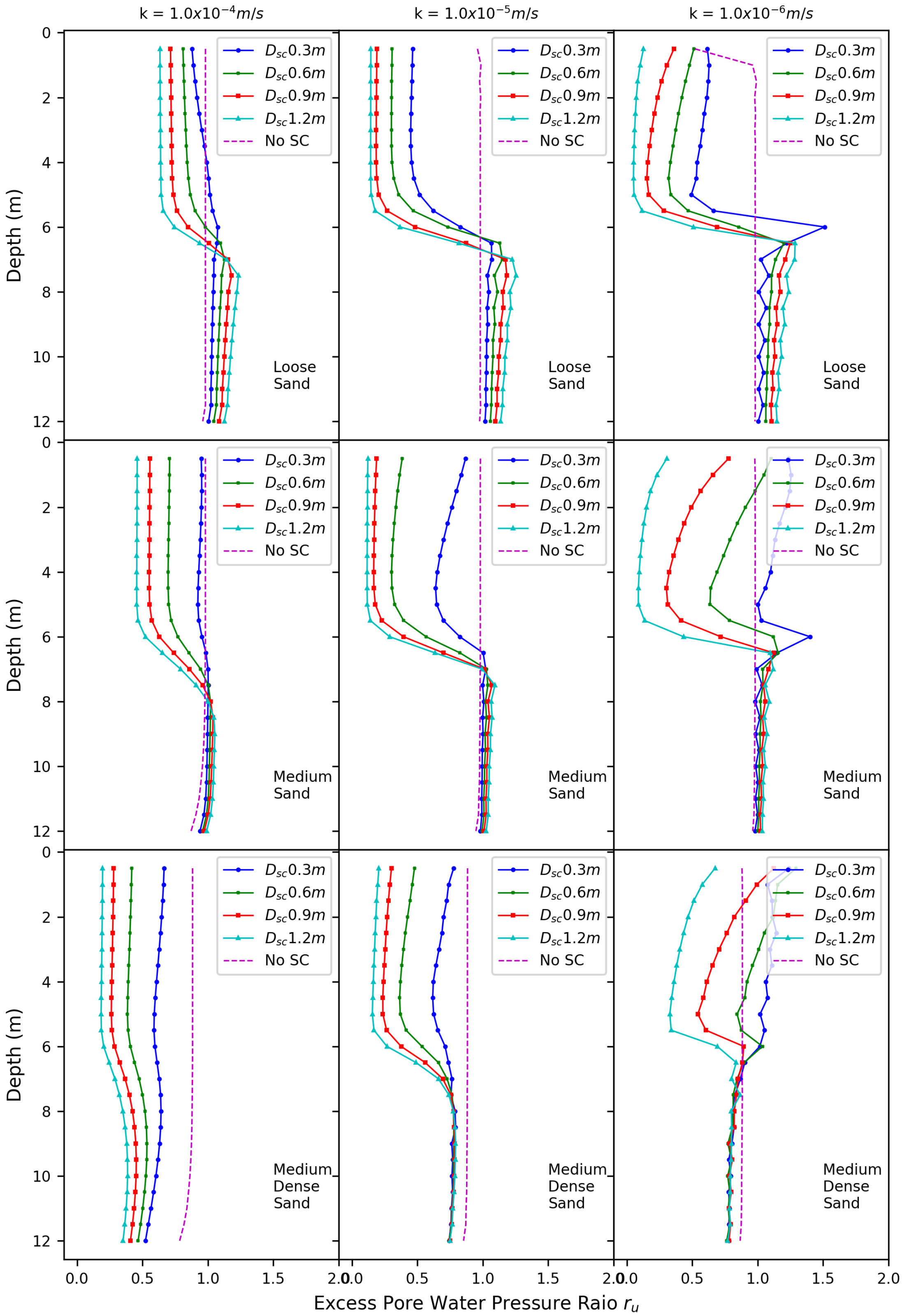

Figure 7.19: EPWPR at the model boundary at $10s$ due to $0.10g$, SC depth = 6 m

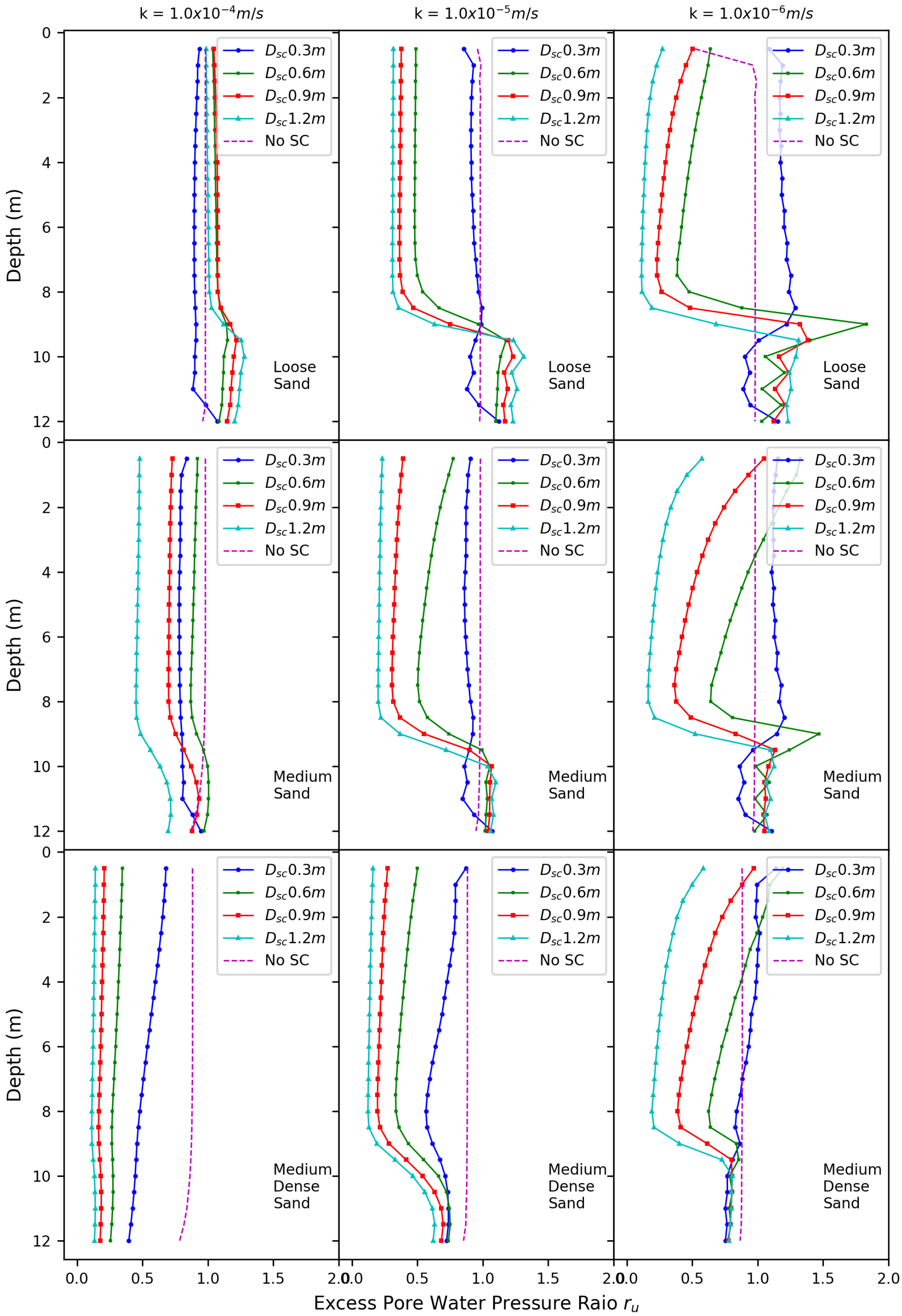

Figure 7.20: EPWPR at the model boundary at $10s$ due to $0.10g$, SC depth = 9 m

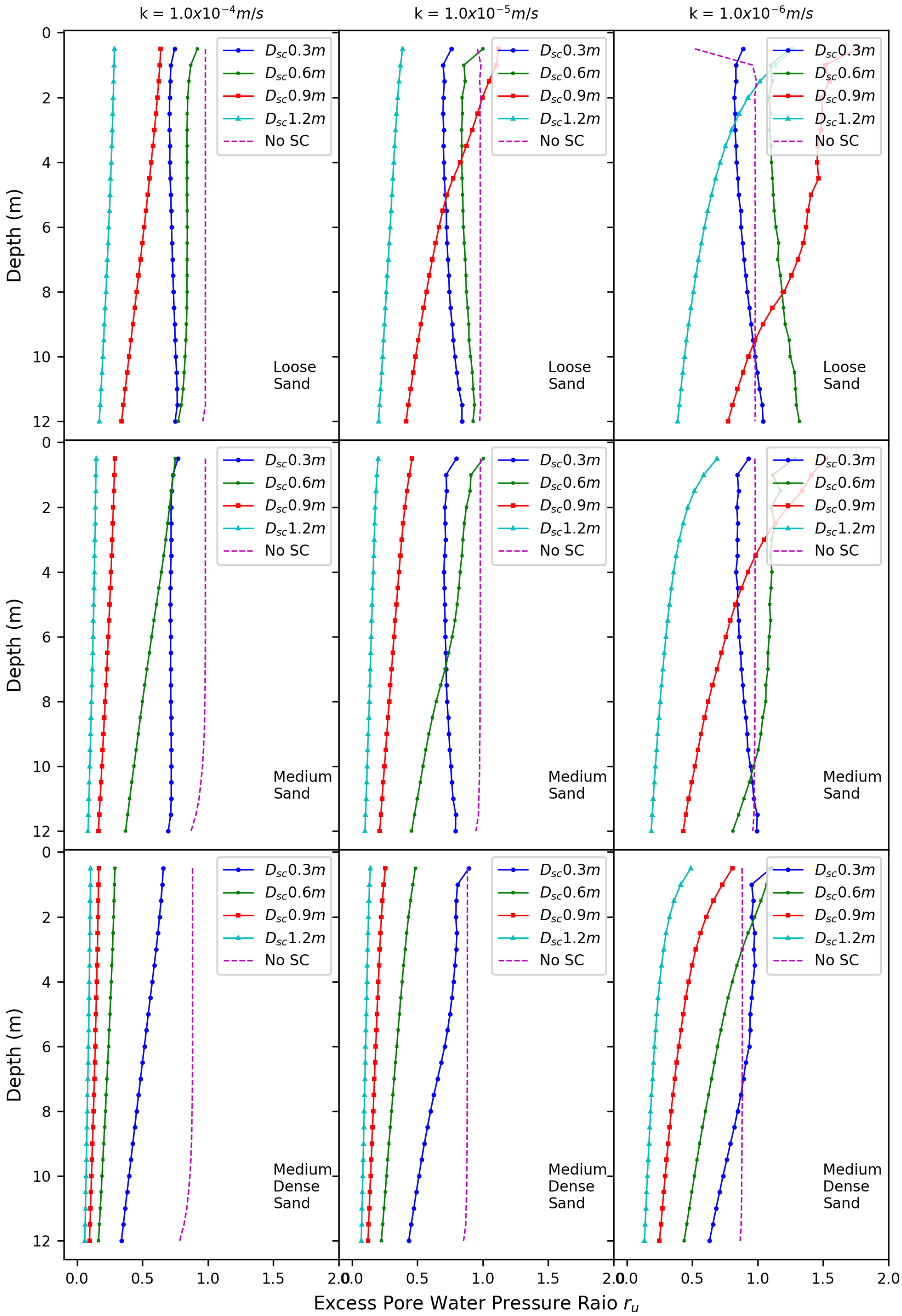

Figure 7.21: EPWPR at the model boundary at $10s$ due to $0.10g$, SC depth = 12 m

7.6.2 Effect of the depth of stone column on EPWP

Fig. 7.14 to Fig. 7.17 shows the Excess Pore Water Pressure (EPWP) for the different models having permeability $1 \times 10^{-4} m/s$, $1 \times 10^{-5} m/s$ and $1 \times 10^{-6} m/s$ with varying stone column depth at the boundary at 10 s when it is subjected to a sinusoidal input motion of $0.15g$. Here, the comparison is made between stone columns of the same diameter but of different depth. Each of the figures is drawn for a specific diameter of the stone column. When the stone column depth increases, the reduction in excess pore water pressure can be seen up to the depth of penetration of the stone column. Also, Fig. 7.18 to Fig. 7.21 shows the Excess Pore Water Pressure Ratio (EPWPR) for the above mentioned cases. It is observed that the excess pore water increases when the depth of the stone column increases for the same diameter of the stone column. This behaviour is observed till the depth of penetration of stone column. Below the stone column, the behaviour is more complex, and no specific trend is observed in the EPWP value. Also, a higher reduction in EPWP is observed when the permeability of the soil is more. The buildup of EPWP is less for denser soil. It is to be noted that when the stone column diameter is 12 m (full depth), the reduction in excess pore water pressure exists till the bottom of the model and is well below the case without the stone column in all the cases studied.

7.7 Summary

To understand the behaviour of stone columns that are partially penetrating (floating stone column), a parametric study was undertaken using a finite element analysis. The effect of diameter and depth of stone columns, ground acceleration, permeability of stratum for loose, medium and medium dense sands were investigated. The parallel option on *OpenSees* was employed to handle the large number of analysis to be carried out by varying the five parameters considered. A

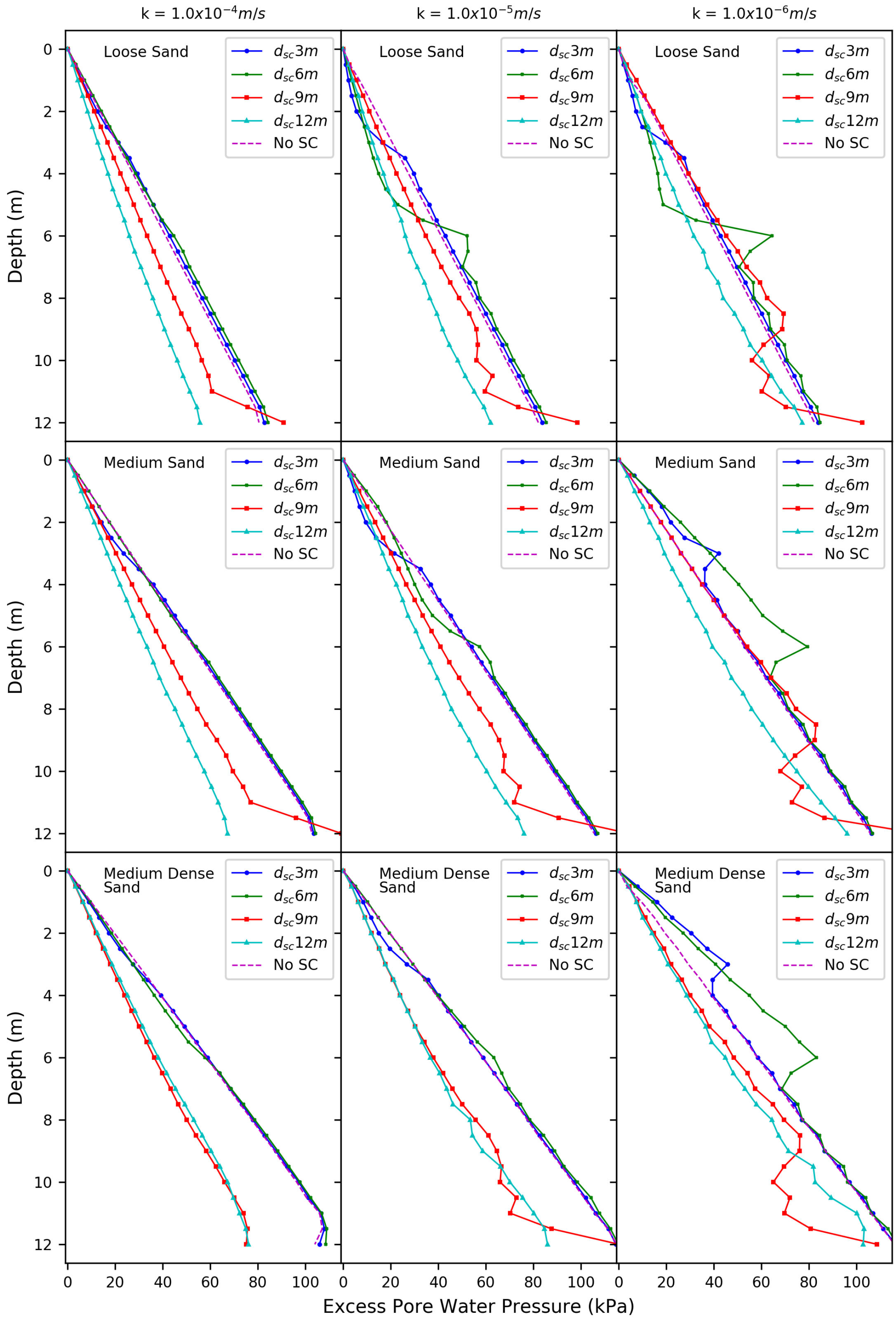

Figure 7.22: EPWP at the model boundary at $10s$ due to $0.15g$, SC dia = 0.30 m

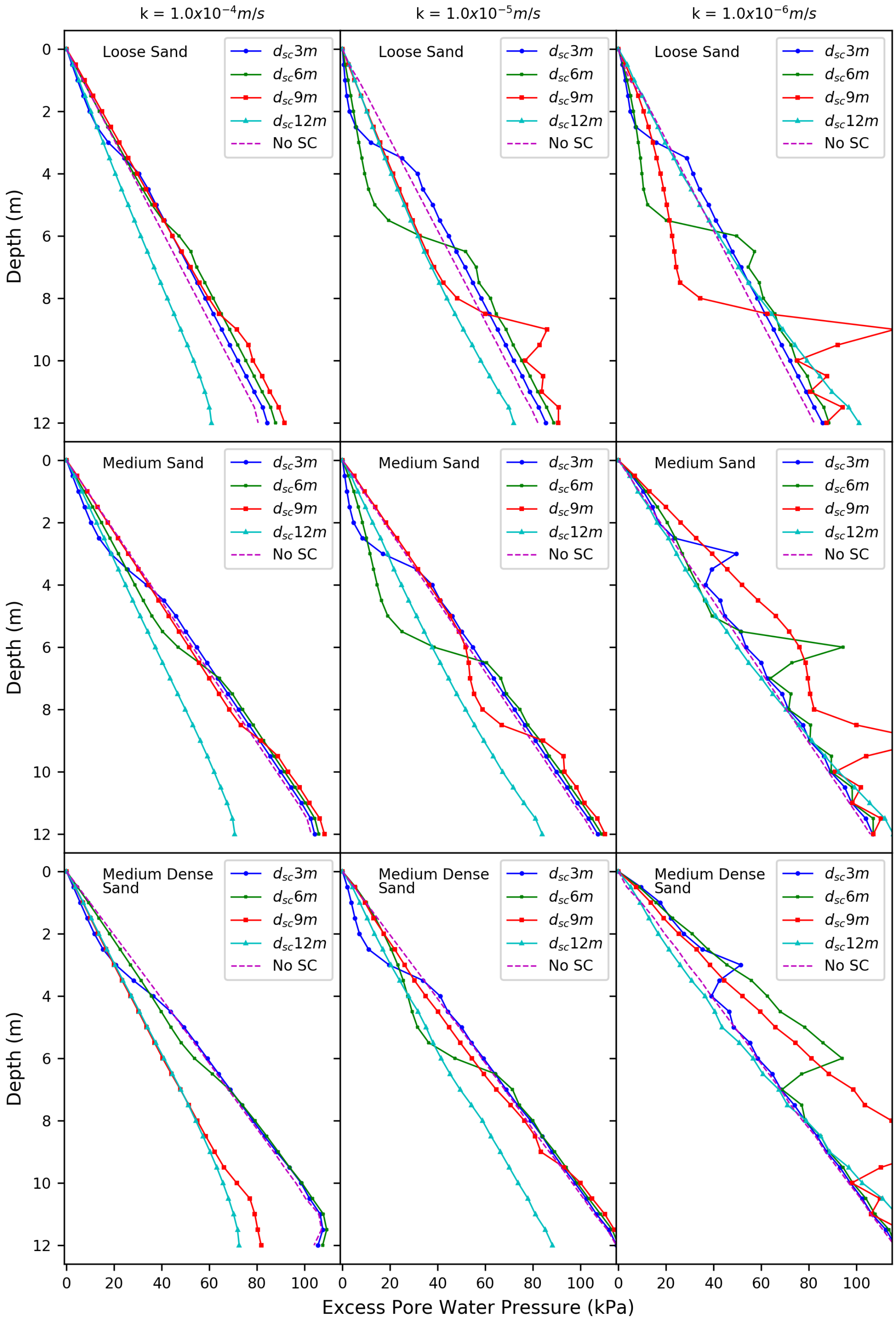

Figure 7.23: EPWP at the model boundary at $10s$ due to $0.15g$, SC dia = 0.6 m

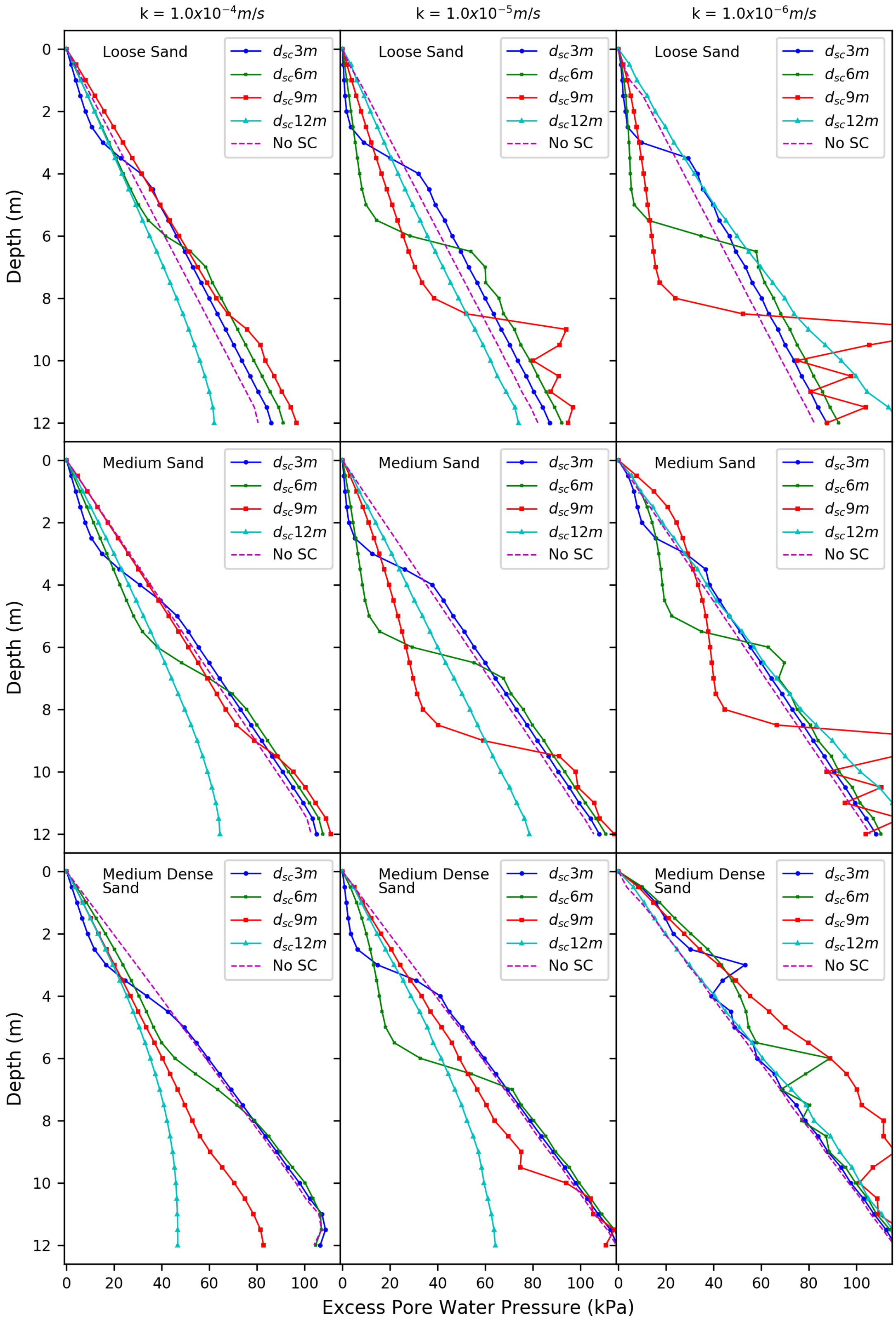

Figure 7.24: EPWP at the model boundary at $10s$ due to $0.15g$, SC dia = 0.9 m

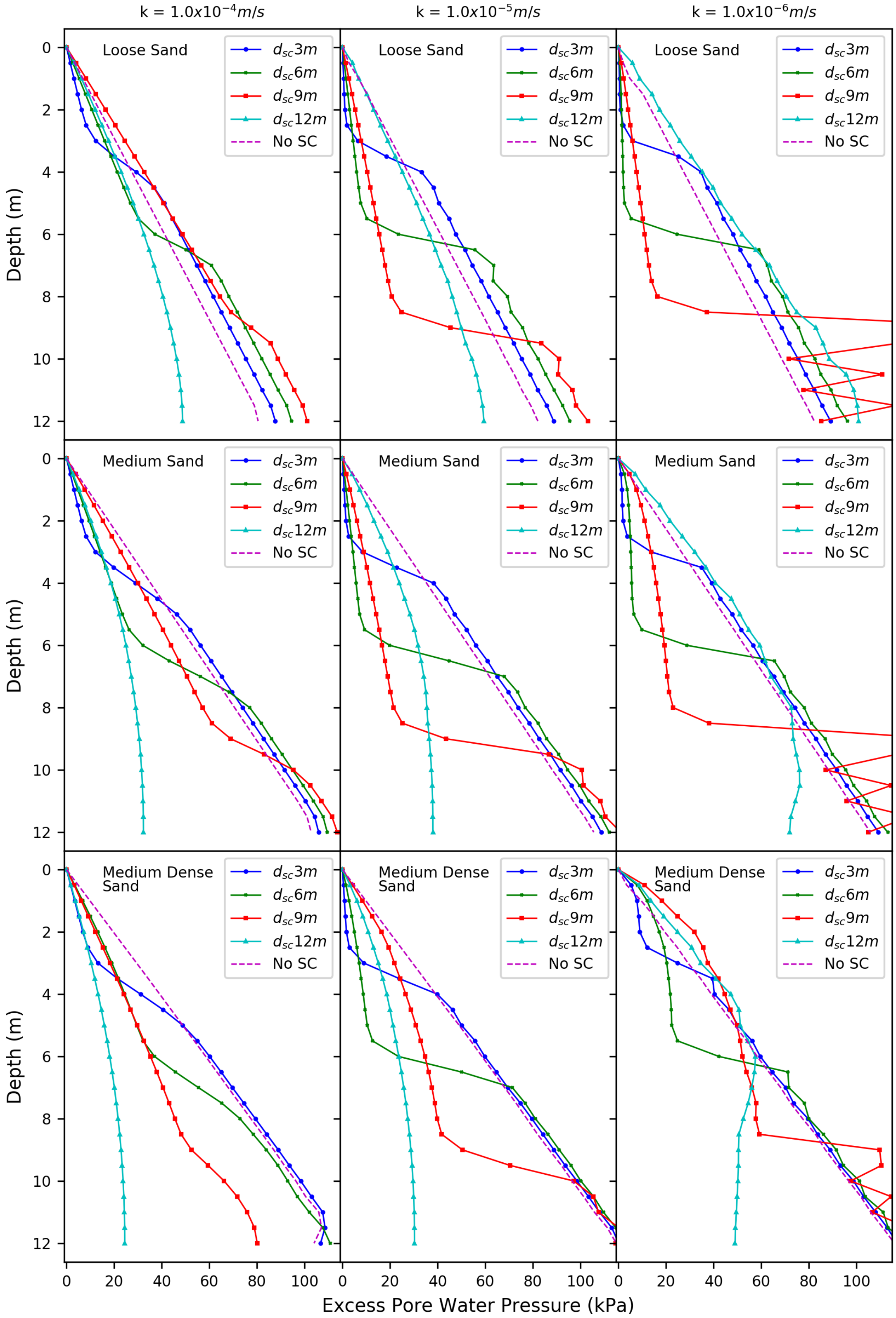

Figure 7.25: EPWP at the model boundary at $10s$ due to $0.15g$, SC dia = 1.2 m

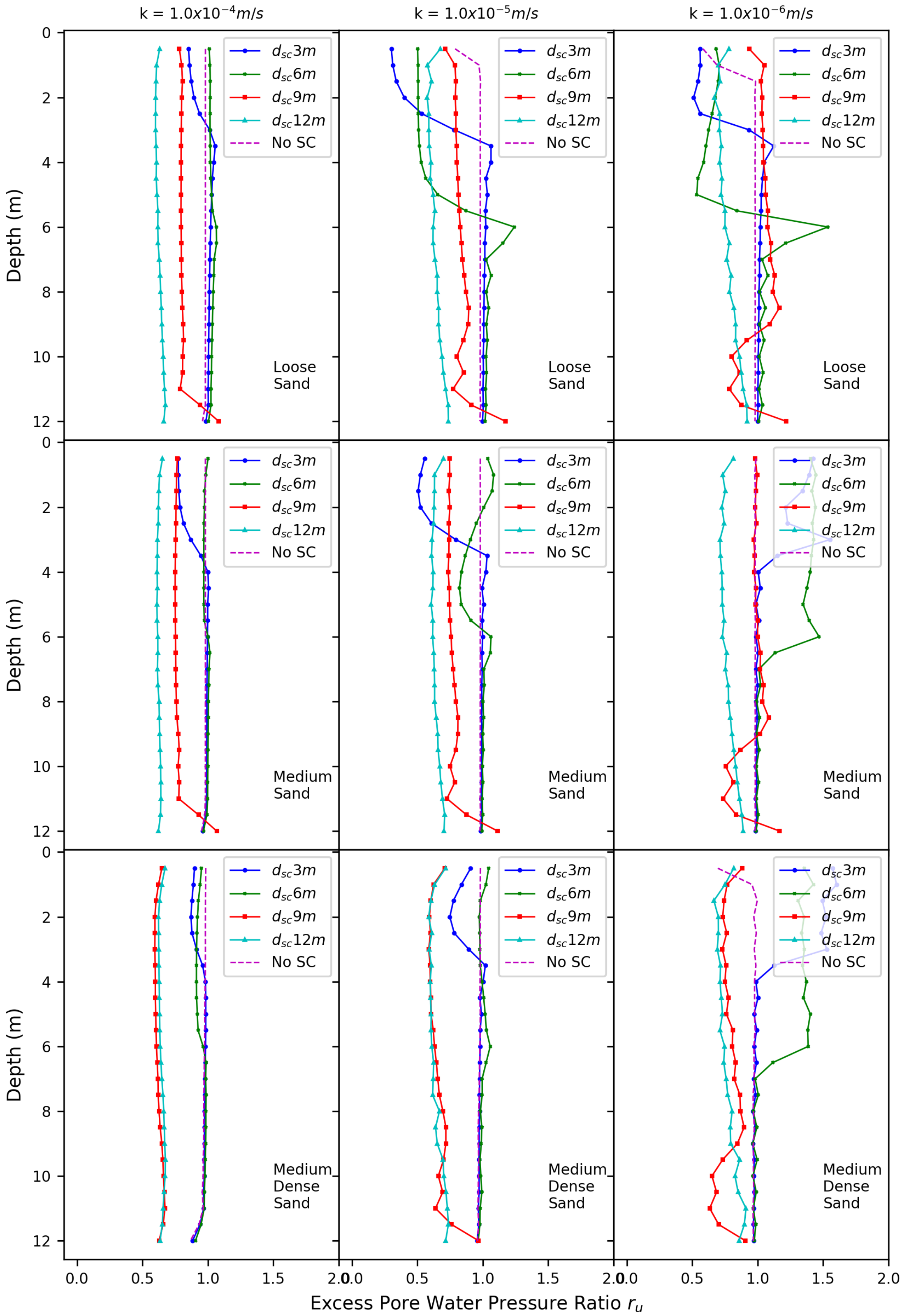

Figure 7.26: EPWPR at the model boundary at $10s$ due to $0.15g$, SC dia = 0.30 m

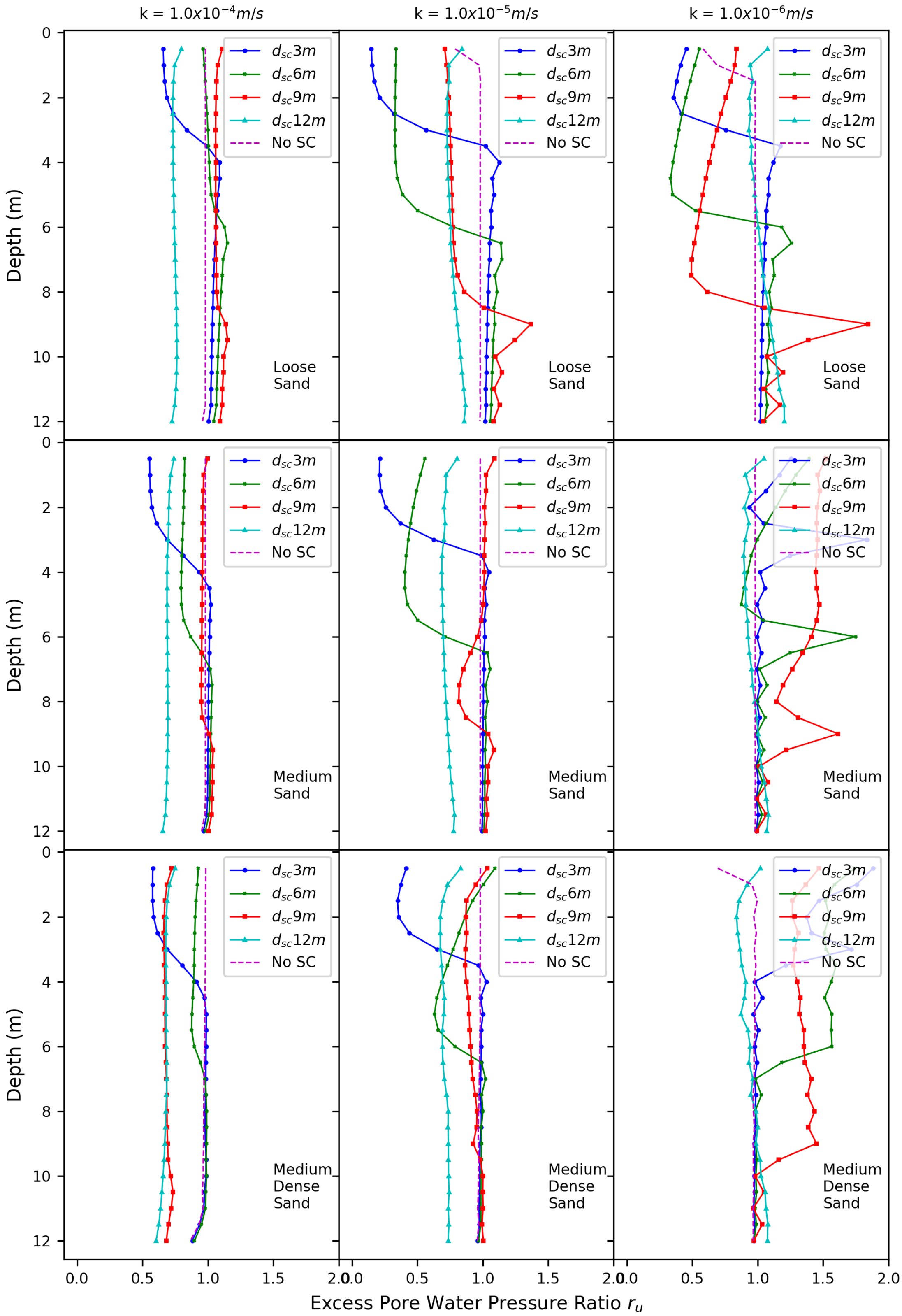

Figure 7.27: EPWPR at the model boundary at $10s$ due to $0.15g$, SC dia = 0.6 m

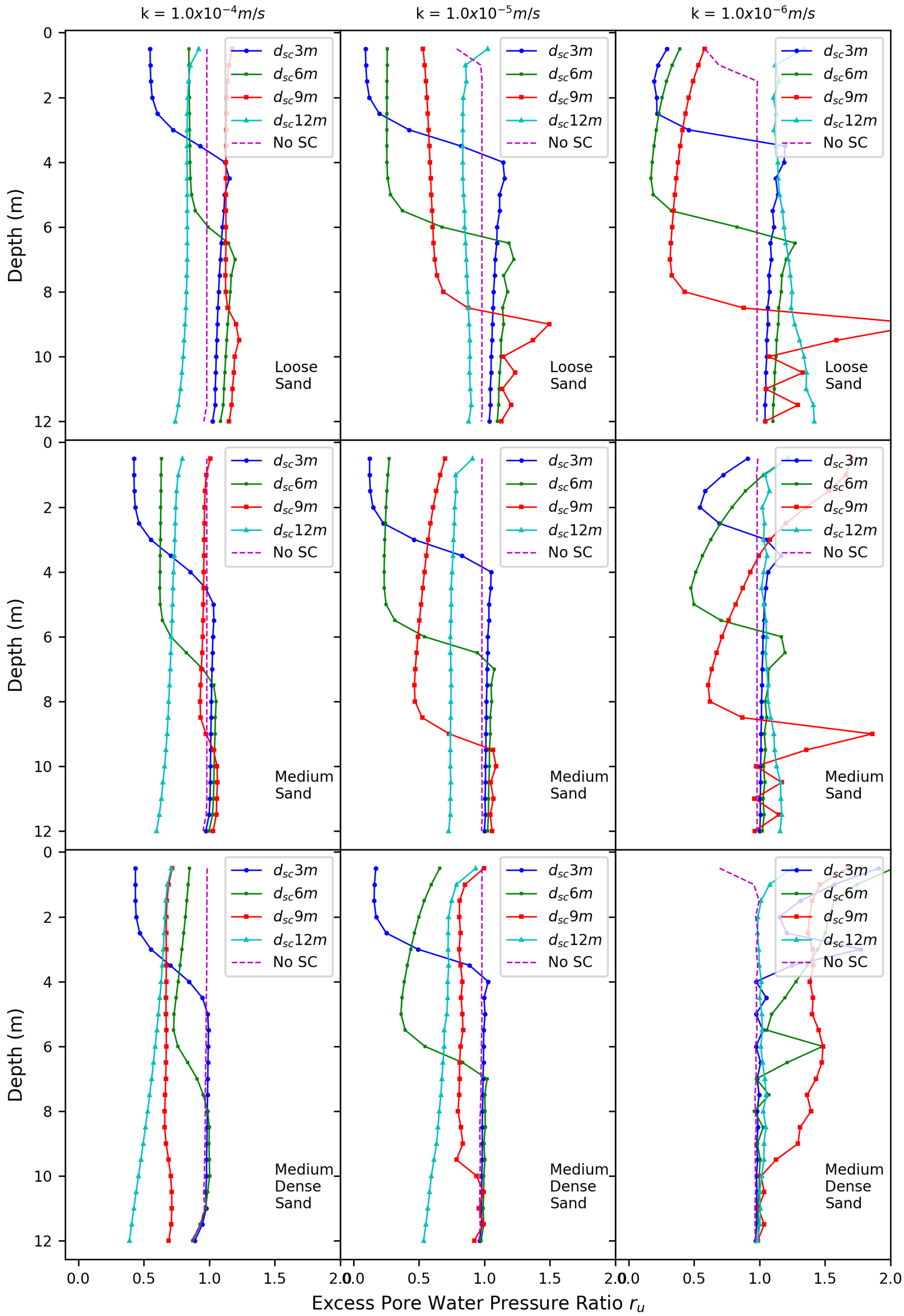

Figure 7.28: EPWPR at the model boundary at $10s$ due to $0.15g$, SC dia = 0.9 m

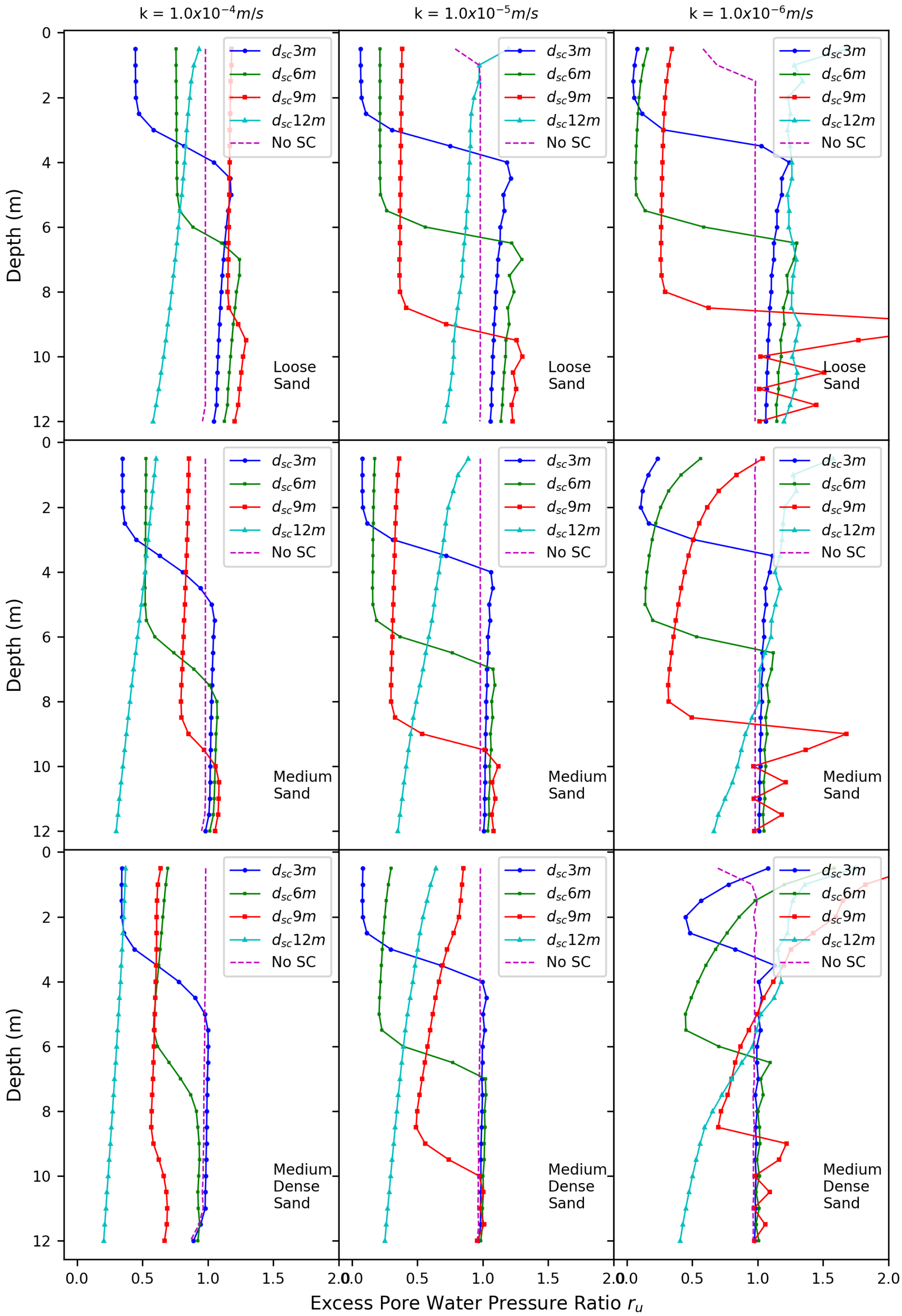

Figure 7.29: EPWPR at the model boundary at $10s$ due to $0.15g$, SC dia = 1.2 m

Table 7.3: Summary of parametric trends observed in numerical simulations

	Excess pore water pressure	
Parameter	upto depth of SC	below SC
Acceleration	↑↑	↑↑
Permeability	↓	↓
Density of soil	↓	↓
Diameter of SC	↓	↑
Depth of SC	↑	↕

The direction of the arrows indicates the effect on excess pore water pressure value for an increase in the parameter, and the number of arrows indicates the relative effect of that parameter. Double-sided arrows indicate that both directions are possible depending on the specific conditions.

total of 1530 analysis was performed and results obtained. The analysis results give an insight into the buildup of excess pore water pressure in the presence of partially penetrating stone columns. It was observed from the results that a partially penetrating stone column has a detrimental effect of the pore pressure buildup below it. The summary of observations made after analysing the results of the FEA parametric study is presented below. A qualitative analysis is presented here, since, the behaviour is extremely complex due to the number of parameters involved and since the effect at different locations in the model vary in an intricate manner with respect to time. Table 7.3 shows the summary of parametric trends observed in numerical simulations.

1. The excess pore water pressure developed is more at higher depths. Almost a linear relationship exists between excess pore water pressure buildup and depth when there is no stone column in the soil.

2. The excess pore water pressure build up increases when the acceleration is more. This behaviour is expected since, when the intensity of shaking is more, the energy to be dissipated is more and is reflected in the form of higher pore water pressure build up.

3. As the density of soil medium increases, there will be lesser voids in between

the soil particles and leads to lesser build up of excess pore water pressure. Also, higher density leads to higher effective stress and hence will require more pore water pressure buildup to initiate liquefaction. This phenomenon is also observed in the cases studied.

4. Higher permeability results in more drainage and rapid dissipation of excess pore water pressure leading to lesser values of r_u influencing the liquefaction behaviour. This phenomenon is observed in all the cases studied.

5. Pore water pressure buildup is less along the periphery of the stone column. As the diameter of the column increases, the area of influence also increases. This may be due to the higher permeability of the stone column compared to the surrounding sand.

6. It is observed that the pore water pressure buildup below the stone column is significantly affected by the presence of the stone column. During shaking, in the absence of the stone column, the excess pore water pressure builds up and drains through the top surface. The flow of water will be in the vertical upward direction. Inserting a stone column in the stratum will alter the direction of flow of water, since, water around the stone column will have a tendency to flow into the stone column due to its high permeability. The drainage path will be completely altered.

7. In loose sand, when the diameter of the stone column increases, pore pressure decreases in the periphery of the column. But, the pore water pressure shows an increasing trend below the stone column when the diameter increases. This may be attributed to the higher stresses due to the larger diameter of the stone column.

8. Partially penetrating stone columns can lead to higher excess pore water pressure buildup below it. Higher stresses due to the stone column and lack of sufficient drainage for the excess pore pressure are two major reasons for this behaviour. This problem predominates in the case of loose sand.

CHAPTER 8

DEVELOPMENT OF PREDICTION MODEL FOR EXCESS PORE WATER PRESSURE

8.1 Introduction

The parametric study has revealed that the development of excess pore water pressure is a very complex phenomenon and depends on several parameters. The relationship is highly non-linear. A model for predicting the excess pore water pressure will be very much useful for design engineers to check if the improved ground is susceptible to liquefaction. The present chapter describes the development of a model for the prediction of excess pore water pressure build-up using the data obtained from FEA.

8.2 Excess pore water pressure prediction model

Fig. 8.1 depicts the model parameters that were chosen for the development of the prediction equation. The excess pore water pressure developed in the improved soil beyond the stone column shown in Fig. 8.1 is used for developing the model. The model for loose sand, medium sand and medium dense sand were developed separately. The other parameters used are permeability ratio k_r (the ratio of stone column permeability to the permeability of soil), input acceleration in g and time of shaking which normalised with the total time of shaking (t_r). The excess pore water pressure value at each node for all the 1440 analysis with stone column was used for finding the coefficients. The number of datasets used for the analysis was approximately 9,00,00,000.

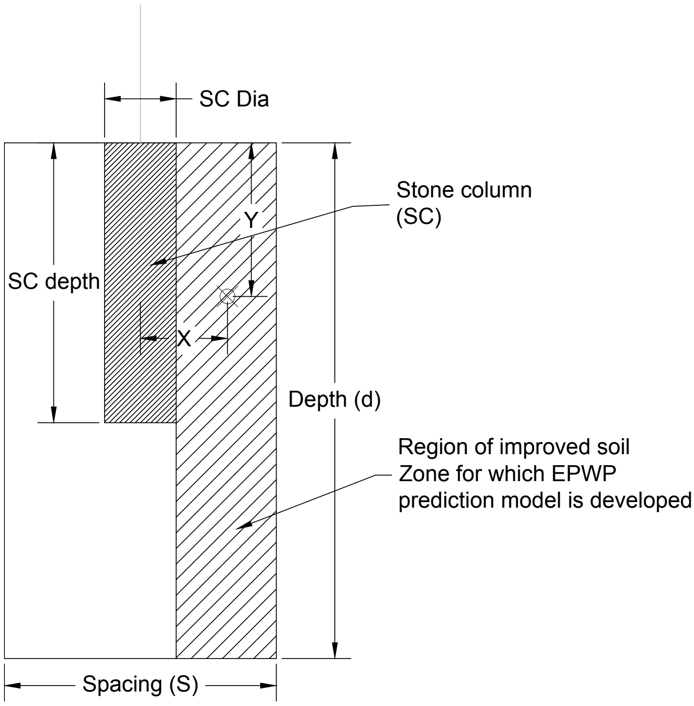

Figure 8.1: Parameters used for predicting excess pore water pressure

The software used was SciPy, an open-source software for mathematics, science, and engineering (Jones *et al.*, 2014). The software has an optimise function which uses non-linear least squares to fit a function, f, to given data. The function is user-defined and can be of any type, linear, trigonometric, power, exponential or logarithmic.

A simple power model was developed accommodating all the parameters directly as shown in equation 8.1. The equation is made non-dimensional by introducing atmospheric pressure ($p_a = 100kPa$) in the excess pore water pressure term. The terms in the equation are described in Table 8.1. The equation is valid where $X > d/2$ where d is the diameter of the stone column

$$\frac{EPWP}{p_a} = C_0 \times [a \times t_r]^{C_1} \times \left[k_r \times \frac{X}{S} \times \frac{1}{A_r^2}\right]^{C_2} \times \left[\frac{Y}{d}\right]^{C_3} \tag{8.1}$$

The coefficients obtained after the fitting is shown in Table 8.2. The coefficient of determination obtained in all the cases are > 0.8, which is satisfactory, considering

Table 8.1: Terms in the prediction model

Notation	Parameter
$EPWP$	Excess Pore Water Pressure in kPa
p_a	Atmospheric pressure in kPa
C_0, C_1, C_2, C_3	Empirical coefficients of equation
a	Acceleration in g
t_r	Time ratio = Time instant / Duration of shaking
k_r	Permeability ratio = Permeability of stone column / Permeability of sand layer
S	Spacing of stone column
A_r	Aspect ratio of stone column = Length of stone column / diameter of stone column
d	Depth of soil layer
X, Y	Coordinates of the point at which EPWP is predicted

Table 8.2: Coefficients obtained for model

Sand type	Coefficients				R^2
	C_0	C_1	C_2	C_3	
Loose Sand	1.400	0.204	0.036	1.232	0.852
Medium Sand	2.461	0.447	0.044	1.099	0.863
Medium Dense Sand	2.878	0.577	0.055	1.026	0.870

the size of the dataset that was used for developing the model. The models are shown in Table 8.3. A comparison of the values obtained from the FEA and the model is depicted in Fig. 8.2, 8.3 and 8.4, indicating the goodness of the model.

To enable easy prediction, charts were prepared with EPWP in kPa on the y axis and $\frac{k_r X}{Sr^2}$ on the x axis. The plots are presented in Fig. 8.5 to Fig. 8.9. Each of the lines in plots represents various values of Y in terms of depth, d. Each chart is prepared for the factor, $a \times t_r$, for loose, medium and dense sand respectively. The charts can be used for predicting values within the range of values considered for analysis given in Table 7.2.

Table 8.3: Prediction models

Type of Sand	Prediction model equation
Loose Sand	$\frac{EPWP}{p_a} = 1.400 \times [a \times t_r]^{0.204} \times \left[k_r \times \frac{X}{S} \times \frac{1}{A_r^2}\right]^{0.036} \times \left[\frac{Y}{d}\right]^{1.232}$
Medium Sand	$\frac{EPWP}{p_a} = 2.461 \times [a \times t_r]^{0.447} \times \left[k_r \times \frac{X}{S} \times \frac{1}{A_r^2}\right]^{0.044} \times \left[\frac{Y}{d}\right]^{1.099}$
Medium Dense Sand	$\frac{EPWP}{p_a} = 2.878 \times [a \times t_r]^{0.577} \times \left[k_r \times \frac{X}{S} \times \frac{1}{A_r^2}\right]^{0.055} \times \left[\frac{Y}{d}\right]^{1.026}$

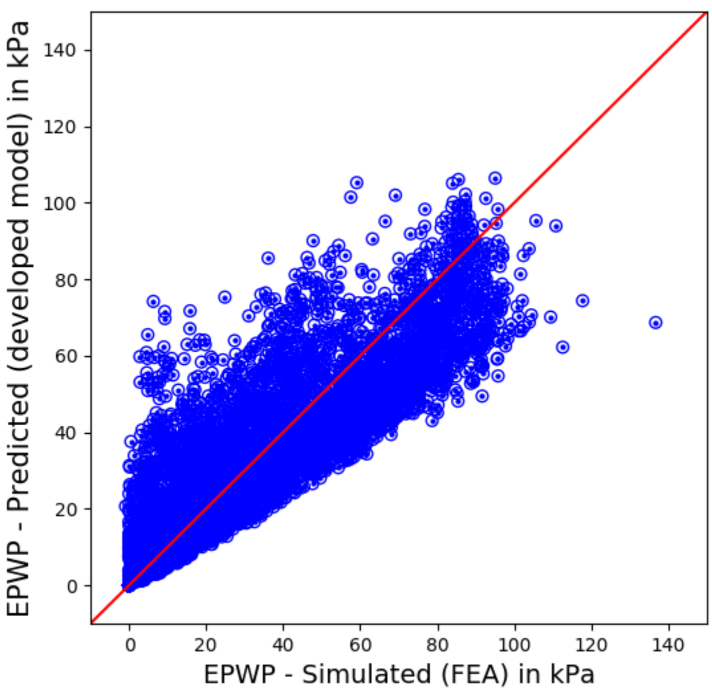

Figure 8.2: Goodness of fit – loose sand

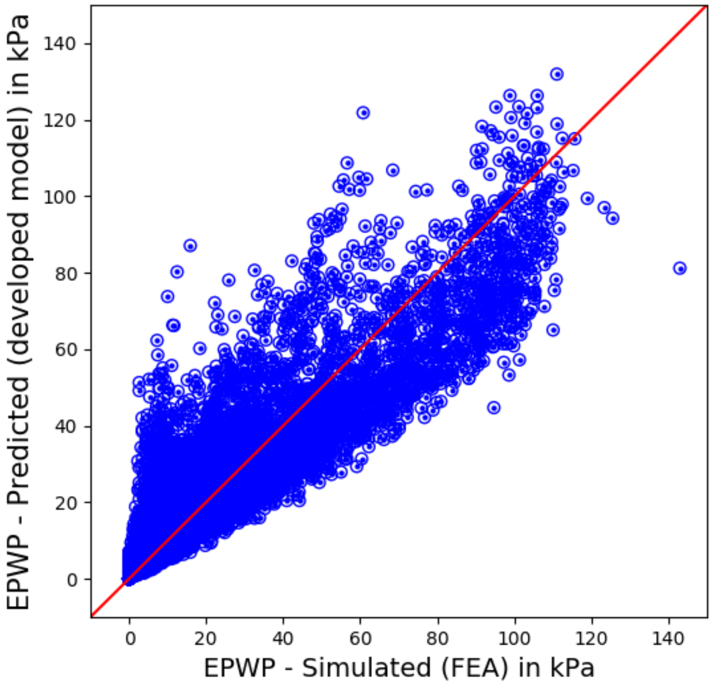

Figure 8.3: Goodness of fit – medium sand

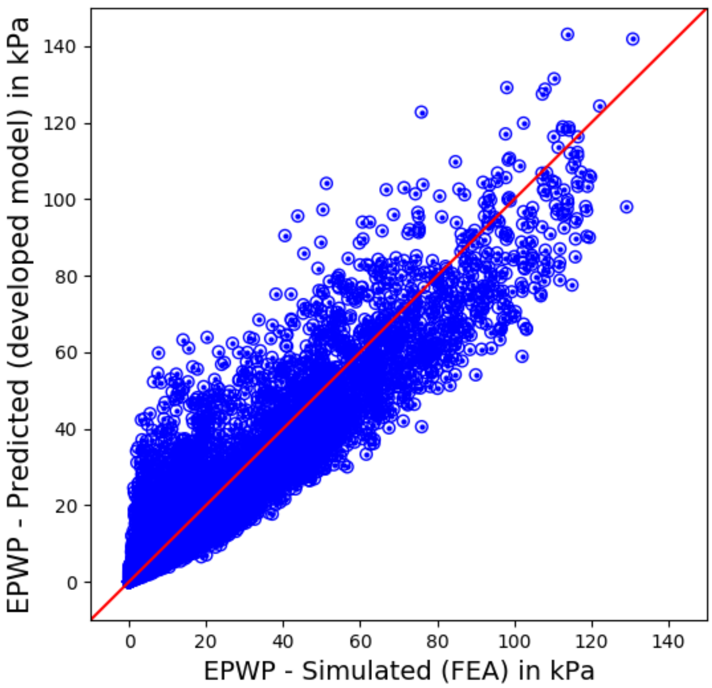

Figure 8.4: Goodness of fit – medium dense sand

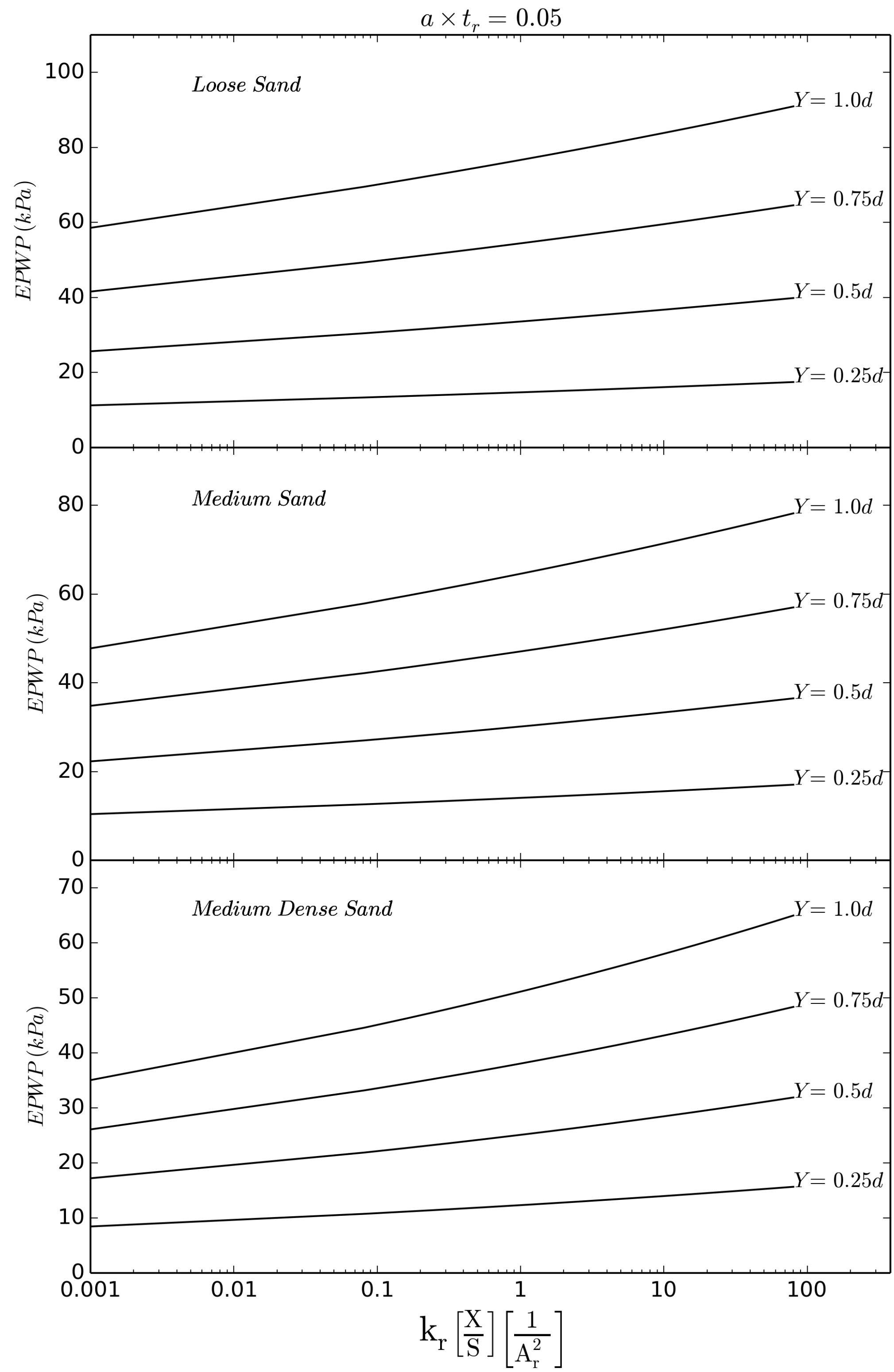

Figure 8.5: EPWP prediction chart $a \times t_r = 0.05$

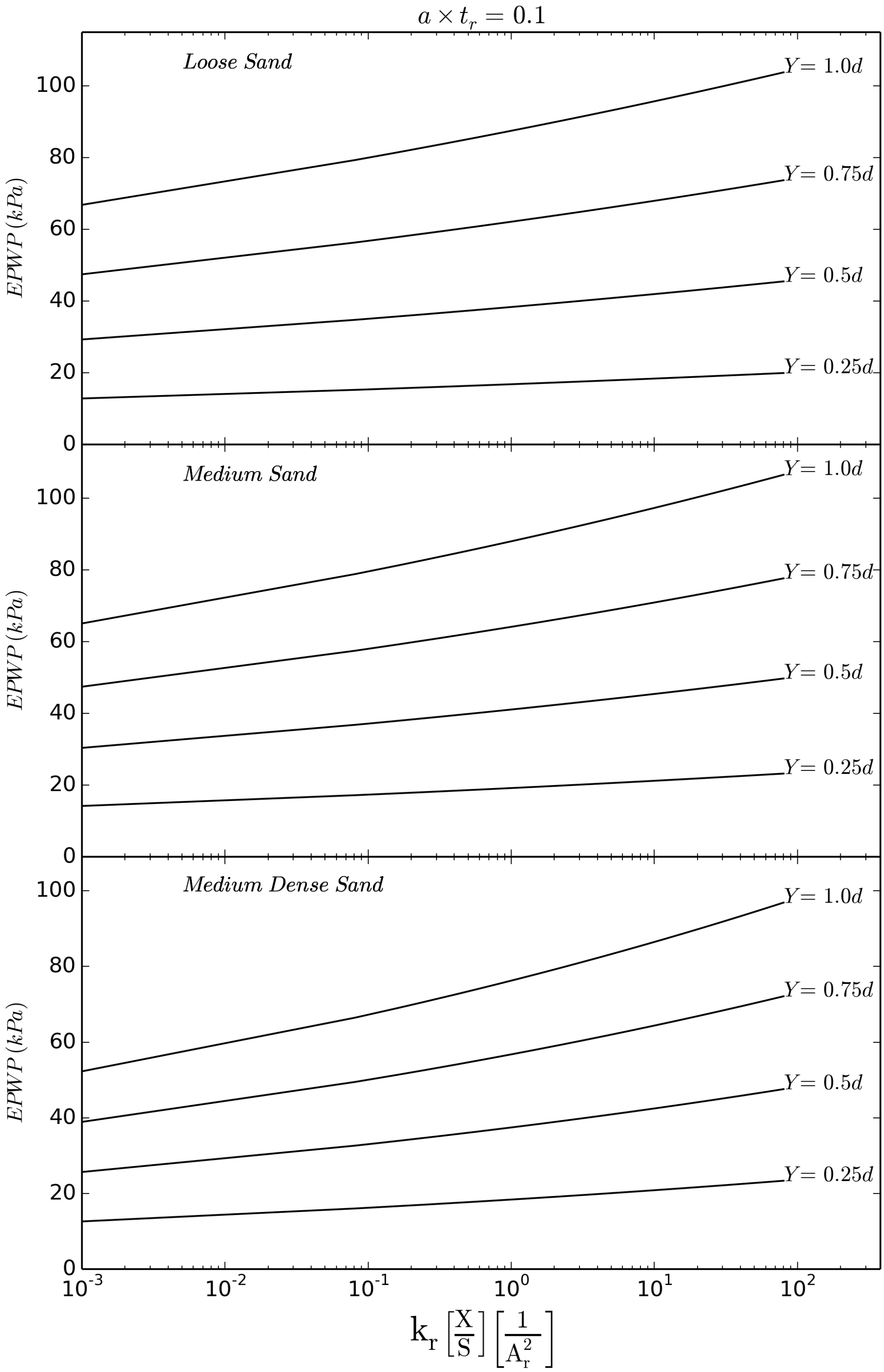

Figure 8.6: EPWP prediction chart $a \times t_r = 0.10$

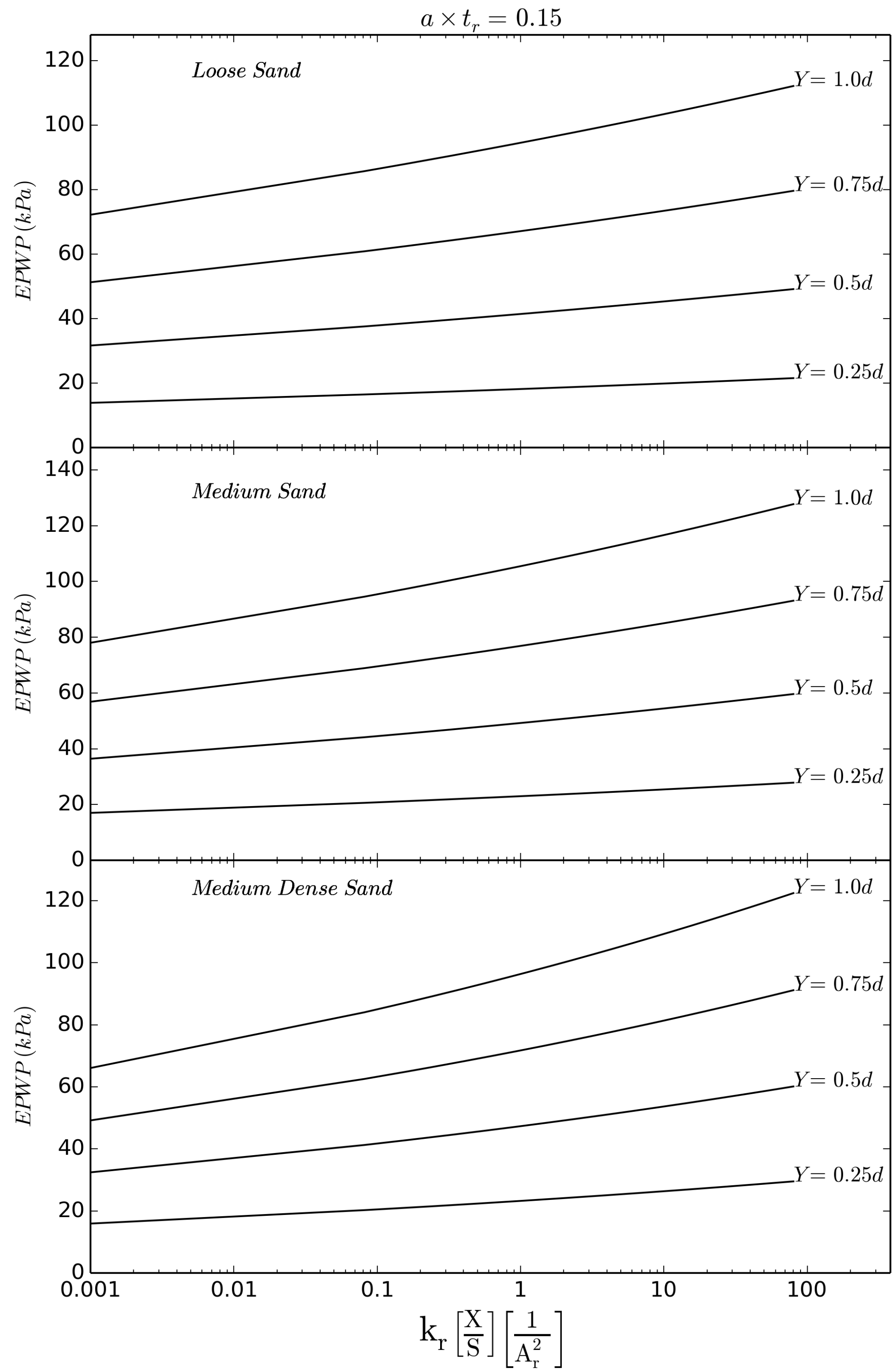

Figure 8.7: EPWP prediction chart $a \times t_r = 0.15$

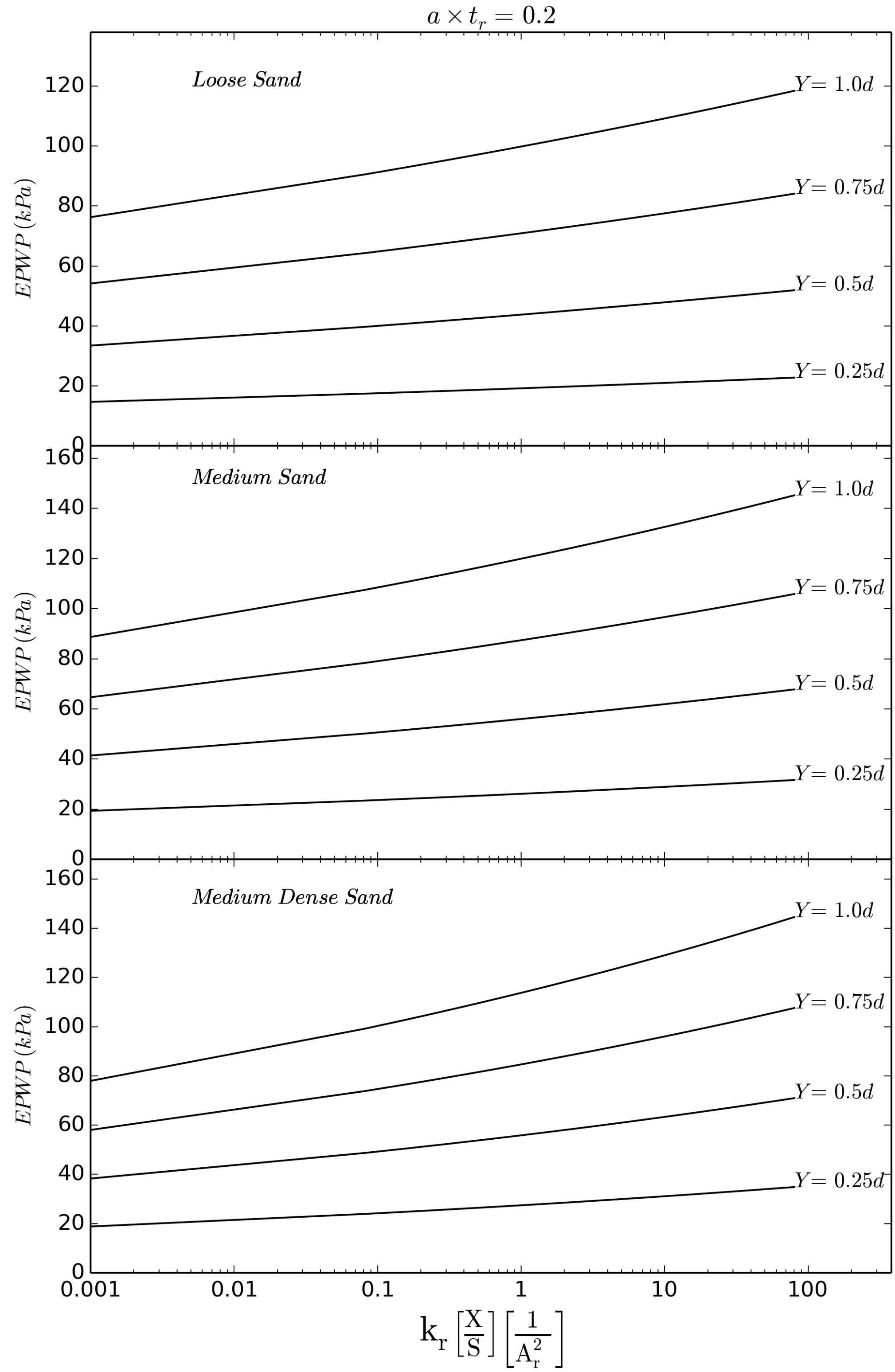

Figure 8.8: EPWP prediction chart $a \times t_r = 0.20$

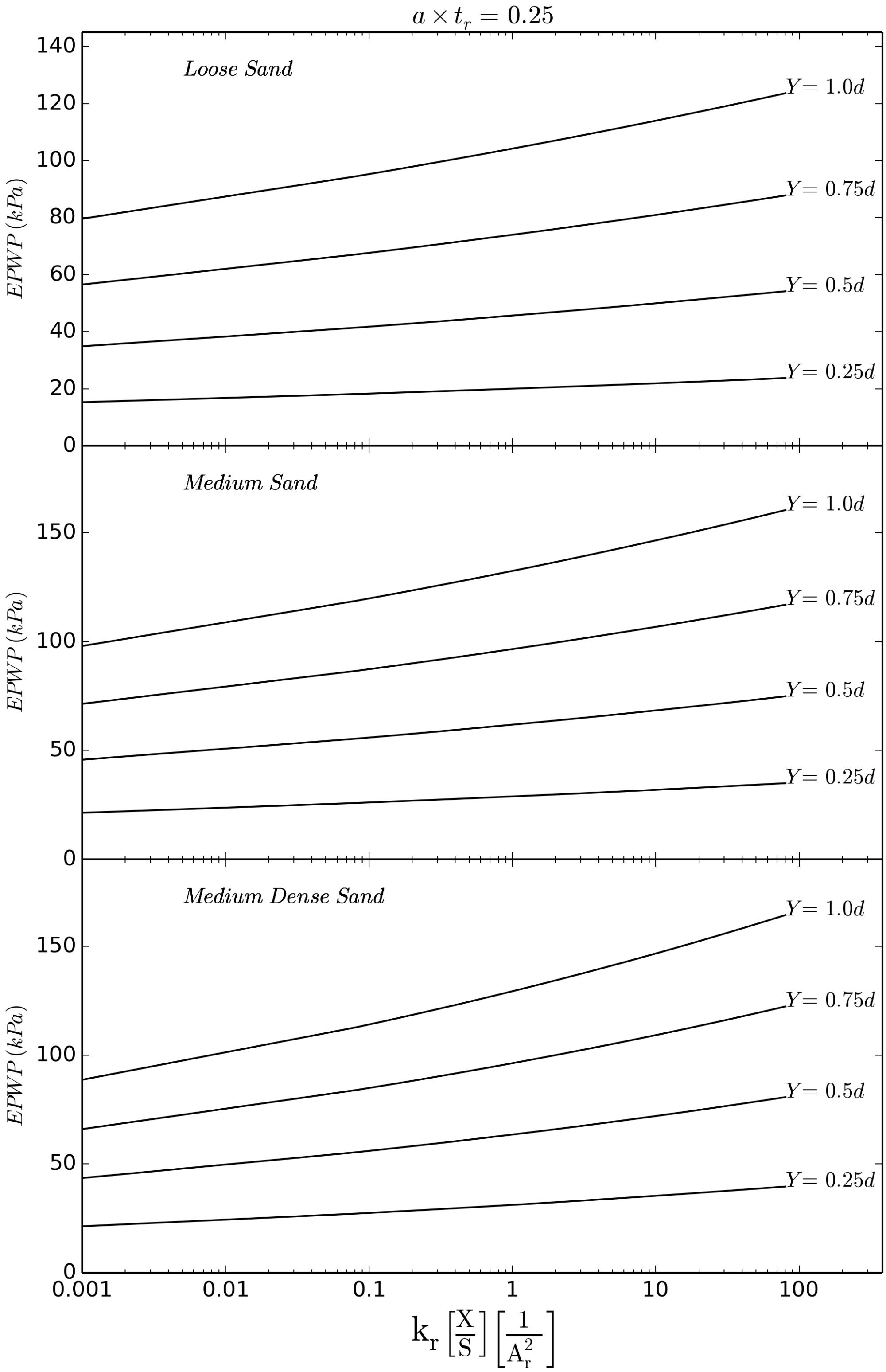

Figure 8.9: EPWP prediction chart $a \times t_r = 0.25$

8.3 Sample calculation

A sample calculation for a typical case is explained below:

A loose sand layer with a relative density of 35% of 10 m depth is improved with stone columns of diameter 0.6 m and 4.0 m depth with a uniform spacing of 1.8 m. The permeability of the layer is $5 \times 10^{-5} m/s$ and stone column is $1 \times 10^{-3} m/s$. The maximum expected ground motion acceleration equivalent to $0.15g$ is expected to last for 10 s.

The expected excess pore water pressure at mid-depth and at a distance of 0.6 m from the centre of the column at 10 s can be calculated as follows.

Step 1: Calculate $a \times t_r = 0.15 \times 10/10 = 0.15$ Choose Fig. 8.7

Step 2: Identify type of sand – Relative density = 35% – Loose sand – Choose graph of loose sand

Step 3: Calculate the factor $\left[k_r \times \dfrac{X}{S} \times \dfrac{1}{A_r^2}\right] = \left[\dfrac{1 \times 10^{-3}}{5 \times 10^{-5}} \times \dfrac{0.6}{1.8} \times \dfrac{1}{(\frac{4.0}{0.6})^2}\right] = 0.15$

Step 4: Calculate $Y/d = 0.5$ (mid depth). Choose the curve corresponding to $Y = 0.5d$

Step 5: Find the EPWP from the y-axis = 41 kPa

8.4 Summary

A statistical method was used to develop models for predicting the excess pore water pressure build-up using the data obtained from FEA for loose, medium and medium dense sand. A set of charts are also prepared to predict the excess pore water pressure employing the empirical relationships obtained.

CHAPTER 9

CONCLUSIONS

9.1 Conclusions

The major objective of the research work was to address the issue of non-availability of laboratory infrastructure for conducting liquefaction studies. It was also aimed to conduct liquefaction studies in the Indian context and to create a better understanding of the behaviour of sand deposits with stone columns.

The present work could meet its objective of developing a shake table with required data acquisition system for conducting laboratory studies to model liquefaction. Further, studies were conducted to find the liquefaction susceptibility of three local sand deposits in the central region of *Kerala*. The effectiveness of the mitigation technique using stone column was studied using experimental investigation by analysing the development and dissipation of pore water pressure. Numerical simulations were used to investigate the effect of different diameter and depth of stone columns in sand deposits of varying densities and permeability.

A cost-effective set up for conducting liquefaction experiments in the laboratory was designed and developed. In addition to a medium sized shaking table, a data acquisition system with sensors for measuring acceleration and excess pore water pressure, and, software for logging the data could be successfully developed. The system was calibrated and tested, and the performance was found to be satisfactory. This is one of the major outcomes of the research.

The major findings of the research study are summarised below:

1. Shake table experiments were conducted to study the behaviour of sand procured from *Cherthala*, *Aluva* and *Puthu Vypin*. The sands were found to be susceptible to liquefaction in loose state, i.e., around 30% relative density when it is subjected to a sinusoidal acceleration of $0.24g$.

2. Out of the three sands studied, *Puthu Vypin* sand having 83% finer sand content of size 0.075 mm-0.425 mm showed highly liquefiable behaviour, while *Cherthala* sand which has 77% of it showed slightly more resistance and that of *Aluva* with 66% showed greater resistance to liquefaction during experiments.

3. The effect of non-plastic fines content on the liquefaction behaviour was studied and observed that fines alter the behaviour during liquefaction. The sand matrix with non-plastic fines tends to remain in a liquefied state during shaking for a longer period of time, and the limiting fines content for this effect was found to be 20% experimentally. This behaviour could be detrimental, since, during liquefaction, sands tend to get consolidated to a denser state and may not liquefy when subjected to dynamic loading again. Higher non-plastic fines content may prevent the sand from reaching a denser state and keep it prone to liquefaction.

4. Stone column is found to be a very effective method for mitigating liquefaction. The shake table experiments confirmed that by increasing the diameter of the stone column, the development of excess pore water pressure could be reduced, leading to better resistance to liquefaction.

5. The free software *OpenSees* platform could be used to model the behaviour of pore pressure development and dissipation in sand during shaking. The experimental investigations with stone columns also could be modelled, and the results are validated.

In order to study the effect of various parameters related to the stone column and surrounding soil on the development and dissipation of pore water pressure, a systematic parametric study was conducted using the same modelling technique used for modelling experimental the previous model. 1530 analyses were conducted to study the significant five parameters affecting the behaviour of sand-stone column subjected to shaking. Owing to the enormous data to be handled for this and to reduce the computing time effectively, a parallel computing technique is resorted for the analysis.

The behaviour of sand-stone column system is very complex in nature due to the number of parameters involved and its interdependence. In such a case, meaningful quantitative conclusions are remote, and hence those depicted below are mostly qualitative. For quantitative evaluation, empirical models and prediction charts are developed and presented in Chapter 8.

6. Almost a linear relationship exists between excess pore water pressure buildup and depth when there is no stone column in the soil. The excess pore water pressure developed is more at higher depths.
7. The excess pore water pressure buildup increases when the ground motion acceleration is more. This behaviour is expected, since, when the intensity of shaking is more, the energy to be dissipated is more and is reflected in the form of higher pore water pressure build up.

8. As the density of soil medium increases, there will be lesser voids in between the soil particles and leads to lesser build up of excess pore water pressure. Also, higher density leads to higher effective stress and hence will require more pore water pressure buildup to initiate liquefaction.

9. Higher permeability results in more drainage and rapid dissipation of excess pore water pressure leading to lesser values of r_u influencing the liquefaction behaviour.

10. The stone column is found to be effective in reducing the excess porewater pressure only in the periphery and not below it. The developed excess pressure below the stone column can adversely affect the behaviour of the system. The contour plots developed for excess pore water pressure reveal this phenomenon.

11. The increase in diameter of the stone column can reduce the development of excess pore water pressure in the periphery. But, this build up is found to increase below the stone column as diameter increases, may be due to the higher stress owing to the weight of the stone column.

12. The excess pore water pressure plots corresponding to different diameter and depths show that the excess pore water pressure value below the stone column reaches up to the case without the stone column or further may exceed that.

13. As far as possible, it is recommended to provide the stone column penetrating to full depth of sand deposit to avoid additional excess pore water pressure below a hanging column.

14. An excess porewater pressure prediction model was developed using the FEA results. The predicted excess pore water pressure values using the model and the values obtained from FEM analysis are shown good agreement. Charts could be prepared using the prediction model for calculating the excess pore water pressure from the intensity of acceleration, the basic soil parameters like permeability, relative density and, the configuration and geometry of the stone column.

The liquefaction studies on sand deposits in *Kerala* presented here throw light on the behaviour of excess pore water pressure development during dynamic shaking, which is expected in the case of the occurrence of an earthquake. The studies also suggest mitigation method using stone column, its analysis and henceforth the developed prediction charts assist the design of the mitigation solution.

9.2 Scope for future work

The present study is not without limitations, and future studies can be pursued to explore further by using sand deposits of different origins, other mitigation methods, 3D modelling techniques etc..

Appendices

APPENDIX A

DATA ACQUISITION SOFTWARE

A.1 Introduction

While developing the sensors and data acquisition system, it was required to have a hardware interface with the computer for acquiring the data. A commonly available microcontroller development board, Arduino was used for prototyping. There were a total of two microcontrollers in the system and it was required to flash a program in the microcontroller to read the data from the sensors and write to the serial port of the computer. The program was written in the Arduino programming language.

The software for acquiring the data was developed using Python. This software has features for calibrating the sensors as well visualising the data while being recorded. The following section shows the program used for the system.

A.2 Program used in microcontroller board - 1

```
#include <avr/io.h>
#include <avr/wdt.h>
#define Reset_AVR() wdt_enable(WDTO_30MS);
while(1) {}
int sensorValue = 0; // value read from the pot
int outputValue = 0; // value output to the PWM (analog out)
int slaverstpin=2;
void setup() {
  // initialize serial communications at 9600 bps:
  Serial.begin(9600);
}
void loop() {
  // read the analog in values:
```

```
  char cmd;
  int i=1;
  float pressure=0,voltage=0,error=0;
  Serial.print("PRS#");
  for(i=0;i<12;i++)
  {
    if ( i==2 || i==10) continue;
    sensorValue = analogRead(i);
    // map it to the range of the analog out:
    Serial.print(sensorValue);
    Serial.print("#");
    // wait 10 milliseconds before the next loop
    // for the analog-to-digital converter to settle
    // after the last reading:
    delay(10);
  }
  Serial.println("");
  delay(10);
}
```

A.3 Program used in microcontroller board - 2

```
#include <avr/io.h>
#include <avr/wdt.h>
#define Reset_AVR() wdt_enable(WDTO_30MS);
while(1) {}
int sensorValue = 0; // value read from the pot
int outputValue = 0; // value output to the PWM (analog out)
int slaverstpin=2;
void setup() {
  // initialize serial communications at 9600 bps:
  Serial.begin(9600);
}
void loop() {
  // read the analog in values:
  char cmd;
  int i=1;
  float pressure=0,voltage=0,error=0;
  Serial.print("MXD#");
  for(i=0;i<12;i++)
  {
    if ( i==4 || i==5 ||i==9) continue;
    sensorValue = analogRead(i);
    // map it to the range of the analog out:
        Serial.print(sensorValue);
    Serial.print("#");
    // wait 10 milliseconds before the next loop
    // for the analog-to-digital converter to settle
    // after the last reading:
    delay(10);
  }
```

```
  Serial.println("");
  delay(10);
}
```

A.4 Program used for acquiring data

```
#####################################################
import sys, serial, random, time, thread, threading, math
from PyQt5 import Qt
from PyQt5 import QtGui
from PyQt5 import QtCore
import PyQt5.Qwt5 as Qwt
from PyQt5.Qwt5.anynumpy import *
#####################################################
class Logger():
  def __init__(self,channel):
    return
  def log(self,mesg):
    print mesg
#####################################################
class kalmanFilter():
  def __init__(self,q,r,p,initial_value):
    self.q=q
    self.p=p
    self.r=r
    self.x=initial_value
  def addSample(self,measurement):
    self.p=self.p+self.q
    self.k=self.p/(self.p+self.r)
    self.x= self.x + self.k*(measurement-self.x)
    self.p=(1-self.k)*self.p
    return self.x
#####################################################
class Recorder():
  def __init__(self,filename):
    self.filename=filename
    self.recorder=open(filename,"w")
  def record(self,data):
    self.recorder.writelines(data)
  def close(self):
    self.recorder.close()
#####################################################
class mainPlot(Qt.QWidget):
  def __init__(self, *args):

    #create a logger to handle logs

    self.uiLogger=Logger(sys.stdout)
    self.ACSrecorder=Recorder("acc"+str(time.time())+".csv")
    self.PRSrecorder=Recorder("prs"+str(time.time())+".csv")
    self.ACSRAWrecorder=Recorder("rawacc"+str(time.time())+".csv")
```

```
    # Initialize sensors #Detect and Attach all sensors
    print "Connecting to sensors"
    self.sensor1=Sensor("/dev/ttyACM0",1,self.uiLogger)
    self.sensor2=Sensor("/dev/ttyACM1",1,self.uiLogger)

    time.sleep(1)

    #setup kalaman filters for accelerometers
    self.A1filter=kalmanFilter(0.4, 256, 100, 0)
    self.A2filter=kalmanFilter(0.4, 256, 100, 0)
    self.A3filter=kalmanFilter(0.4, 256, 100, 0)
    self.A4filter=kalmanFilter(0.4, 256, 100, 0)


    self.acsdata=[]
    self.prsdata=[]

    self.acsError=[0,0,0,0]
    self.prsError=[0,0,0,0,0,0,0,0,0,0,0,0,0,0,0]
    self.acsCalibrate=0
    self.prsCalibrate=0
    self.timeInterval=10 #time interval
    self.recordCounter=0
    self.record=0
#####################################################

    prsPenColors=[Qt.Qt.red,Qt.Qt.green,Qt.Qt.white,Qt.Qt.cyan,Qt.
       Qt.blue,Qt.Qt.red,Qt.Qt.green,Qt.Qt.white,Qt.Qt.cyan,Qt.Qt.
       blue,Qt.Qt.red,Qt.Qt.green,Qt.Qt.white,Qt.Qt.cyan,Qt.Qt.
       blue]#fifteen pens
    acsPenColors=[Qt.Qt.red,Qt.Qt.green] #two pens
    Qt.QWidget.__init__(self, *args)
    self.hbox = QtGui.QHBoxLayout(self)
#####################################################
    #Pressure graph
    self.prsPlot=Qwt.QwtPlot(self)
    self.prsPlot.setTitle('Pressure Sensor')
    self.prsPlot.setCanvasBackground(Qt.Qt.black)
    self.prsPlot.plotLayout().setCanvasMargin(0)
    self.prsPlot.plotLayout().setAlignCanvasToScales(True)

    self.curveP1 = Qwt.QwtPlotCurve("1")
    self.curveP1.attach(self.prsPlot)
    self.curveP2 = Qwt.QwtPlotCurve("2")
    self.curveP2.attach(self.prsPlot)
    self.curveP3 = Qwt.QwtPlotCurve("3")
    self.curveP3.attach(self.prsPlot)
    self.curveP4 = Qwt.QwtPlotCurve("4")
    self.curveP4.attach(self.prsPlot)
    self.curveP5 = Qwt.QwtPlotCurve("5")
    self.curveP5.attach(self.prsPlot)
    self.curveP6 = Qwt.QwtPlotCurve("6")
    self.curveP6.attach(self.prsPlot)
    self.curveP7 = Qwt.QwtPlotCurve("7")
```

```
self.curveP7.attach(self.prsPlot)
self.curveP8 = Qwt.QwtPlotCurve("8")
self.curveP8.attach(self.prsPlot)
self.curveP9 = Qwt.QwtPlotCurve("9")
self.curveP9.attach(self.prsPlot)
self.curveP10 = Qwt.QwtPlotCurve("10")
self.curveP10.attach(self.prsPlot)
self.curveP11 = Qwt.QwtPlotCurve("11")
self.curveP11.attach(self.prsPlot)
self.curveP12 = Qwt.QwtPlotCurve("12")
self.curveP12.attach(self.prsPlot)
self.curveP13 = Qwt.QwtPlotCurve("13")
self.curveP13.attach(self.prsPlot)
self.curveP14 = Qwt.QwtPlotCurve("14")
self.curveP14.attach(self.prsPlot)
self.curveP15 = Qwt.QwtPlotCurve("15")
self.curveP15.attach(self.prsPlot)

self.curveP1.setPen(Qt.QPen(prsPenColors[0]))
self.curveP2.setPen(Qt.QPen(prsPenColors[1]))
self.curveP3.setPen(Qt.QPen(prsPenColors[2]))
self.curveP4.setPen(Qt.QPen(prsPenColors[3]))
self.curveP5.setPen(Qt.QPen(prsPenColors[4]))
self.curveP6.setPen(Qt.QPen(prsPenColors[5]))
self.curveP7.setPen(Qt.QPen(prsPenColors[6]))
self.curveP8.setPen(Qt.QPen(prsPenColors[7]))
self.curveP9.setPen(Qt.QPen(prsPenColors[8]))
self.curveP10.setPen(Qt.QPen(prsPenColors[9]))
self.curveP11.setPen(Qt.QPen(prsPenColors[10]))
self.curveP12.setPen(Qt.QPen(prsPenColors[11]))
self.curveP13.setPen(Qt.QPen(prsPenColors[12]))
self.curveP14.setPen(Qt.QPen(prsPenColors[13]))
self.curveP15.setPen(Qt.QPen(prsPenColors[14]))

self.px = arange(0.0, 100.1, 0.5)
self.p1 = zeros(len(self.px), Float)
self.curveP1.setData(self.px, self.p1)
self.p2 = zeros(len(self.px), Float)
self.curveP2.setData(self.px, self.p2)
self.p3 = zeros(len(self.px), Float)
self.curveP3.setData(self.px, self.p3)
self.p4 = zeros(len(self.px), Float)
self.curveP4.setData(self.px, self.p4)
self.p5 = zeros(len(self.px), Float)
self.curveP5.setData(self.px, self.p5)
self.p6 = zeros(len(self.px), Float)
self.curveP6.setData(self.px, self.p6)
self.p7 = zeros(len(self.px), Float)
self.curveP7.setData(self.px, self.p7)
self.p8 = zeros(len(self.px), Float)
self.curveP8.setData(self.px, self.p8)
self.p9 = zeros(len(self.px), Float)
self.curveP9.setData(self.px, self.p9)
self.p10 = zeros(len(self.px), Float)
self.curveP10.setData(self.px, self.p10)
```

```
    self.p11 = zeros(len(self.px), Float)
    self.curveP11.setData(self.px, self.p11)
    self.p12 = zeros(len(self.px), Float)
    self.curveP12.setData(self.px, self.p12)
    self.p13 = zeros(len(self.px), Float)
    self.curveP13.setData(self.px, self.p13)
    self.p14 = zeros(len(self.px), Float)
    self.curveP14.setData(self.px, self.p14)
    self.p15 = zeros(len(self.px), Float)
    self.curveP15.setData(self.px, self.p15)

#####################################################

    #Acceleration
    self.acsPlot=Qwt.QwtPlot(self)
    self.acsPlot.setTitle('Acceleration Sensor')
    self.acsPlot.setCanvasBackground(Qt.Qt.black)
    self.acsPlot.plotLayout().setCanvasMargin(0)
    self.acsPlot.plotLayout().setAlignCanvasToScales(True)
    #self.layout.addWidget( self.acsPlot, 1, 0)

    self.curveA1 = Qwt.QwtPlotCurve("1")
    self.curveA1.attach(self.acsPlot)
    self.curveA2 = Qwt.QwtPlotCurve("2")
    self.curveA2.attach(self.acsPlot)

    self.curveA1.setPen(Qt.QPen(acsPenColors[0]))
    self.curveA2.setPen(Qt.QPen(acsPenColors[1]))

#####################################################
    self.prsPlot.insertLegend(Qwt.QwtLegend(), Qwt.QwtPlot.
       RightLegend)
    self.acsPlot.insertLegend(Qwt.QwtLegend(), Qwt.QwtPlot.
       RightLegend)
#####################################################
    self.ax = arange(0.0, 100.1, 0.5)
    self.a1 = zeros(len(self.ax), Float)
    self.curveA1.setData(self.ax, self.a1)
    self.a2 = zeros(len(self.ax), Float)
    self.curveA2.setData(self.ax, self.a2)
    self.a3 = zeros(len(self.ax), Float)
#####################################################
    self.prsFrame=QtGui.QFrame(self)
    self.prsFrame.setFrameShape(QtGui.QFrame.StyledPanel)

    self.acsFrame=QtGui.QFrame(self)
    self.acsFrame.setFrameShape(QtGui.QFrame.StyledPanel)
#####################################################
    self.prsSplitter = QtGui.QSplitter(QtCore.Qt.Horizontal)
    self.prsSplitter.addWidget(self.prsPlot)
    self.prsSplitter.addWidget(self.prsFrame)
    self.acsSplitter = QtGui.QSplitter(QtCore.Qt.Horizontal)
    self.acsSplitter.addWidget(self.acsPlot)
    self.acsSplitter.addWidget(self.acsFrame)
#####################################################
```

```
    self.Splitter = QtGui.QSplitter(QtCore.Qt.Vertical)
    self.Splitter.addWidget(self.acsSplitter)
    self.Splitter.addWidget(self.prsSplitter)
    self.hbox.addWidget(self.Splitter)

#####################################################
    #add some button for calibration
    self.A1calbutton= QtGui.QPushButton(self.acsFrame)
    self.A1calbutton.setText("Calibrate ACS")
    self.A1calbutton.setGeometry(30, 40, 100, 30)
    self.connect(self.A1calbutton, Qt.SIGNAL("clicked()"), self.
       calibrateACS)

    self.P1calbutton= QtGui.QPushButton(self.prsFrame)
    self.P1calbutton.setText("Calibrate PRS")
    self.P1calbutton.setGeometry(30, 40, 100, 30)
    self.connect(self.P1calbutton, Qt.SIGNAL("clicked()"), self.
       calibratePRS)


    self.Recbutton= QtGui.QPushButton(self.acsFrame)
    self.Recbutton.setGeometry(150, 40, 100, 30)
    self.Recbutton.setText("Start Record")
    self.connect(self.Recbutton, Qt.SIGNAL("clicked()"), self.
       startRecord)

    self.startTimer(self.timeInterval)
    self.setLayout(self.hbox)
    self.prsPlot.replot()
    self.acsPlot.replot()
#####################################################
  def calibrateACS(self):
    self.acsCalibrate=1
  def calibratePRS(self):
    self.prsCalibrate=1
#####################################################
  def startRecord(self):
    self.record=not self.record
    if self.record==0:
      self.Recbutton.setText("Start Record")
      self.recordCounter=0
    else:
      self.Recbutton.setText("Stop Record")

#####################################################
  def timerEvent(self, e):

    if self.sensor1.type=='MXD' and self.sensor1.STATUS=='OK' and
       self.sensor2.STATUS=='OK' :
      self.acsdata=self.processACSdata(self.sensor1.data[0:5])
      self.prsdata=self.processPRSdata(self.sensor1.data[5:10]+
         self.sensor2.data[1:11])
    elif self.sensor1.type=='PRS' and self.sensor1.STATUS=='OK'
       and self.sensor2.STATUS=='OK':
      self.acsdata=self.processACSdata(self.sensor2.data[0:5])
```

```
      self.prsdata=self.processPRSdata(self.sensor2.data[5:10]+
         self.sensor1.data[1:11])
#####################################################
    #update array and replot
    if  len(self.acsdata)>0:

      self.a1 = concatenate((self.a1[:1], self.a1[:-1]), 1)
      self.a1[0] =self.acsdata[0]
      self.curveA1.setData(self.ax, self.a1)

      self.a2 = concatenate((self.a2[:1], self.a2[:-1]), 1)
      self.a2[0] =self.acsdata[1]
      self.curveA2.setData(self.ax, self.a2)

      self.acsPlot.replot()

    if  len(self.prsdata)>0:

      self.p1 = concatenate((self.p1[:1], self.p1[:-1]), 1)
      self.p1[0] =self.prsdata[0]
      self.curveP1.setData(self.px, self.p1)

      self.p2 = concatenate((self.p2[:1], self.p2[:-1]), 1)
      self.p2[0] =self.prsdata[1]
      self.curveP2.setData(self.px, self.p2)

      self.p3 = concatenate((self.p3[:1], self.p3[:-1]), 1)
      self.p3[0] =self.prsdata[2]
      self.curveP3.setData(self.px, self.p3)

      self.p4 = concatenate((self.p4[:1], self.p4[:-1]), 1)
      self.p4[0] =self.prsdata[3]
      self.curveP4.setData(self.px, self.p4)

      self.p5 = concatenate((self.p5[:1], self.p5[:-1]), 1)
      self.p5[0] =self.prsdata[4]
      self.curveP5.setData(self.px, self.p5)

      self.p6 = concatenate((self.p6[:1], self.p6[:-1]), 1)
      self.p6[0] =self.prsdata[5]
      self.curveP6.setData(self.px, self.p6)

      self.p7 = concatenate((self.p7[:1], self.p7[:-1]), 1)
      self.p7[0] =self.prsdata[6]
      self.curveP7.setData(self.px, self.p7)

      self.p8 = concatenate((self.p8[:1], self.p8[:-1]), 1)
      self.p8[0] =self.prsdata[7]
      self.curveP8.setData(self.px, self.p8)

      self.p9 = concatenate((self.p9[:1], self.p9[:-1]), 1)
      self.p9[0] =self.prsdata[8]
      self.curveP9.setData(self.px, self.p9)

      self.p10 = concatenate((self.p10[:1], self.p10[:-1]), 1)
```

```
      self.p10[0] =self.prsdata[9]
      self.curveP10.setData(self.px, self.p10)

      self.p11 = concatenate((self.p11[:1], self.p11[:-1]), 1)
      self.p11[0] =self.prsdata[10]
      self.curveP11.setData(self.px, self.p11)

      self.p12 = concatenate((self.p12[:1], self.p12[:-1]), 1)
      self.p12[0] =self.prsdata[11]
      self.curveP12.setData(self.px, self.p12)

      self.p13 = concatenate((self.p13[:1], self.p13[:-1]), 1)
      self.p13[0] =self.prsdata[12]
      self.curveP13.setData(self.px, self.p13)

      self.p14 = concatenate((self.p14[:1], self.p14[:-1]), 1)
      self.p14[0] =self.prsdata[13]
      self.curveP14.setData(self.px, self.p14)

      self.p15 = concatenate((self.p15[:1], self.p15[:-1]), 1)
      self.p15[0] =self.prsdata[14]
      self.curveP15.setData(self.px, self.p15)

      self.prsPlot.replot()


#####################################################
    if self.record==1:
      self.PRSrecorder.record(str(self.recordCounter)+","+str(self
         .p1[0])+","+str(self.p2[0])+","+str(self.p3[0])+","+str(
         self.p4[0])+","+str(self.p5[0])+","+str(self.p6[0])+","+
         str(self.p7[0])+","+str(self.p8[0])+","+str(self.p9[0])
         +","+str(self.p10[0])+","+str(self.p11[0])+","+str(self.
         p12[0])+","+str(self.p13[0])+","+str(self.p14[0])+","+str
         (self.p15[0])+"\n")
      self.ACSrecorder.record(str(self.recordCounter)+","+str(self
         .a1[0])+","+str(self.a2[0])+","+str(self.a3[0])+","+str(
         self.a4[0])+"\n")
      self.recordCounter=self.recordCounter+1

    if self.recordCounter>10000000:
      self.recordCounter=0
    return
#####################################################

  def closeEvent(self, event):
    self.sensor1.exitMe=0
    self.sensor2.exitMe=0
    self.ACSrecorder.close()
    #event.accept()

#####################################################

  def processACSdata(self,data):
    filterout=[]
```

```
    try:
      a1=data[1]
      a1=self.calculateG(a1)
      r1=a1
      af1=self.A1filter.addSample(a1)

      a2=data[2]
      a2=self.calculateG(a2)
      r2=a2
      af2=self.A2filter.addSample(a2)

      a3=data[3]
      a3=self.calculateG(a3)
      r3=a3
      af3=self.A3filter.addSample(a3)

      a4=data[4]
      a4=self.calculateG(a4)
      r4=a4
      af4=self.A4filter.addSample(a4)

      if self.acsCalibrate==1:
        self.acsError=[a1,a2,a3,a4]
        self.acsCalibrate=0
      filterout=[af1-self.acsError[0],af2-self.acsError[1],af3-
          self.acsError[2],af4-self.acsError[3]]

      if self.record==1:
        self.ACSRAWrecorder.record(str(self.recordCounter)+","+str
            (r1-self.acsError[0])+","+str(r2-self.acsError[1])+","+
            str(r3-self.acsError[2])+","+str(r4-self.acsError[3])
            +"\n")

    except:
        sys.exc_info()[0]
        self.uiLogger.log("WRN:process_acs_data:empty data array")
        filterout=[0,0,0,0]

    return filterout
####################################################
  def calculatePressure(self,sensorValue):
    error=0.0
    voltage = sensorValue/204.60; #adc conversion(?)
    pressure=(((voltage+error)/5.0)-0.50)/0.0570 #from data sheet
    return pressure
####################################################
  def processPRSdata(self,data):
    dataout=[float(data[0]),float(data[1]),float(data[2]),float(
        data[3]),float(data[4]),float(data[5]),float(data[6]),float
        (data[7]),float(data[8]),float(data[9]),float(data[10]),
        float(data[11]),float(data[12]),float(data[13]),float(data
        [14])]
    dataout=[self.calculatePressure(dataout[0]),self.
        calculatePressure(dataout[1]),self.calculatePressure(
```

```
        dataout[2]),self.calculatePressure(dataout[3]),self.
        calculatePressure(dataout[4]),self.calculatePressure(
        dataout[5]),self.calculatePressure(dataout[6]),self.
        calculatePressure(dataout[7]),self.calculatePressure(
        dataout[8]),self.calculatePressure(dataout[9]),self.
        calculatePressure(dataout[10]),self.calculatePressure(
        dataout[11]),self.calculatePressure(dataout[12]),self.
        calculatePressure(dataout[13]),self.calculatePressure(
        dataout[14])]
    if self.prsCalibrate==1:
      self.prsError=[dataout[0],dataout[1],dataout[2],dataout[3],
         dataout[4],dataout[5],dataout[6],dataout[7],dataout[8],
         dataout[9],dataout[10],dataout[11],dataout[12],dataout
         [13],dataout[14]]
      self.prsCalibrate=0
    dataout=[dataout[0]-self.prsError[0],dataout[1]-self.prsError
        [1],dataout[2]-self.prsError[2],dataout[3]-self.prsError
        [3],dataout[4]-self.prsError[4],dataout[5]-self.prsError
        [5],dataout[6]-self.prsError[6],dataout[7]-self.prsError
        [7],dataout[8]-self.prsError[8],dataout[9]-self.prsError
        [9],dataout[10]-self.prsError[10],dataout[11]-self.prsError
        [11],dataout[12]-self.prsError[12],dataout[13]-self.
        prsError[13],dataout[14]-self.prsError[14]]
    return dataout
#####################################################
  def calculateG(self,adcvalue):
    voltage=interp(float(adcvalue),[0,1023],[0,5])
    volt=voltage-1.35
    g=(volt*1000)/800
    return g*9.81

#####################################################
class basicSensor():
  def __init__(self, device,logger):
    self.device=device
    self.port="NODEVICE"
    self.Logger=logger
    try:
      self.port = serial.Serial(self.device,9600, timeout=1)

    except:
      self.port="NODEVICE"
      self.Logger.log("CRT:basic_sensor_construct:Unable to open
         device "+  self.device)
  def reconnect(self):
    if self.port=='NODEVICE' :
      try:
        self.port = serial.Serial(self.device,9600, timeout=1)
      except:
        self.port="NODEVICE"
  def readValue(self):
    if self.port !='NODEVICE':
      try:
        value=self.port.readline()
        return value
```

```
      except:
        value=-9888
        self.Logger.log("CRT:basic_sensor_readvalue:Unable to read
             from "+  self.device)
        return value

  def close(self):
    if self.port!='NODEVICE':
      try:
        self.Logger.log("MSG:basic_sensor_close:Closing device "+
            self.device)
        self.port.close()
      except:
        self.Logger.log("CRT:basic_sensor_close:Unable to close "+
              self.device)
    else:
      self.Logger.log("CRT:basic_sensor_close:Not opened "+ self.
         device)

#####################################################

class Sensor(threading.Thread):
  def __init__(self,sensor,retry,logger):
    threading.Thread.__init__(self, None)
    self.Logger=logger
    self.retry=retry
    self.exitMe=1
    self.type='NONE'
    self.STATUS='NONE'
    self.data=[]
    self.sensor=basicSensor(sensor,self.Logger)
    self.start()
  def run(self):
    while(self.exitMe):
      #print self.sensor.port
      if self.sensor.port!='NODEVICE':
          data=self.sensor.readValue()
          if data==-9888:
            self.STATUS="READERROR"
          else:
            data=data.replace("\n","").replace("\r","")
            self.data=data[:-1].split("#")
            if self.data[0]=='MXD':
              self.type='MXD'
            elif self.data[0]=='PRS':
              self.type='PRS'
            self.STATUS="OK"
      else:
        if self.retry==1:
          self.sensor.reconnect()
      if self.sensor.port=='NODEVICE':
          self.STATUS="ERROR"

    self.sensor.close()
#####################################################
```

```
app = Qt.QApplication(sys.argv)
QtGui.QApplication.setStyle(QtGui.QStyleFactory.create('Cleanlooks
   '))
demo = mainPlot()
demo.resize(1200, 300)
demo.show()
sys.exit(app.exec_())
#####################################################
```

APPENDIX B

OpenSees INPUT FOR SIMULATING EXPERIMENTAL MODEL

B.1 Introduction

The *OpenSess* input file used for conducting the numerical simulation of the shake table experiments is presented here.

```
#############################################
wipe;
#############################################
set fmass  1.      ;# fluid mass density
set smass  1.93    ;# saturated soil mass density
set n 4.0
set scmass 2.10     ; #saturated stone column mass density
set G     7.5e4    ; # shear modulus of sand
set B     2.0e5    ; # bulk modulus of sand
set GSC 13.e4      ; #shear modulus of stone column
set BSC 3.9e5      ; #bulk modulus of stone column
set phiS 33.       ; # friction angle sand
set phiSC 40.      ; #friction angle stone column
set bulk   2.2e6   ; #fluid-solid combined bulk modulus
set vperm  1.36e-6 ; #vertical permeability (m/s)
set hperm  1.36e-6 ; #horizontal permeability (m/s)
set vpermSC  2.5e-4 ; #vertical permeability of SC (m/s)
set hpermSC  2.5e-4 ; #horizontal permeability of SC (m/s)
set accGravity  9.81  ; #acceleration of gravity
set hperm  [expr $hperm * 0.67/ (log(n) - 0.75)]  ; #converting to
    plain strain permeability
set vperm  $hperm ; #same as horizontal permeability
set press   0.    ; # isotropic consolidation pressure on quad
   element(s)
set accMul  [expr 0.15*$accGravity]  ; # acc. multiplier
set timeShake 80  ; #time for which shaking is done
set period   1.0  ; # Period for applied Sine wave
set deltaT   0.01 ; # time step for analysis
set numSteps 11600 ; # number of time steps
set gamma    0.6   ; # Newmark integration parameter
set massProportionalDamping   0. ; # damping
set InitStiffnessProportionalDamping 0.002; # damping
set ok 0; # to check if analysis is successful
```

```
###############################################################
# BUILD MODEL
#create the ModelBuilder
model basic -ndm 2 -ndf 3
# define material and properties
nDMaterial PressureDependMultiYield 1 2 $smass $G $B $phiS 0.1 80
   0.5 27. 1.5 0.4 2. 10. 0.01 0.7 ; #sand
nDMaterial PressureDependMultiYield 2 2 $scmass $GSC $BSC $phiSC
   0.1 80 0.5 27. 0.03 0.8 5 0.0 0.0 0.0; #SC
# define GRAVITY
set gravY -$accGravity
set gravX 0.
# define nodes
source nodes.tcl
# define elements
#source elements.tcl; # for no SC
#source elements_50.tcl; # for 50mm SC
source elements_100.tcl; # for 100mm SC
#set material to elastic for gravity loading
updateMaterialStage -material 1 -stage 0
updateMaterialStage -material 2 -stage 0
# fix the base
source basefix.tcl
#free surface drainage
source surfacefree.tcl
# tie all disp. DOFs at same level
source tielevelendsOnly.tcl
# fixing ends of box
source sidefix.tcl
###############################################################
# GRAVITY APPLICATION (elastic behavior)
# create the SOE, ConstraintHandler, Integrator, Algorithm and
   Numberer
numberer AMD
system ProfileSPD
test NormDispIncr 1.0e-5 100 2
algorithm Newton
constraints Penalty 1.e18 1.e18
integrator Newmark 1.5  1.
analysis Transient
set ok [analyze 10 5e3]
if {$ok != 0} {
  puts "gravity unsuccessful"
}
if {$ok == 0} {
  puts "gravity successful"
}
# update material stage from elastic (gravity) to plastic
updateMaterialStage -material 1 -stage 1
updateMaterialStage -material 2 -stage 1

if {$ok == 0} {
  set ok [analyze 10 5e3]
}
if {$ok != 0} {
```

```
  puts "plastic stage unsuccessful"
}
if {$ok == 0} {
  puts "plastic stage successful"
}
# rezero time
wipeAnalysis
setTime 0.0
#############################################################
#   base input motion
pattern UniformExcitation  1  1 -accel "Sine 0. $timeShake $period
     -factor $accMul"
#define recorders for disp., excess pore pressure.,acceleration
recorder Node -file $filename -time -nodeRange 1 171 -dof 3 -dT
   $deltaT vel
recorder Node -file disp -time -nodeRange 1 171 -dof 1 2 -dT
   $deltaT disp
recorder Node -file acc -time -nodeRange 1 171 -dof 1 2 -dT
   $deltaT accel
#define recorders for stress and strain
recorder Element -file stress1.out   -time -dT $deltaT  -eleRange
   1 144  material 1 stress
recorder Element -file stress2.out   -time -dT $deltaT  -eleRange
   1 144  material 2 stress
recorder Element -file stress3.out   -time -dT $deltaT  -eleRange
   1 144  material 3 stress
recorder Element -file stress4.out   -time -dT $deltaT  -eleRange
   1 144  material 4 stress
recorder Element -file strain1.out   -time -dT $deltaT  -eleRange
   1 144  material 1 strain
recorder Element -file strain2.out   -time -dT $deltaT  -eleRange
   1 144  material 2 strain
recorder Element -file strain3.out   -time -dT $deltaT  -eleRange
   1 144  material 3 strain
recorder Element -file strain4.out   -time -dT $deltaT  -eleRange
   1 144  material 4 strain
#analysis options
constraints Penalty 1.e18 1.e18
test NormDispIncr 1.e-5 100 2
numberer AMD
system ProfileSPD
algorithm KrylovNewton
rayleigh $massProportionalDamping 0.0
   $InitStiffnessProportionalDamping 0.0
integrator Newmark $gamma  [expr pow($gamma+0.5, 2)/4]
analysis VariableTransient
#analyze
set startT [clock seconds]
if {$ok == 0} {
  set ok [analyze $numSteps $deltaT [expr $deltaT/100] $deltaT 15]
}
if {$ok != 0} {
  puts "Dynamic analysis not successful"
}
set endT [clock seconds]
```

```
if {$ok == 0} {
  puts "Dynamic analysis successful"
puts "Execution time: [expr $endT-$startT] seconds."
}
#############################################
wipe  ;#flush ouput stream
#############################################
```

APPENDIX C

OpenseesMP PARALLEL JOB ALLOCATION PROGRAM

C.1 Introduction

For conducting the parametric study, the parallel version of *OpenSess* was employed. The parallel version helps to utilize multiple cores of the computer and automate the job allocation and analysis. The following section shows the program that was used for conducting parallel analysis.

C.2 Program used for parallel job allocation

```
##############################################
set totalStartT [clock seconds]
set pid [getPID] ;#get the process id
set numP  [getNP] ; #get the number of process
set count 0
##############################################
###The input files corresponding to different models
array set elements_list {
        a {D0.tcl}
        b {D3d3.tcl}
        c {D3d6.tcl}
        d {D3d9.tcl}
        e {D3d12.tcl}
        f {D6d3.tcl}
        g {D6d6.tcl}
        h {D6d9.tcl}
        i {D6d12.tcl}
        j {D9d3.tcl}
        k {D9d6.tcl}
        l {D9d9.tcl}
        m {D9d12.tcl}
        n {D12d3.tcl}
```

```
        o {D12d6.tcl}
        p {D12d9.tcl}
        q {D12d12.tcl}

}
##############################################
###The input files corresponding to different soil
array set materialFile_list {
        a {SL.tcl}
        a {SM.tcl}
        a {SMD.tcl}
}
##############################################
###The input values for different permeability
array set vperm_list {
        a {1e-4}
        b {5e-4}
        c {1e-5}
        d {5e-5}
        e {1e-6}
        f {5e-6}
}
##############################################
###The input values for time of shaking
array set T_list {
        a {10}
}
##############################################
###The input values for time of shaking
array set acc_list {
        a {0.05}
        b {0.10}
        c {0.15}
        d {0.20}
        e {0.25}
}
##############################################
### Job Allocation based on variables
### Definition of file names of output files
foreach ele [lsort [array names elements_list]] {
 set elements "$elements_list($ele)"

 foreach mat [lsort [array names materialFile_list]] {
 set materialFile "$materialFile_list($mat)"

  foreach vpe [lsort [array names vperm_list]] {
  set vperm "$vperm_list($vpe)"

   foreach time [lsort [array names T_list]] {
   set T "$T_list($time)"

    foreach ac [lsort [array names acc_list]] {
    set acc "$acc_list($ac)"
```

```
    set filename "g$acc_list($ac)T$T_list($time)K$vperm_list($vpe)
        S$materialFile_list($mat)$elements_list($ele).out"
    set filenameGstress1 "Gstress1g$acc_list($ac)T$T_list($time)
        K$vperm_list($vpe)S$materialFile_list($mat)$elements_list(
        $ele).out"
    set filenameGstress2 "Gstress2g$acc_list($ac)T$T_list($time)
        K$vperm_list($vpe)S$materialFile_list($mat)$elements_list(
        $ele).out"
    set filenameGstress3 "Gstress3g$acc_list($ac)T$T_list($time)
        K$vperm_list($vpe)S$materialFile_list($mat)$elements_list(
        $ele).out"
    set filenameGstress4 "Gstress4g$acc_list($ac)T$T_list($time)
        K$vperm_list($vpe)S$materialFile_list($mat)$elements_list(
        $ele).out"
    set filenameDystress1 "DyStress1g$acc_list($ac)T$T_list($time)
        K$vperm_list($vpe)S$materialFile_list($mat)$elements_list(
        $ele).out"
    set filenameDystress2 "DyStress2g$acc_list($ac)T$T_list($time)
        K$vperm_list($vpe)S$materialFile_list($mat)$elements_list(
        $ele).out"
    set filenameDystress3 "DyStress3g$acc_list($ac)T$T_list($time)
        K$vperm_list($vpe)S$materialFile_list($mat)$elements_list(
        $ele).out"
    set filenameDystress4 "DyStress4g$acc_list($ac)T$T_list($time)
        K$vperm_list($vpe)S$materialFile_list($mat)$elements_list(
        $ele).out"
    set filenameDystrain1 "DyStrain1g$acc_list($ac)T$T_list($time)
        K$vperm_list($vpe)S$materialFile_list($mat)$elements_list(
        $ele).out"
    set filenameDystrain2 "DyStrain2g$acc_list($ac)T$T_list($time)
        K$vperm_list($vpe)S$materialFile_list($mat)$elements_list(
        $ele).out"
    set filenameDystrain3 "DyStrain3g$acc_list($ac)T$T_list($time)
        K$vperm_list($vpe)S$materialFile_list($mat)$elements_list(
        $ele).out"
    set filenameDystrain4 "DyStrain4g$acc_list($ac)T$T_list($time)
        K$vperm_list($vpe)S$materialFile_list($mat)$elements_list(
        $ele).out"
    set filenamePWP "Pwpg$acc_list($ac)T$T_list($time)K$vperm_list
        ($vpe)S$materialFile_list($mat)$elements_list($ele).out"
    set filenamedisp "Disp$acc_list($ac)T$T_list($time)
        K$vperm_list($vpe)S$materialFile_list($mat)$elements_list(
        $ele).out"
    set filenameacc "Acc$acc_list($ac)T$T_list($time)K$vperm_list(
        $vpe)S$materialFile_list($mat)$elements_list($ele).out"
      if {[expr $count % $numP] == $pid}  {
       puts "started $filename"
       source model.tcl
         }
        incr count 1
       }
      }
    }
  }
}
```

```
###############################################
### Calculation of time required for analysis
set totalEndT [clock seconds]
puts "Execution time: [expr $totalEndT-$totalStartT] seconds"
###############################################
```

C.3 Input used for FEA

```
###############################################
wipe;
###############################################
set fmass  1.         ;# fluid mass density
set bulk   2.2e6      ;#fluid-solid combined bulk modulus
set accGravity  9.81  ;#acceleration of gravity
set press   0.        ;# isotropic consolidation pressure on quad
   element(s)
set accMul  [expr $acc*$accGravity]  ;# input motion accelration
set timeShake $T      ; #time for which shaking is done
set trackTime [expr $timeShake*3] ; #time during which tracking is
    done
set period   1.0      ;# Period for applied Sine wave
set deltaT   0.01     ;# time step for analysis
set numSteps  [expr int($trackTime/$deltaT)]   ;# number of time
   steps
set gamma    0.6      ;# Newmark integration parameter
set massProportionalDamping   0. ;
set InitStiffnessProportionalDamping 0.002;
set thickEle 1.0 ; # Thickness of plane strain element to be used
   in element command
set n 4; #R/r radius of influence zone / radius of drain
set vperm [expr $vperm * 0.67/ (log(n) - 0.75)]; #converting to
   plain strain permeability
set hperm  $vperm  ;#horizontal permeability (m/s) same as
   vertical permeability
set vpermSC  1e-3  ;#vertical permeability of stone column (m/s)
set hpermSC  1e-3  ;#horizontal permeability of stone column (m/s)
set ok 0           ; # to check if analysis is successful
###############################################
# BUILD MODEL
#create the ModelBuilder
model basic -ndm 2 -ndf 3
# define material and properties
source $materialFile
nDMaterial PressureDependMultiYield 2 2 2.1 1.3e5 3.9e5 40 0.1 80
   0.5 27. 0.03 0.8 5 0.0 0.0 0.0
# define GRAVITY
set gravY -$accGravity
set gravX 0.
# define nodes
source nodes.tcl
# define boundary conditions
source boundaries.tcl
# define elements
```

```
source $elements ; #this should be based on analysis
#set material to elastic for gravity loading
updateMaterialStage -material 1 -stage 0
updateMaterialStage -material 2 -stage 0
##############################################
# GRAVITY APPLICATION (elastic behavior)
#creting recorders for stress at all node points
recorder Element -file $filenameGstress1.out   -time -dT $deltaT
    -eleRange 1 336  material 1 stress
recorder Element -file $filenameGstress2.out   -time -dT $deltaT
    -eleRange 1 336  material 2 stress
recorder Element -file $filenameGstress3.out   -time -dT $deltaT
    -eleRange 1 336  material 3 stress
recorder Element -file $filenameGstress4.out   -time -dT $deltaT
    -eleRange 1 336  material 4 stress
# create the SOE, ConstraintHandler, Integrator, Algorithm and
    Numberer
numberer AMD
system ProfileSPD
test NormDispIncr 1.0e-5 1000 0
algorithm KrylovNewton
constraints Penalty 1.e18 1.e18
integrator Newmark 1.5  1.
analysis Transient
set ok [analyze 50 5e3]
if {$ok != 0} {
        puts "gravity unsuccessful $filename"
}
if {$ok == 0} {
        puts "gravity successful $filename"
}
# update material stage from elastic (gravity) to plastic
updateMaterialStage -material 1 -stage 1
updateMaterialStage -material 2 -stage 1
if {$ok == 0} {
        set ok [analyze 1 5e3]
}
if {$ok != 0} {
        puts "plastic stage unsuccessful $filename"
}
if {$ok == 0} {
        puts "plastic stage successful $filename"
}
wipeAnalysis
remove recorders ; # to remove the recorders of stress in gravity
setTime 0.0
##############################################
# NOW APPLY LOADING SEQUENCE AND ANALYZE (plastic)
#   base input motion
pattern UniformExcitation  1  1 -accel "Sine 0. $timeShake $period
     -factor $accMul" ; #this should be based on analysis
#define recorders for disp., excess pore pressure.,acceleration
recorder Node -file $filenamePWP -time -nodeRange 1 375 -dof 3 -dT
     $deltaT vel
recorder Node -file $filenamedisp -time -nodeRange 1 375 -dof 1 2
```

```
   -dT $deltaT disp
recorder Node -file $filenameacc -time -nodeRange 1 375 -dof 1 2 -
   dT $deltaT accel
#define recorders for stress and strain
recorder Element -file $filenameDystress1.out   -time -dT $deltaT
    -eleRange 1 336  material 1 stress
recorder Element -file $filenameDystress2.out   -time -dT $deltaT
    -eleRange 1 336  material 2 stress
recorder Element -file $filenameDystress3.out   -time -dT $deltaT
    -eleRange 1 336  material 3 stress
recorder Element -file $filenameDystress4.out   -time -dT $deltaT
    -eleRange 1 336  material 4 stress
recorder Element -file $filenameDystrain1.out   -time -dT $deltaT
    -eleRange 1 336  material 1 strain
recorder Element -file $filenameDystrain2.out   -time -dT $deltaT
    -eleRange 1 336  material 2 strain
recorder Element -file $filenameDystrain3.out   -time -dT $deltaT
    -eleRange 1 336  material 3 strain
recorder Element -file $filenameDystrain4.out   -time -dT $deltaT
    -eleRange 1 336  material 4 strain
#analysis options
constraints Penalty 1.e18 1.e18
test NormDispIncr 1.e-5 1000 5
numberer AMD
system ProfileSPD
algorithm KrylovNewton
#some mass proportional and initial-stiffness proportional damping
rayleigh $massProportionalDamping 0.0
   $InitStiffnessProportionalDamping 0.0
integrator Newmark $gamma  [expr pow($gamma+0.5, 2)/4]
analysis VariableTransient
#analyze
set startT [clock seconds]
if {$ok == 0} {
        set ok [analyze $numSteps $deltaT [expr $deltaT/100]
           $deltaT 100]
}
if {$ok != 0} {
        puts "Dynamic analysis unsuccessful $filename"
}
set endT [clock seconds]
if {$ok == 0} {
        puts "Dynamic analysis successful $filename"
puts "Execution time is [expr $endT-$startT] seconds for $filename
   "
}
##############################################
wipe  ;#flush ouput stream
##############################################
```

REFERENCES

1. **Abaqus** (2010). Users manual, 6.10-2. *Providence, RI, USA: HKS Inc.*

2. **Adalier, K.** and **A.-W. Elgamal** (2002). Seismic response of adjacent dense and loose saturated sand columns. *Soil Dynamics and Earthquake Engineering*, **22**(2), 115–127.

3. **Airouche, A.**, **H. Bechtoula**, **H. Aknouche**, **B. K. Thoen**, and **D. Benouar** (2014). Experimental identification of the six dof cgs, algeria, shaking table system. *Smart Structures and Systems*, **13**(1), 137–154.

4. **Ammanagi, S.**, **V. Poornima**, **A. Sera**, and **R. Sunder** (2006). Development of a digitally-controlled three-axis earthquake shake table. *Current Science*, 190–203.

5. **Belkhatir, M.**, **T. Schanz**, **A. Arab**, **N. Della**, and **A. Kadri** (2014). Insight into the effects of gradation on the pore pressure generation of sand–silt mixtures. *Geotechnical testing journal*, **37**(5), 922–931.

6. **Ben Salem, Z.**, **W. Frikha**, and **M. Bouassida** (2015). Effect of granular-column installation on excess pore pressure variation during soil liquefaction. *International Journal of Geomechanics*, **16**(2), 04015046.

7. **Bhattacharya, S.** and **R. Dattatrayam** (2002). Earthquake sequence in kerala during december 2000 and january. *Current Science*, **82**(10), 1275.

8. **Bhattacharya, S.**, **A. M. Krishna**, **D. Lombardi**, **A. Crewe**, and **N. Alexander** (2012). Economic mems based 3-axis water proof accelerometer for dynamic geo-engineering applications. *Soil Dynamics and Earthquake Engineering*, **36**, 111–118.

9. **Boominathan, A.**, **C. Ramana**, **M. Bühler**, and **G. Gudehus**, Study on performance of pile walls using laminar shake box. *In 14th World Conference on Earthquake Engineering*. 2004.

10. **Boulanger, R. W.** and **I. Idriss** (2006). Liquefaction susceptibility criteria for silts and clays. *Journal of geotechnical and geoenvironmental engineering*, **132**(11), 1413–1426.

11. **Brennan, A.** and **S. Madabhushi** (2002). Effectiveness of vertical drains in mitigation of liquefaction. *Soil Dynamics and Earthquake Engineering*, **22**(9), 1059–1065.

12. **Chandrasekaran, V.** (2003). Centrifuge modelling in earthquake geotechnical engineering. *Energy*, **3**(1).

13. **Choudhury, D.**, **V. Phanikanth**, **S. Y. Mhaske**, **R. R. Phule**, and **K. Chatterjee** (2015). Seismic liquefaction hazard and site response for design of piles in mumbai city. *Indian Geotechnical Journal*, **45**(1), 62–78.

14. **Coelho, P.**, **S. K. Haigh**, and **S. G. Madabhushi**, Boundary effects in dynamic centrifuge modelling of liquefaction in sand deposits. *In Proceedings of the 16th ASCE engineering mechanics conference, University of Washington, Seattle, USA*. 2003.

15. **Das, A.**, **S. K. Deb**, and **A. Dutta** (2016). Shake table testing of un-reinforced brick masonry building test model isolated by u-frei. *Earthquake Engineering & Structural Dynamics*, **45**(2), 253–272.

16. **Dash, S. R.**, **L. Govindaraju**, and **S. Bhattacharya** (2009). A case study of damages of the kandla port and customs office tower supported on a mat–pile foundation in liquefied soils under the 2001 bhuj earthquake. *Soil Dynamics and Earthquake Engineering*, **29**(2), 333–346.

17. **Donahue, J. L.**, *The liquefaction susceptibility, resistance, and response of silty and clayey soils*. University of California, Berkeley, 2007.

18. **Dou, H.** and **P. M. Byrne** (1997). Model studies of boundary effect on dynamic soil response. *Canadian geotechnical journal*, **34**(3), 460–465.

19. **Dungca, J.**, **J. Kuwano**, **A. Takahashi**, **T. Saruwatari**, **J. Izawa**, **H. Suzuki**, and **K. Tokimatsu** (2006). Shaking table tests on the lateral response of a pile buried in liquefied sand. *Soil Dynamics and Earthquake Engineering*, **26**(2), 287–295.

20. **Elgamal, A.**, **J. Lu**, and **D. Forcellini** (2009). Mitigation of liquefaction-induced lateral deformation in a sloping stratum: three-dimensional numerical simulation. *Journal of geotechnical and geoenvironmental engineering*, **135**(11), 1672–1682.

21. **Elgamal, A.**, **Z. Yang**, and **E. Parra** (2002). Computational modeling of cyclic mobility and post-liquefaction site response. *Soil Dynamics and Earthquake Engineering*, **22**(4), 259–271.

22. **Fabbrocino, G.** and **E. Cosenza**, Shaking tables for seismic simulation, overview of the crdc-amra project. *In The many facets of the seismic risk – Proceedings of the Workshop on Multidisciplinary Approach to Seismic Risk Problems. Doppiavoce Ed., SantAngelo dei Lombardi (Avellino)*. 2003.

23. **Florin, V.**, Liquefaction of saturated sandy soils. *In Proc. of the 5th international conference on soil mechanics and foudation engineering*, volume 1. 1961.

24. **Giri, D.** and **A. Sengupta**, Performance of small scale model slopes in shaking table tests. *In Indian Geotechnical Conference*. IGS Mumbai Chapter and IIT Bombay, 2010.

25. **Goughnour, R. R.** and **J. M. Pestana**, Mechanical behavior of stone columns under seismic loading. *In Proceedings of 2nd International conference on Ground Improvement Techniques, CI-Premier, Singapore*. 1998.

26. **Guo, T.** and **S. Prakash** (1999). Liquefaction of silts and silt-clay mixtures. *Journal of Geotechnical and Geoenvironmental Engineering*, **125**(8), 706–710.

27. **Gupta, M. K.** (1977). *Liquefaction of sands during earthquakes*. Ph.D. thesis, University of Roorkee.

28. **Hazarika, H.** and **A. Boominathan**, Liquefaction and ground failures during the 2001 bhuj earthquake, india. *In Proceedings of International Conference on Performance-Based Design in Earthquake Geotechnical Engineering from case history to practice, Tokyo, Japan*. 2009.

29. **Hird, C.**, **I. Pyrah**, and **D. Russel** (1992). Finite element modelling of vertical drains beneath embankments on soft ground. *Geotechnique*, **42**(3), 499–511.

30. **Howell, R.**, **E. Rathje**, and **R. Boulanger** (2014). Evaluation of simulation models of lateral spread sites treated with prefabricated vertical drains. *Journal of Geotechnical and Geoenvironmental Engineering*, **141**(1), 04014076.

31. **Howell, R. L.** (2013). *The performance of lateral spread sites treated with prefabricated vertical drains: physical and numerical models*. Ph.D. thesis, The University of Texas at Austin.

32. **Idriss, I. M.** and **R. W. Boulanger**, *Soil liquefaction during earthquakes*. Earthquake Engineering Research Institute, 2008.

33. **IIT, K.** (2018). Shake Table for Small Scale Dynamic Model Testing, Department of Civil Engineering, Indian Institute of Technology, Kanpur. `http://home.iitk.ac.in/~dcrai/details/shaketableoct16.pdf`. Accessed: 2018-01-15.

34. **Indraratna, B.** and **I. Redana** (2000). Numerical modeling of vertical drains with smear and well resistance installed in soft clay. *Canadian Geotechnical Journal*, **37**(1), 132–145.

35. **Ishihara, K.** (1993). Liquefaction and flow failure during earthquakes. *Geotechnique*, **43**(3), 351–451.

36. **Ishihara, K.**, **J. Troncoso**, **Y. Kawase**, and **Y. Takahashi** (1980). Cyclic strength characteristics of tailings materials. *Soils and Foundations*, **20**(4), 127–142.

37. **Itasca** (2000). Fast lagrangian analysis of continua FLAC. *Itasca Consulting Group Inc., Minneapolis, Minn.*

38. **Jain, S. K.** and **N. C. Nigam**, Historical developments and current status of earthquake engineering in india. *In Proceedings of the 12th world conference on earthquake engineering. Auckland, New Zealand*. 2000.

39. **Jennings, P. C.** *et al.*, *Earthquake engineering and hazards reduction in China: a trip report of the American Earthquake Engineering and Hazards Reduction Delegation submitted to the Committee on Scholarly Communication with the People's Republic of China*, volume 8. National Academies, 1980.

40. **Jeremić, B.**, **Z. Cheng**, **M. Taiebat**, and **Y. Dafalias** (2008). Numerical simulation of fully saturated porous materials. *International Journal for Numerical and Analytical Methods in Geomechanics*, **32**(13), 1635–1660.

41. **Jones, E.**, **T. Oliphant**, and **P. Peterson** (2014). SciPy: Open Source Scientific Tools for Python.

42. **Joshi, V.**, **B. Lavania**, and **M. Siavoshnia**, Idealizing reinforced earth embankments in dynamic analysis. *In 12th World Conference on Earthquake Engineering*. University of Roorkee, India, 2000.

43. **Karamitros, D. K.**, **G. D. Bouckovalas**, and **Y. K. Chaloulos** (2012). Insight into the seismic liquefaction performance of shallow foundations. *Journal of Geotechnical and Geoenvironmental Engineering*, **139**(4), 599–607.

44. **Karanth, R.**, **P. S. Sohoni**, **G. Mathew**, and **A. Khadkikar** (2001). Geological observations of the 26 january 2001 bhuj earthquake. *Journal of Geological Society of India*, **58**(3), 193–202.

45. **Karimi, Z.** and **S. Dashti** (2016). Seismic performance of shallow founded structures on liquefiable ground: Validation of numerical simulations using centrifuge experiments. *Journal of Geotechnical and Geoenvironmental Engineering*, **142**(6), 04016011.

46. **Koester, J. P.** and **T. Tsuchida** (1988). Earthquake-induced liquefaction of fine-grained soils-considerations from japanese research. Technical report, Army Engineer Waterways Experiment Station Vicksburg ms Geotechnical Lab.

47. **Krahn, J.**, *Dynamic modeling with QUAKE/W: an engineering methodology*. GEO-SLOPE, 2004.

48. **Kramer, S.** (1996). Earthquake geotechnical engineering.

49. **Krishna, A. M.** and **M. Madhav** (2009). Engineering of ground for liquefaction mitigation using granular columnar inclusions: recent developments. *American Journal of Engineering and Applied Sciences*, **2**(3).

50. **Krishna, A. M.**, **M. Madhav**, **G. M. Latha**, *et al.* (2006). Liquefaction mitigation of ground treated with granular piles: Densification effect. *ISET Journal of Earthquake Technology*, **43**(4), 105–120.

51. **Kumar, P.**, **X. Yuan**, **M. R. Kumar**, **R. Kind**, **X. Li**, and **R. Chadha** (2007). The rapid drift of the indian tectonic plate. *Nature*, **449**(7164), 894–897.

52. **Kumar, R. S.**, **S. Sajish**, **S. Kumar**, **P. Chellapandi**, **P. Selvaraj**, and **S. Raghupathy** (2014). Seismic qualification of the unconventional valve by shake table testing. *Applied Mechanics & Materials*.

53. **Liam Finn, W.**, **K. W. Lee**, and **G. Martin** (1977). An effective stress model for liquefaction. *Electronics Letter*, **103**(ASCE 13008 Proceeding).

54. **Liyanathirana, D.** and **H. Poulos** (2002). Numerical simulation of soil liquefaction due to earthquake loading. *Soil Dynamics and Earthquake Engineering*, **22**(7), 511–523.

55. **Luco, J.**, **O. Ozcelik**, and **J. Conte** (2009). Acceleration tracking performance of the ucsd-nees shake table. *Journal of structural engineering*, **136**(5), 481–490.

56. **Madhav, M.** and **A. M. Krishna**, Liquefaction mitigation of sand deposits by granular piles-an overview. *In Geotechnical Engineering for Disaster Mitigation and Rehabilitation*. Springer, 2008, 66–79.

57. **Maheshwari, B.**, **H. Singh**, and **S. Saran** (2012). Effects of reinforcement on liquefaction resistance of solani sand. *Journal of Geotechnical and Geoenvironmental Engineering*, **138**(7), 831–840.

58. **Makran, S.** (2001). Preliminary observations on the origin and effects of the january 26, 2001 bhuj (gujarat, india) earthquake. *EERI Special Earthquake Report - April 2001*.

59. **Marcuson, W. F.** (1978). Definition of terms related to liquefaction. *Journal of the Geotechnical engineering division*, **104**(9), 1197–1200.

60. **Martin, J. B. G.** and **G. Martin**, Quantitative evaluation of stone column techniques for earthquake liquefaction mitigation. *In Proceedings of the Tenth World Conference on Earthquake Engineering: 19-24 July 1992, Madrid, Spain*, volume 3. CRC Press, 1992.

61. **Maslov, N.**, Questions of seismic stability of submerged sandy foundations and structures. *In Proceedings, 4th International Conference on Soil Mechanics and Foundation Engineering*, volume 1. 1957.

62. **Matasović, N.** and **M. Vucetic** (1993). Cyclic characterization of liquefiable sands. *Journal of Geotechnical Engineering*, **119**(11), 1805–1822.

63. **Matsuo, O.**, **K. Yokoyama**, and **Y. Saito** (1998). Shaking table tests and analyses of geosynthetic-reinforced soil retaining walls. *Geosynthetics International*, **5**(1-2), 97–126.

64. **Mazzoni, S.**, **F. McKenna**, **M. H. Scott**, and **G. L. Fenves** (2006). The open system for earthquake engineering simulation (opensees) user command-language manual. *User's Manual. Ver*.

65. **McKenna, F.** and **G. L. Fenves** (2007). Using the opensees interpreter on parallel computers. *NEESit. TN-2007-16*.

66. **Mitchell, J. K.** and **F. J. Wentz**, *Performance of improved ground during the Loma Prieta earthquake*, volume 91. Earthquake Engineering Research Center, University of California Berkeley, 1991.

67. **Mogami, T.**, The behaviour of soil during vibration. *In Proc. of 3rd Int. Conf. on SMFE*. 1953.

68. **Murugesan, S.** and **K. Rajagopal** (2009). Studies on the behavior of single and group of geosynthetic encased stone columns. *Journal of Geotechnical and Geoenvironmental Engineering*, **136**(1), 129–139.

69. **Najjar, S. S.**, **S. Sadek**, and **T. Maakaroun** (2010). Effect of sand columns on the undrained load response of soft clays. *Journal of Geotechnical and Geoenvironmental Engineering*, **136**(9), 1263–1277.

70. **Nath, S. K.**, **K. K. S. Thingbaijam**, and **A. Raj** (2008). Earthquake hazard in northeast indiaa seismic microzonation approach with typical case studies from sikkim himalaya and guwahati city. *Journal of Earth System Science*, **117**(2), 809–831.

71. **National Research Council Committee on Earthquake Engineering Research, U.**, *Liquefaction of soils during earthquakes*, volume 1. National Academies, 1985.

72. **Nayak, N.**, Recent advances in ground improvements by stone column. *In Proceedings of Indian Geotechnical Conference*. 1983.

73. **Ohtani, K.**, **N. Ogawa**, **T. Katayama**, and **H. Shibata**, Construction of e-defense (3-d full-scale earthquake testing facility). *In Proc. of Second International Symposium on New Technologies for Urban Safety of Mega Cities in Asia*. 2003.

74. **Orense, R.**, **I. Morimoto**, **Y. a. Yamamoto**, **T. Yumiyama**, **H. Yamamoto**, and **K. Sugawara** (2003). Study on wall-type gravel drains as liquefaction countermeasure for underground structures. *Soil Dynamics and Earthquake Engineering*, **23**(1), 19–39.

75. **Park, Y.-H.**, **S.-R. Kim**, **S.-H. Kim**, and **M.-M. Kim**, Liquefaction of embankments on sandy soil and the optimum countermeasure against the liquefaction. *In 12th World Conference on Earthquake Engineering*. University of Roorkee, India, 2000.

76. **Peloso, S.**, **A. Pavese**, and **C. Casarotti**, Eucentre trees lab: laboratory for training and research in earthquake engineering and seismology. *In Role of Seismic Testing Facilities in Performance-Based Earthquake Engineering*. Springer, 2012, 65–81.

77. **Petalas, A.** and **V. Galavi** (2013). Plaxis liquefaction model ubc3dplm. *PLAXIS knowledge base*.

78. **Phule, R. R.** and **D. Choudhury**, A critical review of liquefaction susceptibility criteria for fine grained soils subjected to earthquake loading. *In Proceedings of Indian geotechnical conference, IGC-2013, IIT Roorkee, Roorkee, India*. 2013.

79. **Polito, C. P.** and **J. R. Martin II** (2001). Effects of nonplastic fines on the liquefaction resistance of sands. *Journal of Geotechnical and Geoenvironmental Engineering*, **127**(5), 408–415.

80. **Prakashvel, J.**, **C. UmaRani**, **K. Muthumani**, and **N. Gopalakrishnan** (2012). Earthquake response of reinforced concrete frame with open ground storey. *Bonfring International Journal of Industrial Engineering and Management Science*, **2**(4), 91.

81. **Prasad, S.**, **I. Towhata**, **G. Chandradhara**, and **P. Nanjundaswamy** (2004). Shaking table tests in earthquake geotechnical engineering. *Current Science-Bangalore-*, **87**, 1398–1404.

82. **Rajendran, K.**, **C. Rajendran**, **M. Thakkar**, and **M. P. Tuttle** (2001). The 2001 kutch (bhuj) earthquake: Coseismic surface features and their significance. *Current Science*, 1397–1405.

83. **Ramakrishnan, S.**, **M. Budhu**, and **A. Britto** (1998). Laboratory seismic tests of geotextile wrap-faced and geotextile-reinforced segmental retaining walls. *Geosynthetics International*, **5**(1-2), 55–71.

84. **Rao, K.** and **D. N. Satyam** (2007). Liquefaction studies for seismic microzonation of delhi region. *Current science*, 646–654.

85. **Rayamajhi, D.**, **S. A. Ashford**, **R. W. Boulanger**, and **A. Elgamal** (2016*a*). Dense granular columns in liquefiable ground. i: Shear reinforcement and cyclic stress ratio reduction. *Journal of Geotechnical and Geoenvironmental Engineering*, **142**(7), 04016023.

86. **Rayamajhi, D.**, **R. W. Boulanger**, **S. A. Ashford**, and **A. Elgamal** (2016*b*). Dense granular columns in liquefiable ground. ii: Effects on deformations. *Journal of Geotechnical and Geoenvironmental Engineering*, **142**(7), 04016024.

87. **Rayamajhi, D.**, **T. V. Nguyen**, **S. A. Ashford**, **R. W. Boulanger**, **J. Lu**, **A. Elgamal**, and **L. Shao** (2013). Numerical study of shear stress distribution for discrete columns in liquefiable soils. *Journal of Geotechnical and Geoenvironmental Engineering*, **140**(3), 04013034.

88. **Rocker Jr., K.** (1968). *The Liquefaction Behaviour of Sands Subjected to Cyclic Loading*. Ph.D. thesis, Massachusetts Institute of Technology.

89. **Sajudeen, N.** and **S. Latheswary**, Seismic hazard assessment of kerala. *In International Conference on Challenges in Environmental Science and Engineering, 9-13 September, Melbourne, Australia*. 2012.

90. **Sasaki, Y.** and **E. Taniguchi** (1982). Shaking table tests on gravel drains to prevent liquefaction of sand deposits. *Soils and Foundations*, **22**(3), 1–14.

91. **Seed, B.** and **K. L. Lee** (1966). Liquefaction of saturated sands during cyclic loading. *Journal of Soil Mechanics & Foundations Div*, **92**(ASCE# 4972 Proceeding).

92. **Seed, H. B.**, Landslides during earthquakes due to soil liquefaction. *In Terzaghi Lectures: 1963-1972*. ASCE, 1968.

93. **Seed, H. B.** and **J. R. Booker**, *Stabilization of potentially liquefiable sand deposits using gravel drain systems*. Earthquake Engineering Research Center, University of California, 1976.

94. **Seed, H. B.** and **I. M. Idriss** (1971). Simplified procedure for evaluating soil liquefaction potential. *Journal of Soil Mechanics & Foundations Div*, **97**(9), 1249–1273.

95. **Seed, H. B.**, **P. P. Martin**, and **J. Lysmer** (1976). Pore-water pressure changes during soil liquefaction. *Journal of Geotechnical and Geoenvironmental Engineering*, **102**(Proc. Paper# 12074).

96. **Sharma, A.**, **G. Reddy**, **K. Vaze**, *et al.* (2012). Shake table tests on a non-seismically detailed rc frame structure. *Structural Engineering and Mechanics*, **41**(1), 1–24.

97. **Sharp, M. K.**, **R. Dobry**, and **T. Abdoun** (2003). Liquefaction centrifuge modeling of sands of different permeability. *Journal of geotechnical and geoenvironmental engineering*, **129**(12), 1083–1091.

98. **Singh, R.**, **D. Roy**, and **S. K. Jain** (2005). Analysis of earth dams affected by the 2001 bhuj earthquake. *Engineering geology*, **80**(3-4), 282–291.

99. **Sitharam, T.**, **P. Anbazhagan**, and **G. Mahesh** (2007). 3-d subsurface modelling and preliminary liquefaction hazard mapping of bangalore city using spt data and gis. *Indian Geotechnical Journal*, **37**(3), 23–57.

100. **Sladen, J.**, **R. D'hollander**, and **J. Krahn** (1985). The liquefaction of sands, a collapse surface approach. *Canadian Geotechnical Journal*, **22**(4), 564–578.

101. **Sollogoub, P.** (2007). Seismic testing. *Advanced Earthquake Engineering Analysis*, 181–214.

102. **Tan, S. A.**, **S. Tjahyono**, and **K. Oo** (2008). Simplified plane-strain modeling of stone-column reinforced ground. *Journal of Geotechnical and Geoenvironmental Engineering*, **134**(2), 185–194.

103. **Tang, L.**, **S. Cong**, **X. Ling**, **J. Lu**, and **A. Elgamal** (2015). Numerical study on ground improvement for liquefaction mitigation using stone columns encased with geosynthetics. *Geotextiles and Geomembranes*, **43**(2), 190–195.

104. **Thoen, B. K.** and **P. N. Laplace**, Offline tuning of shaking tables. *In Proceedings of the 13th World Conference on Earthquake Engineering*. 2004.

105. **Tsuchida, H.**, Prediction and countermeasure against the liquefaction in sand deposits. *In Abstract of the seminar in the Port and Harbor Research Institute*. 1970.

106. **Uma Maheswari, R.**, **A. Boominathan**, and **G. Dodagoudar**, Effective stress v/s total stress ground response analyses for a typical site in chennai (india). *In International Conferences on Recent Advances in Geotechnical Earthquake Engineering and Soil Dynamics*. Missouri University of Science and Technology, 2010.

107. **University of Berkeley** (2018). University of Berkeley Shaking Table 6 DOF. `https://peer.berkeley.edu/laboratories/shaking_table.html`. Accessed: 2018-01-14.

108. **Varghese, R. M.** and **G. M. Latha**, Initiation of liquefaction in sand under different surcharge and overburden stresses. *In Proceedings of Indian Geotechnical Conference, Roorkee*. 2013.

109. **Varghese, R. M.** and **G. M. Latha** (2014). Shaking table tests to investigate the influence of various factors on the liquefaction resistance of sands. *Natural hazards*, **73**(3), 1337–1351.

110. **Vipin, K.**, **T. Sitharam**, and **S. Kolathayar** (2013). Assessment of seismic hazard and liquefaction potential of gujarat based on probabilistic approaches. *Natural hazards*, **65**(2), 1179–1195.

111. **Wang, B.**, **K. Zen**, **G. Chen**, **Y. Zhang**, and **K. Kasama** (2013). Excess pore pressure dissipation and solidification after liquefaction of saturated sand deposits. *Soil Dynamics and Earthquake Engineering*, **49**, 157–164.

112. **Wang, W.**, *Some findings in soil liquefaction*. Earthquake Engineering Department, Water Conservancy and Hydroelectric Power Scientific Research Institute, 1979.

113. **Wood, D. M.** and **K. Belkheir** (1994). Strain softening and state parameter for sand modelling. *Geotechnique*, **44**(2), 335–339.

114. **Yamamoto, Y.**, **M. Hyodo**, and **R. P. Orense** (2009). Liquefaction resistance of sandy soils under partially drained condition. *Journal of geotechnical and geoenvironmental engineering*, **135**(8), 1032–1043.

115. **Yamamuro, J. A.** and **P. V. Lade** (1998). Steady-state concepts and static liquefaction of silty sands. *Journal of geotechnical and geoenvironmental engineering*, **124**(9), 868–877.

116. **Yang, Z.**, **A. Elgamal**, and **E. Parra** (2003). Computational model for cyclic mobility and associated shear deformation. *Journal of Geotechnical and Geoenvironmental Engineering*, **129**(12), 1119–1127.

117. **Zienkiewicz, O.** and **T. Shiomi** (1984). Dynamic behaviour of saturated porous media; the generalized biot formulation and its numerical solution. *International journal for numerical and analytical methods in geomechanics*, **8**(1), 71–96.

LIST OF PAPERS BASED ON THESIS

Journals

1. **Unni, K.G.,** Beena, K.S. and Mahesh, C (2018). Development of 1-D Shake Table Testing Facility for Liquefaction Studies, *Journal of Institution of Engineers India Series A* **99**, 423 - 432. DOI: `https://doi.org/10.1007/s40030-018-0299-2`

2. **G. Unni Kartha,** K. S. Beena and C. P. Mohamed Thahir (2018). Shake Table Studies on Embankments on Liquefiable Soil, *Soil Dynamics and Earthquake Geotechnical Engineering. Lecture Notes in Civil Engineering* **15**, 101 - 109. DOI: `https://doi.org/10.1007/978-981-13-0562-7_12`

Conferences

1. **Beena, K. S.,** Unni Kartha, G. (2014). Stone columns for liquefaction mitigation: An experimental investigation, *6th International Geotechnical Symposium on Disaster Mitigation in Special Geoenvironmental Conditions*, 169 - 172.

CURRICULUM VITAE

UNNI KARTHA G
Assistant Professor
Dept. of Civil Engineering
Federal Institute of Science and Technology (FISAT)
Angamaly, Kerala - 683577

Education

Degree	Institution	Period	Remarks
SSLC	BSS Gurukulam HS, Alathur	1992 -1993	First class with distinction, 82.5%
Pre-Degree	Govt. Victoria College, Palakkad	1993 -1995	First class, 79.1%
B.Tech	NSS Engineering College, Palakkad	1995 - 1999	First class with honours, 75.2%
M.Tech	Govt. College of Technology, Coimbatore	2000 - 2002	First class with first rank, 82.9
Ph.D	Cochin University of Science and Technology, Cochin	Registered on 04/08/2009	

Fields of research interest

Structural Dynamics, Earthquake Geotechnical Engineering, Finite Element Analysis

Publications

International Journal	2
International Conference	2
National Conference	4

Software skill set

Languages : Python, TCL

Software packages and platforms: AutoCAD, STAAD, OpenSees, Scilab, GNU Octave, LaTeX

Operating system: Linux, macOS

Personal details

Age and date of birth	40 Years, 31/01/1978
Gender	Male
Nationality	Indian
Languages	English, Malayalam, Hindi
e-mail	unnikartha@gmail.com
Permanent Address	Dwaraka, FISAT Gardens, Mookkannor, Angamaly - 683 577